REPUBLIC OF TÜRKİYE
YILDIZ TECHNICAL UNIVERSITY
GRADUATE SCHOOL OF SCIENCE AND ENGINEERING

ONE DIMENSIONAL MODELLING AND EXPERIMENTAL INVESTIGATION OF MECHANICAL DEHUMIDIFICATION SYSTEM

Şerife SATOĞLU

MASTER OF SCIENCE

Department of Energy Technologies

Program of Energy Technologies

Supervisor

Prof. Dr. Hakan DEMİR

January, 2025

REPUBLIC OF TÜRKİYE

YILDIZ TECHNICAL UNIVERSITY

GRADUATE SCHOOL OF SCIENCE AND ENGINEERING

ONE DIMENSIONAL MODELLING AND EXPERIMENTAL INVESTIGATION OF MECHANICAL DEHUMIDIFICATION SYSTEM

A thesis submitted by Şerife SATOĞLU in partial fulfillment of the requirements for the degree of **MASTER OF SCIENCE** is approved by the committee on 12.02.2025 in Department of Energy Technologies, Program of Energy Technologies.

Prof. Dr. Hakan DEMIR
Yıldız Technical University
Supervisor

Approved By the Examining Committee

Prof. Dr. Hakan DEMIR, Supervisor
Yildiz Technical University _____

Doç. Dr. Zafer GEMICI, Member
Yildiz Technical University _____

Prof. Dr. Ali Ihsan KOCA, Member
Istanbul Technical University _____

I hereby declare that I have obtained the required legal permissions during data collection and exploitation procedures, that I have made the in-text citations and cited the references properly, that I haven't falsified and/or fabricated research data and results of the study and that I have abided by the principles of the scientific research and ethics during my Thesis Study under the title of "One Dimensional Modelling and Experimental Investigation of Mechanical Dehumidification System" supervised by my supervisor, Prof. Dr. Hakan DEMIR. In the case of a discovery of false statement, I am to acknowledge any legal consequence.

Şerife SATOĞLU

Signature

Dedicated to my family

and friends

ACKNOWLEDGEMENTS

I would like to thank firstly my supervisor, Prof. Dr. Hakan Demir, whose insight and knowledge in the subject matter and understanding and patience in our working conditions have steered me through this research. Secondly, I would like to thank Emre Arpaci, whose work as part of his PhD and whose help and support at every stage of experimentation have allowed me to shape and finalize my project.

I would especially like to thank my sister, Asst. Prof. Merve Yüsra Doğan, who has never held back her care and effort even all the way from across the world and pushed me through the process.

I would also like to acknowledge my immediate family, friends and coworkers who have not given up on me and always encouraged me in my academic studies.

Şerife SATOĞLU

TABLE OF CONTENTS

LIST OF ABBREVIATIONS viii

LIST OF FIGURES x

LIST OF TABLES xiv

ABSTRACT xv

ÖZET xvii

1 INTRODUCTION 1

1.1 Statement of Purpose 1

1.2 Mechanical Dehumidification in the Industry 2

1.3 Essential Benefits of Dehumidification 4

1.4 Project Scope 5

2 THEORETICAL CONCEPTS 6

2.1 Dehumidification Process 6

2.1.1 Refrigerant Mechanical Dehumidification 6

2.1.2 Dehumidification with Heat Pumps 8

2.1.3 Comparison between Heat Pump and Refrigerant Based Dehumidifier 9

2.2 Psychrometric Chart Analysis of Dehumidification Process 11

3 LITERATURE REVIEW 14

3.1 Classification of Heat Pump Systems 14

3.2 Classification of Dehumidification systems 17

3.3 Dehumidification Applications in the Industry 18

3.4 Heat pump drying in food and agricultural industries 19

3.5 Limitations of heat pumps 21

3.6 Progress and Recent developments in dehumidification technology 21

3.7 Psychrometric analysis 22

3.8 Modelling of mechanical dehumidification 23

3.9 Mathematical modeling of dehumidification processes 24

4 EXPERIMENTAL INVESTIGATION 27

4.1 Dehumidifier 27
4.1.1 Dissembling 28
4.2 Preliminary Setup 31
4.2.1 Tools and setup details 31
4.2.2 Experiment 34
4.3 Dryer Oven Setup 37
4.3.1 Dryer Oven Setup Details and Measurement Tools 38
4.3.2 Experiment 41
5 MODELLING **43**
5.1 Simcenter Amesim 43
5.1.1 Overview of Simcenter Amesim 43
5.1.2 Historical Development 44
5.1.3 Working Principles 44
5.2 Modelling 47
5.2.1 Overview of Simcenter Amesim Modelling 47
5.2.2 Submodels 47
5.2.3 Final Model 66
6 CONCLUSION **69**
6.1 Validation 69
6.2 Test Results 74
6.3 Variations on the Model 84
6.4 Conclusion 87
6.5 Future Work 88
6.6 Future of Dehumidification 88
REFERENCES **90**
PUBLICATIONS FROM THE THESIS **97**

LIST OF SYMBOLS

x_i	Variable
$u(t)$	Function of Time
u'	First Derivative
u''	Second Derivative
y_i	Actual value
$\hat{y}_i$	Forecast value
n	Number of fitted points

LIST OF ABBREVIATIONS

AMCHPD	Automated Multi Commodity Heat Pump Dryer
CAD	Computer Aided Design
CFC	Chlorofluorocarbon
CFD	Computational Fluid Dynamics
DAE	Differential Algebraic Equation
DBT	Dry-Bulb Temperature
DHE	Dehumidification Efficiency
DOE	Design of Experiments
EES	Engineering Equation Solver
EV	Electric Vehicle
FMU	Functional Mock-Up
GCC	GNU Compiler Collection
GUI	Graphical User Interface
HACCP	Hazard Analysis and Critical Control Points
HDH	Humidification-Dehumidification
HPD	Heat Pump Dryer
HP-ORC	Heat Pumps with Organic Rankine Cycles
HR	Humidity Ratio
HVAC	Heating, Ventilation, and Air Conditioning
MAE	Mean Absolute Error
MAPE	Mean Absolute Percentage Error

MSE	Mean Squared Error
MER	Moisture Extraction Rate
ODE	Ordinary Differential Equation
PINN	Physics Informed Neural Network
RBD	Refrigerant Based Dehumidifiers
RH	Relative Humidity
SAHPD	Solar-Assisted Heat Pump Dryer
SDWRS	Solar Desiccant Wheel System
SEC	Specific Energy Consumption
SLDR	Solar Liquid Desiccant Radiation
SMER	Specific Moisture Extraction Rate
TRNSYS	Transient System Simulation Tool
WBT	Wet-Bulb Temperature

LIST OF FIGURES

Figure 2.1 Illustration of a refrigerant based dehumidifier **7**

Figure 2.2 The psychrometric chart for air **12**

Figure 2.3 Dehumidification on Pyschrometric Chart **13**

Figure 3.1 Classification of heat pump development **15**

Figure 3.2 Table heat pump dryer classification **16**

Figure 3.3 Classification of heat pump dryers **16**

Figure 4.1 Views of dehumidifier used in experiment **28**

Figure 4.2 Data sheet on the dehumidifier **28**

Figure 4.3 Exploded view and component list of the Trotec TK100 dehumidifier **29**

Figure 4.4 Open panel views of dehumidifier **30**

Figure 4.5 Separated heat exchanger and compressor **30**

Figure 4.6 Dehumidifier with cardboard canal **32**

Figure 4.7 Testo flow measurement instruments **32**

Figure 4.8 Log-Tchebycheff rule **33**

Figure 4.9 Steam spray setup in classroom **35**

Figure 4.10 Dryer Oven **37**

Figure 4.11 Flexible duct connection to the cabin **38**

Figure 4.12 Thermocouples in the oven cabin **38**

Figure 4.13 Positioning of Sense humidity sensor **39**

Figure 4.14 Positioning of the EMS humidity sensor **39**

Figure 4.15 Agilent data logger **39**

Figure 4.16 Handmade stainless steel duct for inlet **40**

Figure 4.17 Measuring with velocity probe **40**

Figure 4.18 Manual measuring **41**

Figure 4.19 Weighing tomato trays **41**

Figure 5.1 Compressor submodel icon **47**

Figure 5.2 Compressor port inlet and outlet **48**

Figure 5.3 External variables for compressor submodel **48**

Figure 5.4 Parameters entered and signal input for compressor submodel.....**49**
Figure 5.5 Compressor data sheet **50**
Figure 5.6 Heat exchanger submodel icon **50**
Figure 5.7 The features of designer app **51**
Figure 5.8 Arrangement types offered for heat exchanger tubes **52**
Figure 5.9 Geometry parameters defined for heat exchanger **52**
Figure 5.10 Creating a repeatable pattern for the heat exchanger.....**52**
Figure 5.11 External variables for the heat exchanger submodel **53**
Figure 5.12 Heat exchangers of the dehumidifier **53**
Figure 5.13 Condenser geometry illustrated by the designer app **54**
Figure 5.14 Condenser parameters entered in the designer app.....**54**
Figure 5.15 Evaporator geometry illustrated by the designer app **55**
Figure 5.16 Evaporator parameters entered in the designer app **55**
Figure 5.17 Capillary tube submodel icon **55**
Figure 5.18 External variables for the capillary submodel **56**
Figure 5.19 Parameters entered for capillary tube **56**
Figure 5.20 Adiabatic pipe icon **57**
Figure 5.21 External variables for adiabatic pipe submodels **57**
Figure 5.22 Parameters for adiabatic pipe connecting compressor to evaporator **57**
Figure 5.23 Parameters for adiabatic pipe connecting compressor to condenser **58**
Figure 5.24 Moist air source submodel icon **58**
Figure 5.25 External variables for moist air source submodel.....**59**
Figure 5.26 Constant input signal icon.....**59**
Figure 5.27 Parameter for air pressure input for moist air source.....**59**
Figure 5.28 Interpolate signal input icon **60**
Figure 5.29 Interpolation types for interpolate signal input submodel **61**
Figure 5.30 Parameters entered for moist air source submodel **62**
Figure 5.31 Screenshot of data files entered for moist air source inputs **63**
Figure 5.32 Refrigerant submodel icon.....**63**
Figure 5.33 Parameters entered for refrigerant submodel.....**65**
Figure 5.34 Moist air sink submodel icon.....**65**
Figure 5.35 External variables for moist air sink submodel **65**
Figure 5.36 Solid submodel icon.....**66**
Figure 5.37 Parameters entered for solid submodel.....**66**

Figure 5.38 One dimensional dehumidifier model.....**67**

Figure 5.39 Run parameters used for the model **68**

Figure 5.40 Performance analyzer results **68**

Figure 6.1 Results from the preliminary setup at ambient temperature: exit temperature shown as blue and inlet temperature shown as red (degrees C on y-axis) **70**

Figure 6.2 Results from the preliminary setup at ambient temperature: exit relative humidity shown in blue and inlet relative humidity shown in red (% value on the y-axis).....**70**

Figure 6.3 Results from the preliminary setup at humid conditions: exit temperature shown as blue and inlet temperature shown as red (degrees C on y-axis) – Experiment 1 .....**71**

Figure 6.4 Results from the preliminary setup at humid conditions: exit temperature shown as blue and inlet temperature shown as red (degrees C on y-axis) – Experiment 2 .....**71**

Figure 6.5 Results from the preliminary setup at humid conditions: exit temperature shown as blue and inlet temperature shown as red (degrees C on y-axis) – Experiment 3 .....**72**

Figure 6.6 Results from the preliminary setup at humid conditions: exit relative humidity shown in blue and inlet relative humidity shown in red (% value on the y-axis) – Experiment 1 .....**72**

Figure 6.7 Results from the preliminary setup at humid conditions: exit relative humidity shown in blue and inlet relative humidity shown in red (% value on the y-axis) – Experiment 2 .....**73**

Figure 6.8 Results from the preliminary setup at humid conditions: exit relative humidity shown in blue and inlet relative humidity shown in red (% value on the y-axis) – Experiment 3 .....**73**

Figure 6.9 Experiment starting evaporator inlet and ending condenser outlet air properties **74**

Figure 6.10 Model starting evaporator inlet and ending condenser outlet air properties **74**

Figure 6.11 Psychrometric air properties at starting evaporator inlet and ending condenser outlet points **75**

Figure 6.12 Psychrometric dehumidification process of the dryer oven experiment **75**

Figure 6.13 Psychrometric dehumidification process of the simulation model **76**

Figure 6.14 Model exit temperature results for dryer oven setup shown in blue, inlet temperature shown in red (degrees C on the y-axis) **77**

Figure 6.15 Model exit relative humidity results for dryer oven setup shown in blue, inlet relative humidity shown in red (% values on the y-axis) **77**

Figure 6.16 Comparison graph for dryer oven and model output temperature data **78**

Figure 6.17 Comparison graph for dryer oven and model output relative humidity data **79**

Figure 6.18 Correlation between experiment and model data temperature at evaporator inlet **81**

Figure 6.19 Correlation between experiment and model data temperature at condenser exit **82**

Figure 6.20 Correlation between experiment and model data relative humidity at evaporator inlet **82**

Figure 6.21 Correlation between experiment and model data relative humidity at temperature at condenser exit **83**

Figure 6.22 Comparison graph for model output temperature using R290 and R410a **85**

Figure 6.23 Comparison graph for model output relative humidity using R290 and R410a **85**

Figure 6.24 Comparison graph for model output temperature using R290, R32 and R410a **86**

Figure 6.25 Comparison graph for model output relative humidity using R290, R32 and R410a..... **86**

LIST OF TABLES

Table 2.1 Comparison between heat pump drying and refrigerant based dehumidifying **11**

Table 4.1 Measurement of dehumidifier parts **31**

Table 4.2 Technical data for air properties measuring instruments **33**

Table 4.3 Measurement of air properties for first preliminary setup **34**

Table 4.4 First set of measurements for the steam spray setup **35**

Table 4.5 Second set of measurements for the steam spray setup **36**

Table 4.6 Third set of measurements for the steam spray setup **36**

Table 4.7 Format of data logger results for dryer oven **42**

Table 4.8 Velocity measurements **42**

Table 5.1 List of refrigerants available **64**

Table 6.1 List of experiments **69**

Table 6.2 Evaluation metric results on time series comparisons **80**

ABSTRACT

One Dimensional Modelling and Experimental Investigation of Mechanical Dehumidification System

Şerife SATOĞLU

Department of Energy Technologies

Program of Energy Technologies

Master of Science Thesis

Supervisor: Prof. Dr. Hakan DEMIR

Mechanical dehumidification is a process used to remove excess moisture from the air by employing mechanical refrigeration principles. This process plays a crucial role in various industries and environments where precise humidity control is imperative for ensuring comfort, safety, product quality, and equipment reliability. Among these sectors, the food and beverage industry prominently utilizes dehumidification processes to uphold optimal conditions for food processing, storage, and preservation.

This study aimed to construct a comprehensive one-dimensional modeling framework for mechanical dehumidification systems and validate it through experimental investigation. Leveraging Simcenter Amesim, a robust simulation software widely embraced in engineering circles for its prowess in modeling, simulating, and analyzing multidisciplinary systems, we emulated the Trotec TTK 100E model dehumidifier. One-dimensional modeling can simplify psychrometric analysis by considering the changes in air properties such as temperature and humidity ratio as the air passes through the dehumidifier which was a primary analytical approach in this study. The findings of this investigation contribute

substantively to the design parameters for a heat pump dryer oven configuration geared towards the analysis of dehumidification in food products.

Keywords: Mechanical dehumidification, Simcenter Amesim, Heat Pump Dryer.

ÖZET

Mekanik Nem Alma Sisteminin Bir Boyutlu Modellenmesi ve Deneysel Incelenmesi

Şerife SATOĞLU

Enerji Teknolojileri Anabilim Dalı
Enerji Teknolojileri Programı
Yüksek Lisans Tezi

Danışman: Prof. Dr. Hakan DEMİR

Mekanik nem alma, mekanik soğutma prensipleri kullanılarak havadaki fazla nemin uzaklaştırılması için kullanılan bir işlemdir. Bu süreç, konfor, güvenlik, ürün kalitesi ve ekipman güvenilirliğini sağlamak için hassas nem kontrolünün zorunlu olduğu çeşitli endüstrilerde ve ortamlarda çok önemli bir rol oynar. Bu sektörler arasında yiyecek ve içecek endüstrisi, gıda işleme, depolama ve muhafaza için en uygun koşulları sağlamak amacıyla nem alma süreçlerini belirgin bir şekilde kullanmaktadır.

Bu çalışma, mekanik nem alma sistemleri için kapsamlı bir tek boyutlu modelleme çerçevesi oluşturmuş ve deneysel inceleme yoluyla doğrulamaya çalışmıştır. Çok disiplinli sistemleri modelleme, simüle etme ve analiz etme becerisi nedeniyle mühendislik çevrelerinde yaygın olarak kabul gören sağlam bir simülasyon yazılımı olan Simcenter Amesim'den yararlanarak Trotec TTK 100E model nem alma cihazını modellenmiştir. Nem alma cihazından geçerken sıcaklık ve nem oranı gibi hava özelliklerinde meydana gelen değişiklikleri dikkate alarak tek boyutlu modelleme bu çalışmada birincil analitik yaklaşım olan psikrometrik analizi ile basitleştirilmiştir. Bu araştırmanın bulguları, gıda ürünlerinde nem alma analizine

yönelik bir ısı pompalı kurutma fırını konfigürasyonunun tasarım parametrelerine önemli ölçüde katkıda bulunacaktır.

Anahtar Kelimeler: Mekanik nem alma, Simcenter Amesim, Isı pompalı kurutma.

1
INTRODUCTION

1.1 Statement of Purpose

Mechanical dehumidification process aims to remove moisture from the air, and various different methods can be employed for this purpose. Experimental investigations of mechanical dehumidification methods themselves involve testing various procedures and devices.

Among the most common methods of mechanical dehumidification are desiccant, refrigeration-based, adsorption, membrane or hygroscopic liquid-based dehumidification. While desiccant dehumidifiers use materials like silica gel or lithium chloride, adsorption dehumidifiers use adsorbent materials like zeolites to absorb moisture from the air. The leading experimental investigation method that both of these dehumidification systems are based on is testing the efficiency of different kind of materials. The performance of desiccant dehumidifiers is optimized by varying parameters like airflow rate, humidity levels, and temperature, which is a continuous area of investigation. The research for optimizing adsorption dehumidifiers is mainly focused on examining regeneration methods and optimizing cycle. Membrane dehumidifiers use semi-permeable membranes, and testing various membrane materials, pore sizes, and operating conditions is the way to enhance moisture removal efficiency. Dehumidifiers using hygroscopic liquids like concentrated salt solutions explore different types of solutions, concentrations, and regeneration techniques.

Refrigerant Based Dehumidifiers (RBD) cool air to condense moisture, then return it to its original temperature. Experimental investigations for refrigerant based

dehumidifiers include adjusting refrigerant types, compressor designs, or heat exchanger configurations.

Hybrid systems that combine multiple dehumidification techniques are also prominent areas of research to improve efficiency. Measuring and analyzing moisture removal rate, energy consumption, dew point, relative humidity, and temperature profiles is the primary approach to evaluate the effectiveness of any type of dehumidification process. Varying performance metrics with the goal to enhance efficacy, diminish energy usage, and optimize performance across diverse applications like HVAC systems, industrial processes, and environmental control illustrate a variety of experimental methodologies employed to explore mechanical dehumidification techniques.

This research is based on a RBD system, where we experimentally analyze its dehumidification process and model it one dimensionally with a simulation software.

1.2 Mechanical Dehumidification in the Industry

Controlling humidity levels is essential in many industries and environments, hence the mechanical dehumidification process is applied extensively.

Excessive humidity can result in discomfort, mold growth and other issues, therefore removing surplus moisture from the air is essential to establish a pleasant indoor environment. Consequently, mechanical dehumidification is often integrated into air conditioning systems in residential, commercial, and industrial buildings as part of comfort cooling principles. In spaces prone to moisture buildup such as basements, crawl spaces or warehouses, mechanical dehumidifiers are especially employed to prevent mold and mildew growth and protect stored items, building materials and equipment. Heating, ventilation, and air conditioning (HVAC) systems commonly incorporate mechanical dehumidifiers to improve energy efficiency as well since the dehumidification process reduces the workload on air conditioners.

Many industries require a controlled environment for production, testing and storage of sensitive materials. Leading such industries is the pharmaceutical industry. Manufacturing facilities and laboratories employ mechanical

dehumidification principles to maintain precise control over humidity levels for product quality, safety and compliance with regulatory standards for sensitive medications and research materials.

High humidity levels can also be detrimental for sensitive electronics. Mechanical dehumidification is used in environments such as data centers protecting equipment and ensuring uninterrupted operation. Document and artifact preservation also requires controlling humidity levels to avoid degradation, mold growth or insect infestations; therefore museums, libraries, archives, and historical buildings often employ mechanical dehumidification systems to protect valuable documents, artifacts, and artworks from deterioration.

High humidity levels are inherent to facilities where evaporation is prevalent, such as indoor pools, spa areas, or other recreational water facilities. To prevent structural damage, corrosion, and discomfort for occupants, dehumidifiers are frequently employed in such facilities.

Moisture is also an essential part of life in many settings. For plant growth and health, the right balance of moisture is crucial, so greenhouses and indoor farming facilities need to establish and maintain a controlled agricultural setting. In such places, dehumidifiers regulate humidity levels for optimal growing conditions. For storage facilities, preserving quality and integrity of perishable items is the main objective, and especially for cold storage warehouses where frost buildup and condensation is a great risk, mechanical dehumidification systems help to stabilize humiditiy levels to prevent any moisture-related damage.

Last but not least, mechanical dehumidification plays a vital role in the food and beverage industry, where this research is aiming to serve in the long run. In general, maintaining optimal humidity levels help preserve the quality and shelf life of products in food or beverage processing facilities and storage warehouses since moisture related spoilage, degradation and mold growth are common occurrences.

Overall, mechanical dehumidification is vital in various environments, industries and applications for comfort, safety, quality and reliability aspects. There are certain points to consider while employing dehumidifiers for any setting. Understanding the specific moisture control requirements for a given system is fundamental. For example, different food products have divergent moisture content

conditions and needs. Therefore, the dehumidificaiton systems to be incorporated will differ depending on products being processed or stored. Also, dehumidification equipment selection will depend on factors such as the scale of operation, ambient conditions, energy efficiency requirements, and the level of humidity control needed. Placement, proper installation and integration to the facility without causing disruptions to production processes is another concern. Automated control systems can be added to help continuous monitoring and control of humidity levels by adjusting operations of dehumidifiers based on real-time humidity readings. Dehumidifiers can also work as part of comprehensive environmental control systems, integrated with other processes such as air filtration, ventilation, and temperature control depending on the need of the specific process. Regulatory standards and guidelines for specific industries guide the selection of dehumidification systems such as the role Hazard Analysis and Critical Control Points (HACCP) regulatory system plays in the Food industry to ensure Food safety. Optimizing operational and energy costs can also be decisive for choosing dehumidifiers for various industries and regular maintance is necessary to achieve optimal performance levels. Abiding to these concerns, many indsutries benefit from implementing an effective dehumidification process.

1.3 Essential Benefits of Dehumidification

There are several reasons why dehumidification is essential for human well-being and comfort. Among many heatlh benefits, inhibiting the growth of allergens such as dust mites, mold or mildew is key for preventing respiratory problems. Dehumidification also can make indoor spaces feel less hot or sticky resulting in a more comfortable atmosphere. Prevention of property damage and preservation of goods are other complimentary benefits, playing a role in preserving the integrity and longevity of many buildings and sensitive possessions respectively. Dehumidification also aids in energy efficiency in air conditoning systems as they operate better with lower humidity levels.

Overall, the dehumidification process helps create healthy, comfortable, and structurally sound environments while also protecting valuable assets and benefitting energy efficiency.

1.4 Project Scope

This research based on one dimensional modeling and experimental analysis of mechanical dehumidification work started as part of a larger project that is undergoing at Yıldız Heat Lab, led by Prof. Dr. Özgür Atayılmaz and conducted by Res. Asst. Emre Arpaci as basis of his doctoral studies focusing on a food drying project, namely "Experimental and Numerical Investigation of Heat Pump Microwave Assisted Food Drying System." One part of his project examines heat pump drying of food and for experimental analysis he has built a closed loop drying oven using our Trotec 100 K dehumidifier as the heat pump of the system. The thesis presented here aims to model said dehumidifier using Simcenter Amesim program; the output of the project will be used as basis of modeling of the heat pump dryer oven in our laboratory. The scope of this research is the experimental analysis of a refrigeration-based dehumidifier system for food processing and one-dimensional modeling of its dehumidification process with simulation software.

2
THEORETICAL CONCEPTS

Dehumidification is an essential process in climate control, particularly in indoor environments where humidity levels must be maintained to prevent structural damage, ensure optimal indoor air quality, structural integrity, and occupant comfort. Psychrometric analysis forms the foundation for understanding and designing efficient dehumidification systems. This analysis provides the framework by illustrating the relationship between air temperature, moisture content and energy. By employing psychrometric principles, this project has integrated theoretical concepts with practical applications, advancing the design and validation of dehumidification systems. This chapter explores the theoretical underpinnings of the process, focusing on psychrometric principles, methodologies, and practical applications.

2.1 Dehumidification Process

Dehumidification primarily involves the removal of moisture from air using various methods such as refrigerant based dehumidification, desiccant based dehumidification, hybrid systems and heat pump drying. In this chapter we focus on refrigerant-based dehumidification and heat pumps.

2.1.1 Refrigerant Mechanical Dehumidification

The mechanical dehumidification process subject to this research is refrigerant based mechanical dehumidification. Refrigerant dehumidifiers use a refrigerant that flows between warm and cold coils and change phase during the process. Figure 2.1 shows the components of this system and illustrates where the moist air enters, and dry air exits the device.

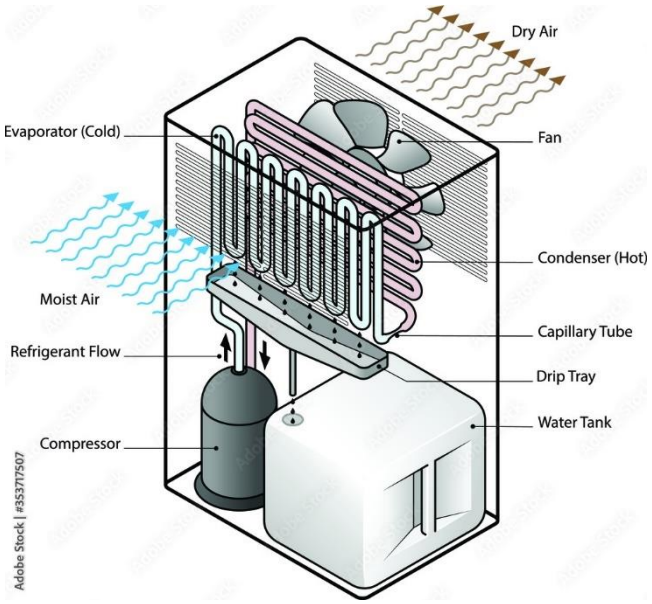


Figure 2.1 Illustration of a refrigerant based dehumidifier

The process begins with air intake. The machine draws in air from the space where dehumidification is required, and this air is typically warm and humid. There is often a filtering system to remove dust, pollen or other particulate matter to keep the dehumidifier's components clean and ensure efficient operation.

Then there is a coil that contains a refrigerant, and air goes over this cooling coil also called the evaporator (marked as evaporator in Figure 2.1). The compressor keeps the pressure of the refrigerant high within the evaporator to keep the tubing cold. The refrigerant absorbs heat from the air, cooling it down and causing its ability to hold moisture to decrease. This results in the condensation of water vapor into liquid water on the surface of the cooling coil.

A collection tray or pan is present to collect the condensed water dripping down the cooling coil. This collected water can be drained away or reused depending on the design.

If maintaining a certain temperature is a necessity, the cooled air may be reheated in some settings before being let out, avoiding overcooling. The hot condenser reheats the air, and the dehumidified air is then released back into the space through a fan.

This process operates continuously until the desired humidity level is established. The capacity and efficiency of the dehumidifier can be adjusted as to the needs and requirements of the application with the air being cycled through the dehumidifier.

2.1.2 Dehumidification with Heat Pumps

While dedicated dehumidifiers are designed with the specific purpose of removing moisture from the air and can therefore handle high humidity levels, heat pumps also inherently dehumidify air while working to heat and cool spaces.

Mechanical dehumidification using heat pump dryers is an efficient method for removing moisture from various products, ensuring high-quality output with optimized energy consumption. This approach integrates refrigeration cycles and controlled drying environments, making it an effective solution for industrial and agricultural applications.

The heat pump dryer works by recovering the latent and sensible heat from the exhaust air, increasing energy efficiency while providing precise control over drying conditions such as temperature and humidity. The fundamental design typically involves a compressor, evaporator, and condenser. Various types include solar-assisted, air source and ground source heat pump dryers.

Solar-assisted heat pump dryers integrate solar energy to preheat the air or assist the heat pump, significantly reducing operational costs. Air source heat pump dryers utilize ambient air for dehumidification and are suitable for various agricultural and industrial products. Ground source heat pump dryers draw heat from the ground, offering higher efficiency in specific climatic conditions.

Key performance indicators for heat pump dryers include Specific Moisture Extraction Rate (SMER), Moisture Extraction Rate (MER) and Specific Energy Consumption (SEC). SMER measures the efficiency of water removal per unit of energy consumed. MER indicates the mass of moisture removed per hour. SEC quantifies the energy required to remove a unit of moisture.

There are several advantages to heat pump dryers. Heat pump dryers achieve higher energy efficiency compared to conventional methods, reducing operational costs. In terms of product quality, precise control over drying conditions maintains the integrity of heat-sensitive materials delivering better results. Modern systems reduce dependence on harmful refrigerants and emphasize sustainability benefiting environmental impacts of these systems.

Thera are also several limitations to heat pump dryer systems. Most notably, initial investment costs can be higher than conventional dryers. The requirement for

regular maintenance to ensure optimal performance is also a limiting economic factor.

Mechanical dehumidification with heat pump dryers represents a significant advancement in drying technology, balancing energy efficiency with superior product quality. Continued innovations in hybrid systems, such as solar and ground-source integrations, promise further enhancements in performance and sustainability.

Heat pump drying and refrigerant-based dehumidifying are both processes used to remove moisture from the air, but they have distinct mechanisms, applications, and purposes.

In terms of principle of operation, heat pump drying, as the name suggests, utilizes a heat pump to circulate air in a controlled drying environment. The heat pump extracts heat from one side (evaporator) and releases it on the other side (condenser). This allows for both cooling and heating within the same system. Warm air absorbs moisture from the material being dried. This moisture-laden air is then cooled in the evaporator, causing water to condense and separate. The dried, reheated air is recirculated. The process is energy-efficient since the heat is recycled within the system. Refrigerant-based dehumidifying on the other hand, operates on a refrigeration cycle to cool the air below its dew point. Air is drawn through a cold coil (evaporator), where moisture condenses out of the air. The dehumidified air is reheated using the heat extracted during the cooling phase or through an additional heating element. This system focuses primarily on reducing humidity in spaces like basements, homes, or industrial environments, not necessarily for drying materials.

2.1.3 Comparison between Heat Pump and Refrigerant Based Dehumidifier

In terms of purpose and applications, heat pump drying is primarily used for drying solid materials, such as agricultural products (grains, fruits, vegetables), textiles, wood, and ceramics. It is ideal for applications where precise temperature and humidity control is required to avoid product damage or quality loss. Refrigerant-based dehumidifying, on the other hand, is used for general air dehumidification in buildings, warehouses, or industrial facilities. It is not optimized for drying specific materials but instead for creating a comfortable or controlled environment.

In terms of energy efficiency, heat pump drying is better because the system recycles the heat generated during operation. It is suitable for high efficiency drying processes with minimal energy wastage. Refrigerant based dehumidifying, on the other hand, is less energy-efficient compared to heat pump drying when used for drying purposes, as it does not recycle heat to the same extent. Energy efficiency is adequate for typical air dehumidification tasks but not for industrial scale drying.

In terms of temperature and humidity control, heat pump drying offers better control over both temperature and humidity. It allows for lower temperature drying, which is important for heat-sensitive materials. Refrigerant-based dehumidifying on the other hand Primarily focuses on reducing humidity and has limited temperature control capabilities. Air temperature may increase slightly after dehumidification due to reheating but is not finely controlled.

In terms of equipment design, heat pump drying includes components for both heating and cooling cycles. It typically has a closed-loop design to maintain a stable drying environment. Refrigerant-based dehumidifying consists of a cooling coil, a condensation system, and sometimes a heater for reheating. It is usually open-loop systems that condition the air in a room or space.

The choice between the two depends on the application. For drying specific materials efficiently and preserving quality, heat pump drying is preferred. For reducing ambient humidity, refrigerant-based dehumidifiers are more suitable. You can refer to Table 2.1 for a summary of comparison between these two systems. For our project, we are using a RBD as a heat pump in our dryer oven.

Table 2.1 Comparison between heat pump drying and refrigerant based dehumidifying

Feature	**Heat Pump Drying**	**Refrigerant Dehumidifying**
Primary Goal	Material drying	Air dehumidification
Energy Efficiency	High	Moderate
Temperature Control	Precise	Limited
Applications	Industrial drying (agriculture, wood)	Indoor humidity control
Heat Recycling	Yes	Minimal

2.2 Psychrometric Chart Analysis of Dehumidification Process

The psychrometric chart is a graphical representation of the thermodynamic properties of moist air. The psychrometric chart is foundational to understanding the dehumidification process, illustrating the relationships between air temperature, humidity, and energy. An example of this chart for air is given in Figure 2.2. Key parameters include Dry-Bulb Temperature (DBT), which is measured with a standard thermometer, and Wet-Bulb Temperature (WBT), which reflects evaporative cooling. Other essential variables are Relative Humidity (RH), defined as the ratio of actual water vapor pressure to the saturation pressure, and the Humidity Ratio (HR), which measures the mass of water vapor per unit mass of dry air. Enthalpy and specific volume further describe the energy content and space occupied by the air-water vapor mixture.

At the top of the psychrometric chart lies the saturation curve, which indicates the maximum water vapor air can hold at a specific temperature. This curve is pivotal in identifying condensation points during cooling processes, marking the onset of dehumidification.

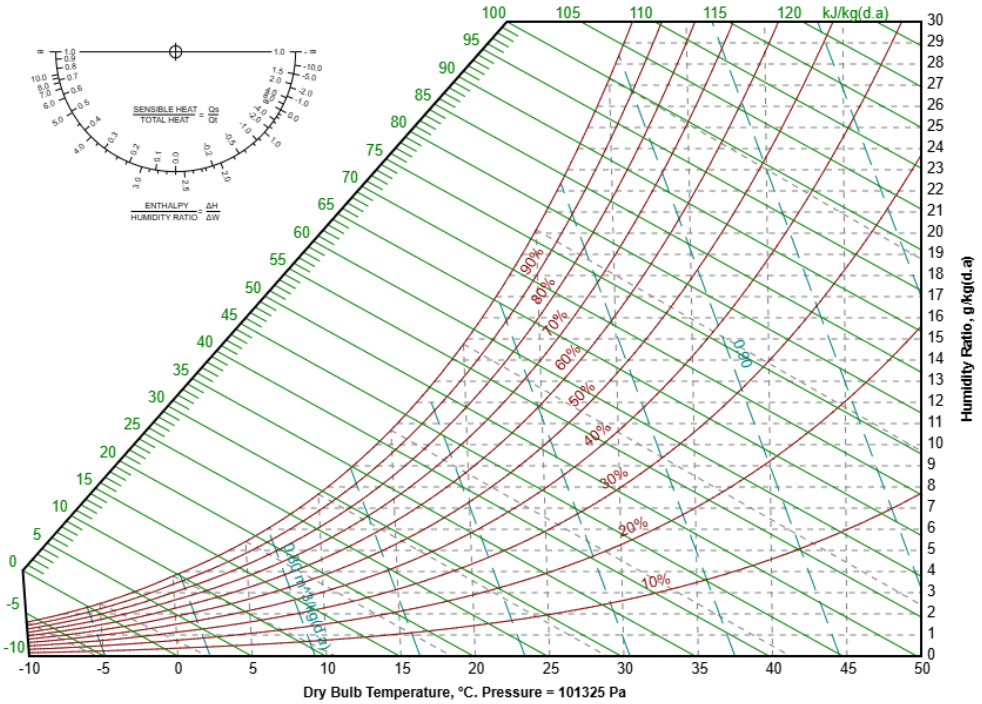


Figure 2.2 The psychrometric chart for air [1]

Refrigerant based dehumidification involves cooling air below its dew point, causing water vapor to condense. This process, represented on a psychrometric chart, includes sensible cooling (reducing DBT without affecting HR) and latent cooling (condensation of moisture). Optional reheating enhances comfort by increasing the DBT of the drier air. Complementing this, desiccant-based systems utilize hygroscopic materials such as silica gel to remove moisture, especially in low-temperature or low-humidity conditions. Air passes through a desiccant wheel or bed in moisture adsorption step and heated air removes moisture from the desiccant, making it reusable in regeneration step. Hybrid systems, combining refrigerant and desiccant technologies, provide enhanced efficiency, particularly in environments with fluctuating conditions.

On a psychrometric chart, Refrigerant based dehumidification process is represented as a downward movement along a constant HR line, followed by a leftward shift along a constant RH curve (Figure 2.3).

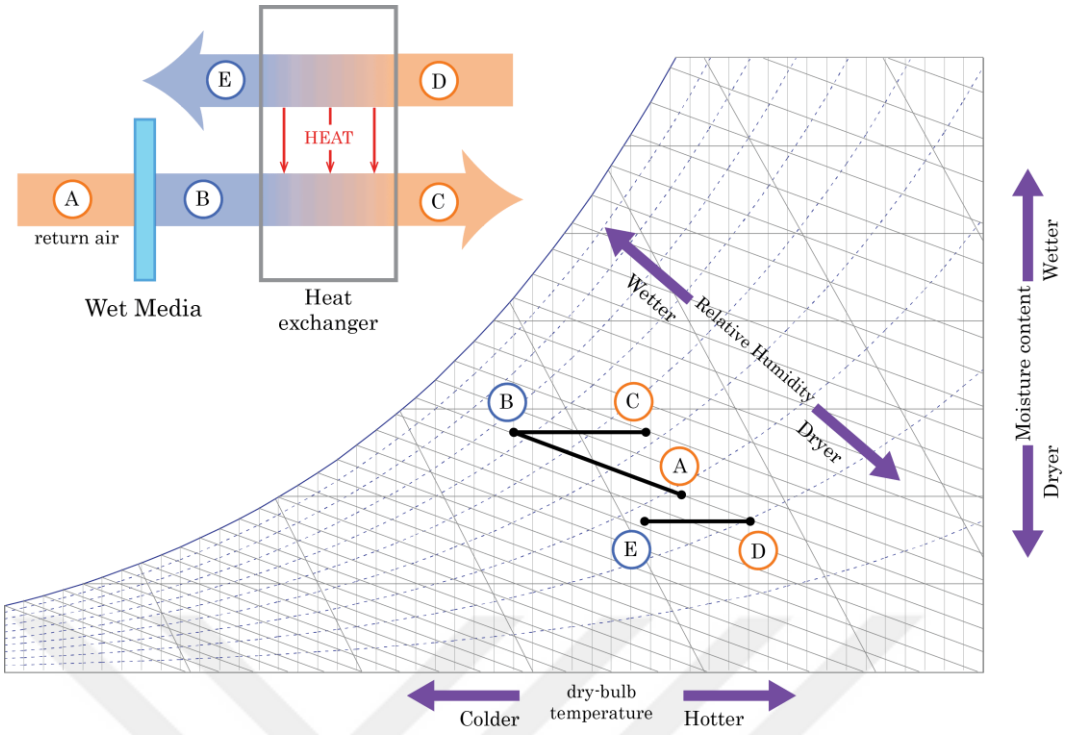


Figure 2.3 Dehumidification on Pyschrometric Chart [2]

Psychrometric analysis is indispensable in designing effective and efficient dehumidification systems. By understanding air properties and their interactions, engineers can optimize moisture removal, system performance, minimize energy consumption, and achieve desired comfort levels. The integration of psychrometric insights with modern technologies, such as hybrid and desiccant systems, promises further advancements in energy efficiency and system reliability.

3
LITERATURE REVIEW

While the scope of this research is the experimental analysis of a refrigeration-based dehumidifier system for food processing and one-dimensional modeling of its dehumidification process with a simulation software, the work is part of a larger project that is undergoing at Yıldız Heat Lab, focusing on food drying via heat pump dehumidification. Therefore, this review encompasses a broad scope covering mechanical dehumidification systems and heat pump drying with an emphasis on food drying. It also covers mathematical modelling of dehumidification, and Simcenter Amesim software in general.

In 1974 King has put the standard on what must be achieved for successful food drying in terms of product quality and drying economy [3]. Product quality is satisfactory provided there are minimum chemical and biochemical disintegration reactions, product structure is preserved, only selective removal of water is achieved without affecting volatile materials such as aroma, final product has the desired color, simple and rapid rehydration is possible, and there is no microbial contamination after the drying process. For drying economy, there need to be minimum product loss, rapid removal of water (higher capacity per unit amount of drying equipment), a cheap energy source, and uncomplicated drying equipment with high reliability requiring minimum labor [3]. These standards are what we keep in mind while considering food drying using heat pumps and other dehumidification systems.

3.1 Classification of Heat Pump Systems

There has been research on heat pump drying systems in terms of the above-mentioned standards for food drying. “Heat pumps appear to have attracted interest

as a means of energy recovery since the idea was first proposed by Lord Calvin in 1852," hence they have been utilized in many processes. Heat pump systems are mostly used in heating and cooling applications and dehumidifying, or in other words drying applications, which are an extension of this project. The progress of research in heat pump systems have been steadily increasing over the years. The range of research has been broad, and it can be categorized in a few different ways. There has been research about heat pump dryers with regards to product quality for special food and agriculture industries, with regards to performance analysis and with regards to operating systems etc. to name a few. Schematic presentation of heat pump development presented by Goh et al. can be seen in Figure 3.1.

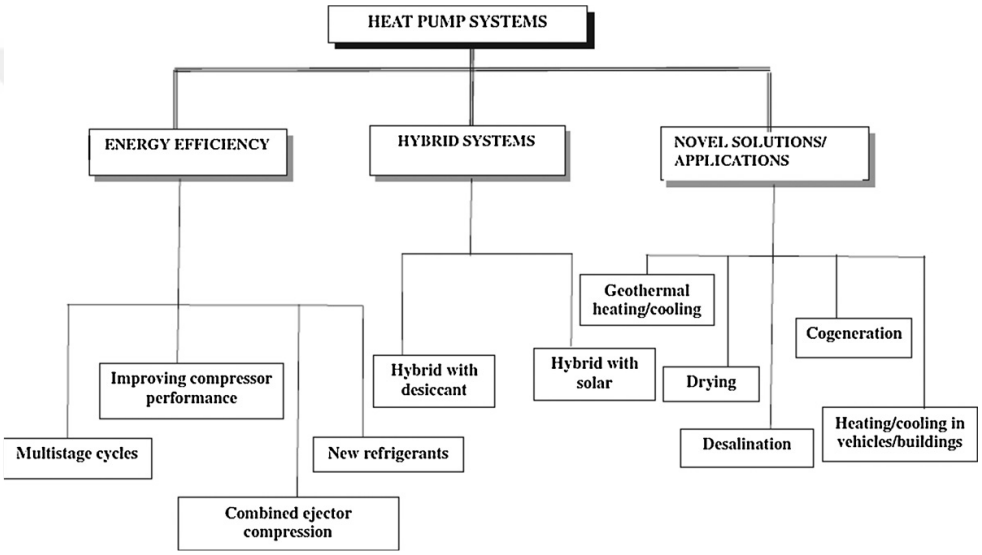


Figure 3.1 Classification of heat pump development [4]

In 2002 Chua et al. wrote a review about heat pump drying, outlining operating principles and limitations, and advantages, giving examples from food and timber industries and concluding with a new example design. They stated that new developments in HPD might focus on control process and on individual component advancements, such as compressors [5]. They also presented a generalized classification scheme, where they grouped HPD systems according to their processing mode, number of dry stages, auxiliary input, etc [5].

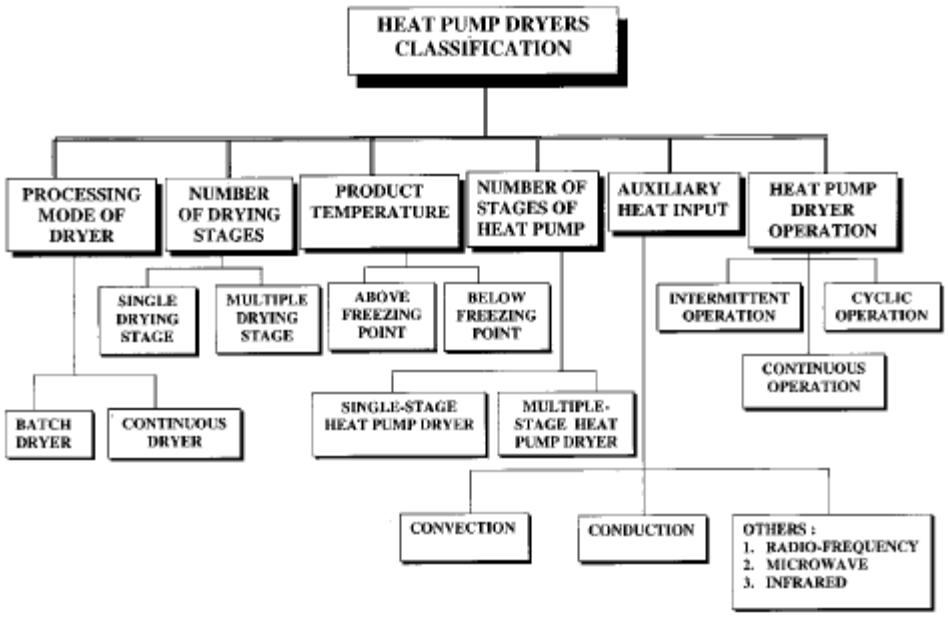


Figure 3.2 Table heat pump dryer classification [5]

In a comprehensive review of heat pump systems for drying applications in 2011, Goh et al. presented another classification of heat pump dryers in terms of source material. They gave details on the evolution of heat pump systems, including air source, solar-assisted, ground source, and chemical heat pumps [4].

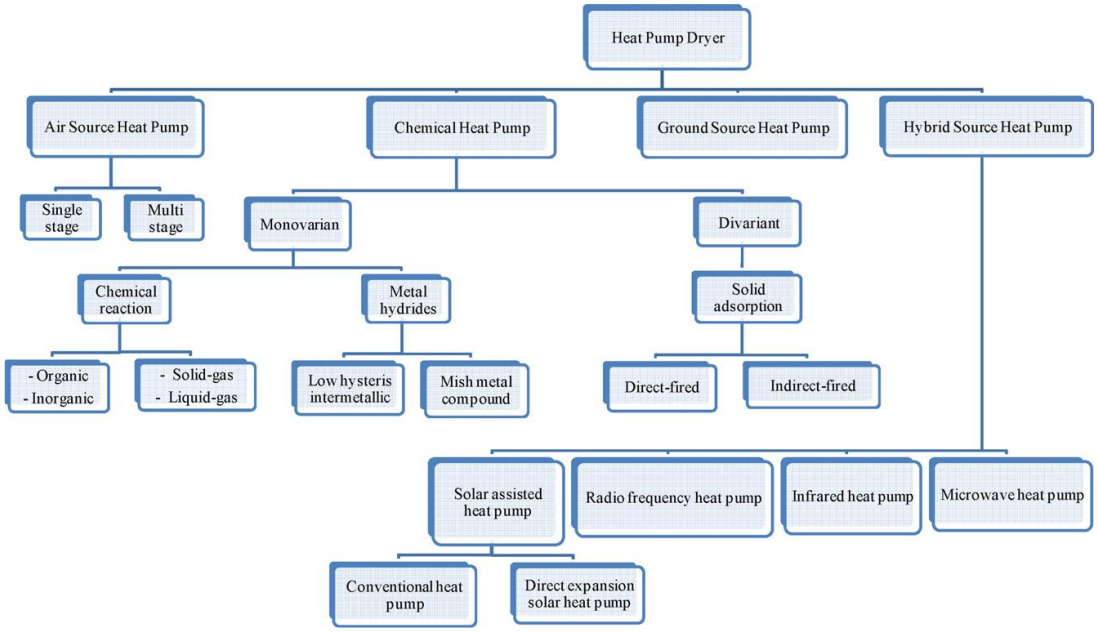


Figure 3.3 Classification of heat pump dryers [4]

In their review, Goh et al., have evaluated that the evolution of heat pump drying starting with air source heat pump going towards hybrid systems, such as solar assisted or microwave assisted systems. They discuss the integration of heat pumps with other systems to enhance performance and reduce costs. They conclude that hybrid systems might have better performance but will be more costly [4].

Heat pump dehumidification types can be classified into several categories based on their configurations and applications. One notable type is the multifunction compression heat pump, designed specifically for greenhouses to dehumidify and heat simultaneously [6]. Additionally, systems like solar liquid desiccant radiation air-conditioning (SLDRS) and solar desiccant wheel systems (SDWRS) combine solar energy with heat pumps for enhanced dehumidification capabilities, with SLDRS demonstrating superior efficiency [7]. Furthermore, integrating heat pumps into humidification-dehumidification desalination systems has shown significant improvements in performance and efficiency [8]. Overall, variations exist between direct and indirect dehumidifiers, with direct systems often providing better performance in specific contexts [8].

Heat pump dryers can be categorized into several types based on their design and application. Common types include tray dryers, fluidized bed dryers, and combined dryers that integrate both tray and bed systems to optimize drying efficiency [9]. Additionally, solar-assisted heat pump dryers (SAHPD) combine solar thermal energy with heat pump technologies, leading to enhanced drying performance and reduced operational costs [10]. Within domestic applications, heat pump dryers are compared against electric and gas dryers, showcasing superior energy efficiency and moisture extraction rates [11]. Each type of heat pump dryer exhibits distinct performance characteristics, influenced by factors such as drying conditions and product type [12][13]. Overall, the selection of a heat pump dryer is crucial for specific drying needs and energy conservation goals.

3.2 Classification of Dehumidification systems

Dehumidification systems can be classified into several categories based on their applications and technologies. Key classifications include Humidification-Dehumidification (HDH) systems, which are often integrated into hybrid desalination processes to enhance water efficiency [14]. Additionally, desiccant

dehumidification systems, particularly using liquid desiccants, are employed in HVAC applications to improve energy utilization and reduce the latent heat load [15]. Heat pump systems also serve an essential role in dehumidification, particularly in drying applications where their efficiency is enhanced at lower relative humidity levels [16]. Lastly, air conditioning systems utilize various dehumidification strategies, including thermal processes that leverage low-temperature thermal energy [17]. Each classification addresses different operational efficiencies and humidity control needs.

Refrigerant dehumidification is an effective method for food drying, particularly in low-temperature applications where preserving the quality of the food is crucial [18]. The integration of heat pump technology using refrigerants like R12 can facilitate controlled drying processes, eliminating excess moisture while maintaining the desired product quality [18]. Additionally, methods that combine thermal and electrical elements, such as hybrid drying systems, demonstrate enhanced drying efficiency by utilizing various energy sources [19]. The use of efficient refrigerants not only improves the drying process but also aligns with environmental sustainability goals in food preservation technologies [20]. Overall, refrigerant-based dehumidification plays a significant role in advancing food drying techniques, making them more efficient and sustainable.

3.3 Dehumidification Applications in the Industry

Heat pump dehumidification utilizes advanced technology to efficiently remove moisture from the air, enhancing energy efficiency and comfort in various applications, including vehicles and industrial settings. For instance, a two-stage humidification-dehumidification heat pump system has shown significant performance improvements in desalination processes by enhancing heat and mass transfer [21]. Similarly, studies on heat exchangers in electric vehicles reveal that optimizing refrigerant flow rates can effectively increase dehumidification rates while ensuring cabin comfort [13]. Additionally, heat pump systems applied in drying processes, like corn drying, demonstrate substantial energy savings and lower lifecycle costs compared to traditional methods, offering a specific moisture extraction rate of 3.39 kg/kWh [22]. Overall, heat pump systems represent a promising solution for effective dehumidification across various sectors [23] [13].

There are also location specific studies for heat pump drying applications done all around the world. An example for this can be the review on using heat pump pumps in Cocao drying in Nigeria done by Ikem et al in 2016 [24]. Another review was done for South Africa in 2014, discussing the opportunities for the development of heat pump drying systems locally by [25].

A notable application of dehumidification is in swimming pool environments, where high evaporation rates present unique challenges. Factors influencing evaporation rates include the pool area, water and air temperatures, and air velocity above the pool surface [26]. Using equations such as Shah's evaporation formula, engineers can estimate these rates, guiding the design of efficient dehumidification systems. A case study involving swimming pool environments highlighted the practical application of these calculations, showcasing the complexity of balancing high evaporation rates with efficient dehumidification [27].

3.4 Heat pump drying in food and agricultural industries

In agriculture grains, tomatoes, various leaves, and vegetables are main subjects of heat pump drying research. There is also much research done on fruits, especially locally grown grapes, apples or tropic fruits, such as guava or papaya. Through such research, the effects of different drying systems on various products and drying conditions have been evaluated and are being compared [4].

Regarding food products, Goh et al. emphasize HPDs energy efficiency and ability to maintain product quality and they summarize the key benefits of using HPDs. They state that heat pump dryers recover latent and sensible heat, reducing energy consumption by up to 40% compared to conventional dryers [4]. HPDs also allow precise control of drying parameters (temperature, humidity, and airflow) hence improving the quality of heat-sensitive products [4]. These benefits make heat pump systems an attractive option for various drying applications, particularly in the food and agriculture sectors.

Heat pump dehumidification leverages thermodynamic properties to enhance energy efficiency and drying speed. Its application in systems like the Automated Multi Commodity Heat Pump Dryer (AMCHPD) has demonstrated high dehumidification efficiency (DHE), achieving average relative humidity reductions

suitable for extracting moisture from various fruits and vegetables [28]. Moreover, integrating heat recovery and renewable energy sources further optimizes these processes, contributing to sustainable food production [29]. The technology not only ensures effective moisture removal but also minimizes food loss and preserves product quality by maintaining controlled drying environments [30]. Overall, heat pump dehumidification presents a robust solution for enhancing the efficiency and sustainability of food drying operations.

Heat pump dehumidification techniques for food drying showcase various innovative systems designed to enhance energy efficiency and drying performance. For instance, İşkan et al [31] demonstrated that integrating infrared lamps and carbon fiber heaters with a heat pump drying system led to faster moisture removal and lower energy consumption. Zhuman et al. [32] focused on a unit that allows for both drying and refrigeration, achieving significant energy savings through optimal system design. Li et al. [22] proposed a multi-stage dehumidification heat pump corn drying system, significantly outperforming traditional methods in energy consumption and cost-effectiveness. Moreover, the study by M et al. [9] highlighted the effectiveness of different drying chamber designs, emphasizing the importance of tailored configurations for improved moisture removal rates. Overall, these advancements illustrate the potential of heat pump technology in efficient food drying applications.

Recent developments have focused on improving energy efficiency and product quality. Innovations include the integration of solar, infrared, and ultrasound technologies to enhance drying performance while minimizing energy consumption [33][34]. Research highlights the ability of heat pump dryers to independently control temperature and humidity, which is crucial for preserving the nutritional quality of heat-sensitive products [35] . Additionally, advancements in the design of heat pump systems aim to reduce drying times and operational costs, with new hybrid technologies emerging as promising approaches for enhancing the drying process [36]. These developments collectively contribute to the growing application of heat pump dryers in the food industry.

3.5 Limitations of heat pumps

Heat pump systems work with higher efficiency compared to other systems and result with less energy consumption and better-quality products. However, there are certain known limitations of heat pump dryers as well. These limitations were summarized by Gürlek et al. In their review, they discuss challenges such as higher initial investment and regular maintenance requirements on the compressors, refrigerant filters, heat exchangers, etc. to keep the dryer in optimum operating conditions as main constraints. Environmental impacts of use of ozone-damaging CFCs (Chlorofluorocarbons) in many heat pump systems and of possible refrigerant leakages have been a concern for the use of HPD as well [3]

3.6 Progress and Recent developments in dehumidification technology

In a more recent review done in 2020, the progress of new dehumidification technology has been seen towards liquid to dehumidification and air dehumidification due to its fluidity. For preservation and protection of cultural relics this paper emphasizes on three new types of dehumidification technologies, namely "condensation heat recovery type refrigeration temperature regulation dehumidification technology, electroosmosis regeneration solid dehumidification technology, and ionic liquid dehumidification technology." These technical solutions are said to offer higher efficiency dehumidification for humidity control of cultural and electronic products [37].

The historic progress of heat pump dehumidification systems has evolved significantly, demonstrating enhanced efficiency and performance in various applications. Recent studies propose innovative configurations, such as indirect heat pump-assisted mechanical vapor compression systems, which show improved gain-output ratios and specific power consumption metrics [38]. Furthermore, combining air source heat pumps with dehumidification units effectively utilizes waste heat, leading to higher primary energy utilization rates [39]. The introduction of solar liquid desiccant air conditioning systems, driven by photovoltaic thermal and air source heat pumps, allows for independent temperature and humidity control with reduced carbon emissions [40]. Moreover, advancements in heat

exchangers for electric vehicles indicate improved dehumidification rates and thermal comfort under varying conditions [41]. Collectively, these innovations signify a notable trajectory towards more efficient and sustainable dehumidification solutions.

Recent developments in heat pump dehumidification systems highlight their integration and optimization across various industries. The combination of heat pumps with Organic Rankine Cycles (HP-ORC) in building applications showcases enhanced performance and energy efficiency, addressing functional challenges and identifying areas for future research [42]. In the food industry, advancements in heat pump dryers demonstrate their efficacy in drying fruit crops, facilitating controlled conditions that preserve quality and enhancing energy efficiency through various hybrid techniques [34]. Additionally, improvements in ground heat exchanger performance for geothermal heat pump systems indicate a shift towards more sustainable and effective temperature regulation solutions [43]. In essence, ongoing research is driving the innovation of heat pump technologies, expanding their applications in energy demand reduction and quality preservation across multiple sectors.

Recent developments in heat pump dryers (HPD) highlight their growing efficiency and effectiveness in various applications, particularly in food drying. Notably, advancements include the integration of solar thermal energy to create solar-assisted heat pump systems, which significantly reduce operational costs and enhance product quality [10]. Additionally, the versatility of HPD allows for better control over temperature and humidity, ensuring superior food preservation [33]. Recent studies also emphasize the environmental benefits of HPD, as they do not emit harmful gases, marking an important shift towards sustainable drying solutions. Overall, the progression in performance metrics such as energy efficiency, moisture extraction rates, and reduced drying times position HPD as a crucial technology in energy-intensive drying processes [35].

3.7 Psychrometric analysis

Psychrometric analysis is crucial for understanding dehumidification processes in various air conditioning systems. It involves assessing how temperature and humidity interact under different conditions, particularly in systems like desiccant

rotary wheels and swimming pool dehumidification units [26]. For instance, Xue et al. highlighted that the dehumidification performance is significantly affected by air inlet conditions, emphasizing the importance of psychrometric parameters in optimizing system efficiency. Additionally, Borane et al. demonstrated that rotary dehumidification systems can effectively manage indoor humidity while minimizing energy consumption, especially under varying meteorological conditions [44]. The integration of psychrometric analysis with optimization techniques, as discussed by Ghiaus et al., facilitates effective design and control of dehumidification systems, ultimately contributing to improved energy performance in HVAC applications [45] [46].

3.8 Modelling of mechanical dehumidification

Modelling of mechanical dehumidification encompasses various approaches to optimize efficiency and effectiveness in different applications. Kuru and Dumlutaş [47] focused on direct contact dehumidification in washer-dryer machines, utilizing computational fluid dynamics (CFD) for system modeling and assessing temperature and moisture interactions. Maslak and Nimmermark [48] modeled thermal energy use in a tomato greenhouse, demonstrating how a heat exchanger could enhance dehumidification efficiency, revealing significant energy savings. Gendelis et al. [49] developed a mathematical model for a dual-layer shell recuperation system for biogas dehumidification, emphasizing the role of condensation in heat management without additional components. Lastly, Chu et al. [50] presented an integrated mechanical system for residential dehumidification using a solar-assisted heat pump, optimizing energy management through Transient System Simulation Tool (TRNSYS) simulations. Such modeling efforts highlight diverse methods to improve mechanical dehumidification across various contexts.

One-dimensional modeling plays a crucial role in various mechanical dehumidification applications by simplifying complex systems while maintaining essential physical characteristics. For instance, Singh et al. [51] demonstrate the effectiveness of physics-informed neural networks (PINNs) in addressing solid mechanics problems, such as those found in aerospace applications, by utilizing one-dimensional models like cantilever beams. Similarly, Clavica et al. [52] employ one-dimensional equations to analyze airflow in the respiratory system,

highlighting the balance between accuracy and computational efficiency. These techniques can also be adapted to assess mechanical behaviors in dehumidification processes, allowing for effective simulations that consider material properties and environmental conditions. Overall, one-dimensional modeling serves as a valuable tool for analyzing dynamic systems, improving both understanding and performance in mechanical applications.

3.9 Mathematical modeling of dehumidification processes

Mathematical modeling of dehumidification processes is crucial for enhancing efficiency across various applications, including agricultural, desalination, and energy systems. Russo et al. propose a model for air dehumidification using Peltier modules, highlighting the importance of reducing air humidity in food processing [53]. Zarei et al. [54]and Abd-ur-Rehman et al. [55] extend these concepts by exploring humidification-dehumidification (HDH) systems, emphasizing the effects of design parameters on freshwater production. Gendelis et al. focus on gas dehumidification in biogas systems through dual-layer heat exchangers, optimizing condensation rates [49]. Finally, Enayatollahi et al. develop a theoretical model for solar-powered HDH systems, identifying optimal flow rates and external conditions for maximum water production [56]. These studies collectively illustrate the versatility and necessity of mathematical modeling in improving dehumidification technology.

Software modeling of dehumidification processes

Software modeling of dehumidification processes is a critical aspect of designing efficient systems for various applications, such as desalination and HVAC. For example, Laknizil et al. utilize MATLAB for modeling a humidification-dehumidification desalination system, employing mass and heat balance principles to optimize energy consumption [57]. Similarly, Barochia et al. employ Aspen Plus for modeling a zero liquid discharge desalination process, highlighting the importance of simulation for energy efficiency [58]. Furthermore, Marion et al. use TRNSYS to model a cogeneration system for air dehumidification, showcasing its application in building energy management [59]. Jafarinejad et al. also focus on energy recovery measures in direct expansion systems using EnergyPlus and Engineering Equation Solver (EES) software to improve fresh air dehumidification

[60]. These approaches illustrate the diverse applications and importance of software modeling in enhancing dehumidification efficiency across various sectors.

Simcenter Amesim is a powerful simulation tool used across various fields, including medical and automotive applications. For instance, it facilitated the modeling of a two-patient single ventilator system, demonstrating safe pairing based on lung compliance [61]. In the automotive sector, it plays a crucial role in the design and validation of electric vehicles (EVs), allowing for virtual testing and validation against real-world data [62]. Moreover, it supports thermal management studies, such as optimizing battery air cooling systems in EVs to enhance performance and efficiency [63]. The tool's capability to provide detailed simulation results helps accelerate the development of mechatronic devices and improves the design process by reducing reliance on costly physical testing [62].

The software is versatile in simulating thermal management systems and fluid dynamics, as seen in studies examining battery cooling for electric vehicles [63] and validating electric vehicle models [62]. The concepts of thermal regulation and fluid flow management in environments, notably under varying conditions, could be directly applicable to dehumidification systems, where maintaining specific humidity levels is crucial. Utilizing simulation tools like Simcenter Amesim can enhance the design and efficiency of dehumidification mechanisms by allowing detailed analysis of performance parameters under diverse operational scenarios [61]. It is therefore widely used for modeling and simulating applications relevant to dehumidification processes.

Projects involving heat pump systems for drying processes also use Simcenter Amesim as a preferred tool for analysis. In the context of dynamic modeling, as demonstrated in the PUMP-HEAT H2020 project, Simcenter Amesim is employed to develop and validate models of heat pumps and their interactions within combined cycle power plants [64]. The software facilitates the integration of heat pumps with thermal storage systems, crucial for enhancing operational flexibility and efficiency. By simulating the thermodynamic behavior and interactions of subsystems, including heat pumps, engineers can optimize designs and predict performance in drying applications, thereby reducing energy consumption and improving overall system efficacy [65]. This approach highlights the versatility and

efficacy of Simcenter Amesim in optimizing thermal processes in industrial applications.

Simcenter Amesim is also a tool choice for modeling and simulating mechanical systems, including those related to dehumidification. In one study, it was employed to analyze mechanical resonance in reciprocating compressors, showcasing how simulations can improve system dynamics by minimizing torque fluctuations [66]. Additionally, it has been utilized in the design of mechatronic systems, highlighting its versatility in various engineering applications [67]. For specific uses in systems requiring precise control, such as a seabed cone penetration test system, Simcenter Amesim enabled the development of control mechanisms to maintain consistent operation, showcasing its ability to handle complex dynamic simulations [68]. Overall, the software's capabilities can be applied to optimize mechanical dehumidification processes by enhancing efficiency and control.

In this project we use Simcenter Amesim to one-dimensionally model the dehumidification process of a refrigerant based dehumidifier system for food processing, and compare the results to our experimental observation.

4
EXPERIMENTAL INVESTIGATION

Our goal is to one dimensionally model a mechanical dehumidification system successfully. The dehumidification system we chose to model is a retail sold dehumidifier which was later used in a food drying oven as the dehumidification component of the dryer. In this chapter we describe the dehumidifier we attempted to model and the two different experimental setups. The first setup is the one we experimented on to validate our model which we call the preliminary setup, and the second one is the dryer oven setup that we tested our model with.

4.1 Dehumidifier

The humidifier used in this project is a Trotec model TK100 shown in Figure 4.1. It was chosen as it represents a small scale, compact, refrigerant based air dehumidifier. It was lent for this project by Kartal Gıda San. ve Tic. A.Ş. Kartal Gida which is a flour mill that has branched into producing baking mixes. Kartal Gıda used this dehumidifier for a specific mixture process where the ingredients used required lower than normal storage humidity levels. Using this device helped us mimic the settings and equipment of an actual food processing facility. The data sheet of the device can be seen in Figure 4.2.



Figure 4.1 Views of dehumidifier used in experiment



Figure 4.2 Data sheet on the dehumidifier

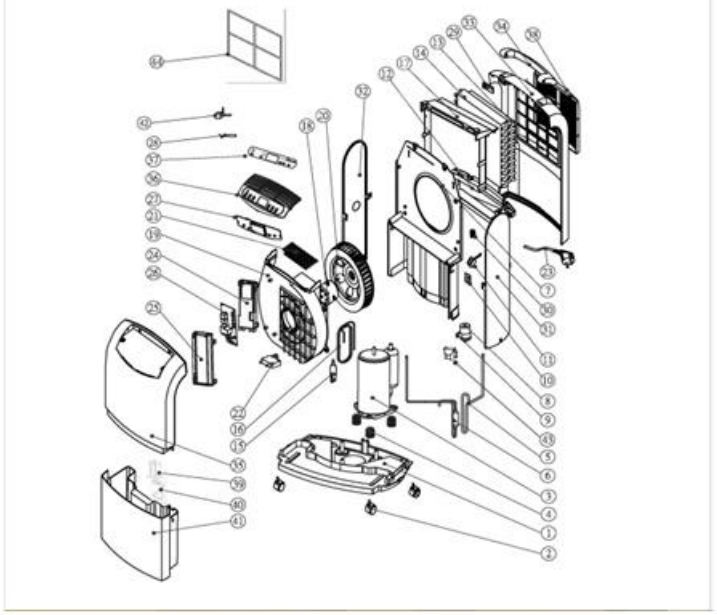
4.1.1 Dissembling

The correctly model this specific dehumidifier we needed to acquire the specific and correct measurements of the system components. This required us to dissemble the machine.

Since this specific equipment has been used in a dusty environment, specifically a powder mixing food facility, we first cleaned it to bring it to its ideal working condition like a brand new machine. This ensured that the equipment operated in full efficiency as it is crucial to get correct results from running experiments.

Once all clean, a test was run to make sure that machine worked fine. After making sure all equipment was in working condition, we started dissembling and taking specific measurements for each part. Graphical representation of dissembled parts

and their names are listed in Figure 4.3 as taken from the registered user manual of the machine [69]. Open panel views are shown in Figure 4.4 where the evaporator can be seen as the blue part and the condenser is an identical looking section behind it that is not visible from the outside. The right picture shows the enclosed fan. The compressor and heat exchangers after disassembly can be seen in Figure 4.5.



No.	Spare Part	QTY	No.	Spare Part	QTY	No.	Spare Part	QTY
1	BASE PAN	1	16	CAPILLARY TUBE	1	31	SIDE PLATE	1
2	TURING WHEEL ASS'Y	4	17	FIX TURE	1	32	SIDE PLATE	1
3	COMPRESSOR ASS'Y	1	18	FAN MOTOR	1	33	PEAR PANEL	1
4	RUBBER	3	19	FAN CASING	1	34	HANDLE	1
5	SUCTION PIPE	1	20	BLOWER WHEEL	1	35	FRONT PANEL	1
6	DISCHARGE PIPE	1	21	SCREEN	1	36	CONTROL PLATE	1
7	PLATE	1	22	CAPACITOR	1	37	CONTROL PANEL	1
8	CAPACITOR	1	23	POWER SUPPLY CORD COMPLETE	1	38	INTAKE GRILLE	1
9	FIX METAL	1	24	FIX TURE	1	39	TANK LID	1
10	SENSOR (FOR HUMIDITY)	1	25	COVER	1	40	FIX TUBE	1
11	REED SWITCH	1	26	CONTROL BOARD	1	41	DRAIN BUCKET	1
12	DRAINAGE PAN	1	27	PC BOARD	1	42	2-WAY REVERSING VALVE ASS'Y	1
13	EVAPORATOR ASS'Y	1	28	SENSOR (FOR EVAPORATOR)	1	43	COVER	1
14	CONDENSER ASS'Y	1	29	FIX TURE	1	44	AIR FILTER	1
15	Y TUBE	1	30	FIX METAL	1			

Figure 4.3 Exploded view and component list of the Trotec TK100 dehumidifier [69]



Figure 4.4 Open panel views of dehumidifier

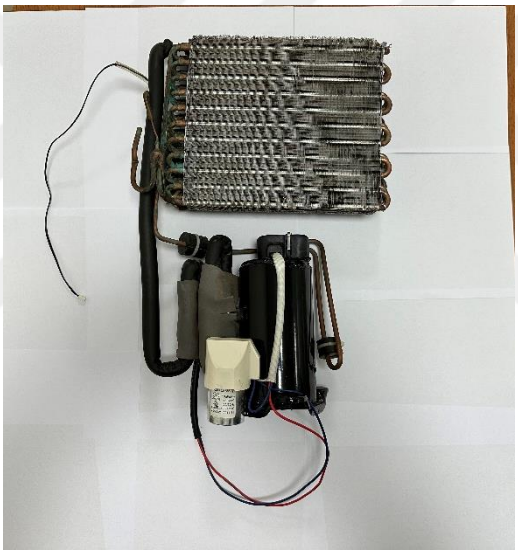


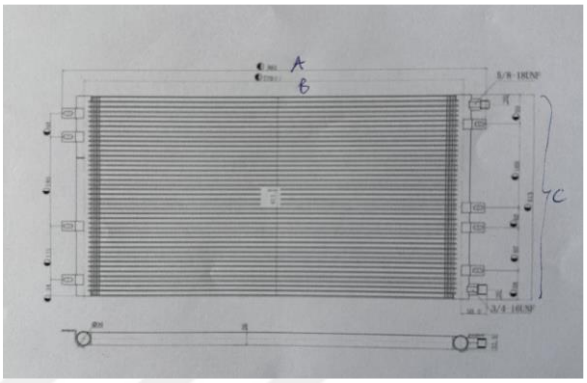
Figure 4.5 Separated heat exchanger and compressor

4.1.1.1 Measuring Parts

For both the condenser and the evaporator part of the dehumidifier, we took measurements of the panel as a whole and additional measurements for coils. The measurements for coil diameters, the distance between fins and tubes, and size measurements for the panel are the main measurements we took as listed in Table 4.1. Also, measurements for the capillary tube and other piping, as well as the data sheet for the compressor are listed in Table 4.1.

Table 4.1 Measurement of dehumidifier parts

		Condenser	Evaporator
	Unit		
Outer Tube Length A	cm	29	29
Inner Tube Length B	cm	25	25
Height C	cm	23	23
Copper Tube Diameter	mm	7.2	7.8
Copper Tube Diameter	mm	7.8	8.5
Thickness	cm	2.56	2.56
Fin pitch	mm	1.25	1.25
Fin thickness	mm	0.2	0.2
Copper Tube Pitch (center to center)	cm	2	2
Capillary Tube			
Diameter	mm	2.2	
Length	cm	38	
Isolated Thick Tube between Condenser and Evaporator			
Diameter	cm	1.92	
Length	cm	127.5	



4.2 Preliminary Setup

4.2.1 Tools and setup details

As part of our experimental investigation, we needed to determine the inlet air properties. To make sure that we got a standard measurement from the inlet, we prepared a cardboard tunnel like structure and attached it to the air entrance of our dehumidifier as seen in Figure 4.6. This was the final dehumidifier set up that we used to take measurements.



Figure 4.6 Dehumidifier with cardboard canal

There was primarily one set of tools that we used to measure the ambient, inlet and outlet air properties, mainly temperature and relative humidity and inlet air velocity. This toolset, Testo 440 Humidity Kit and Hot Wire Probe, was provided by our heat lab at Yildiz Technical University and is shown in Figure 4.7. The technical data for all air properties measuring instruments are given in Table 4.2.

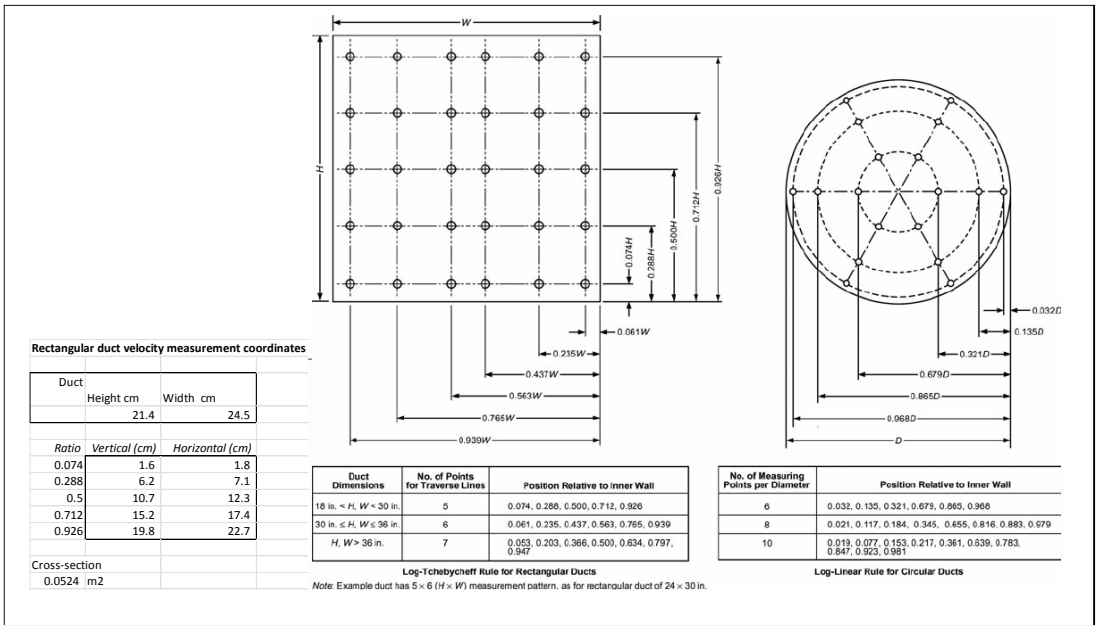


Figure 4.7 Testo flow measurement instruments

Table 4.2 Technical data for air properties measuring instruments

EMS ST-NT-2XX	**Measurng Range**	**Sensitvity**	**Accuracy**
Temperature	0 - 50°C / (-20) - (+80)°C	± 0,1 °C	± 0,3 °C
Humidity	0 to 100 %	± % 1	± % 3 Rh
Sense - SHD.355.D	**Measurng Range**	**Sensitvity**	**Accuracy**
Temperature	(-30) - (+50) / 70 / 100°C		
Humidity	0 to 100%rH		3% Rh
Testo 440 Humidity Kit	**Measuring range**	**Resolution**	**Accuracy**
Humidity	0 to 100 %RH	0.1 %RH	long-term stability: ±1 %RH / year ±0.03 %RH/K (k=1) ±2 %RH (5 to 90 %RH)
Testo 440 Hot Wire	**Measuring range**	**Resolution**	**Accuracy**
Velocity	0 to 30 m/s	0.01 m/s	±(0.5 m/s + 5 % of mv) (0 to 20 m/s) ±(0.03 m/s + 4 % of mv) (20.01 to 30 m/s)

We calculated the coordinates of measuring points at the entrance of the inlet tunnel using the Log-Tchebycheff rule as the industry standard. Our calculated coordinates are shown in Figure 4.8 alongside the Log-Tchebycheff diagram.



Rectangular duct velocity measurement coordinates

Duct		
	Height cm	Width cm
	21.4	24.5
Ratio	*Vertical (cm)*	*Horizontal (cm)*
0.074	1.6	1.8
0.288	6.2	7.1
0.5	10.7	12.3
0.712	15.2	17.4
0.926	19.8	22.7
Cross-section		
0.0524	m2	

Duct Dimensions	No. of Points for Traverse Lines	Position Relative to Inner Wall
18 in. < *H*, *W* < 30 in.	5	0.074, 0.288, 0.500, 0.712, 0.926
30 in. ≤ *H*, *W* ≤ 36 in.	6	0.061, 0.235, 0.437, 0.563, 0.765, 0.939
H, *W* > 36 in.	7	0.053, 0.203, 0.366, 0.500, 0.634, 0.797, 0.947

Log-Tchebycheff Rule for Rectangular Ducts

Note: Example duct has 5 × 6 (*H* × *W*) measurement pattern, as for rectangular duct of 24 × 30 in.

No. of Measuring Points per Diameter	Position Relative to Inner Wall
6	0.032, 0.135, 0.321, 0.679, 0.865, 0.968
8	0.021, 0.117, 0.184, 0.345, 0.655, 0.816, 0.883, 0.979
10	0.019, 0.077, 0.153, 0.217, 0.361, 0.639, 0.783, 0.847, 0.923, 0.981

Log-Linear Rule for Circular Ducts

Figure 4.8 Log-Tchebycheff rule [70]

4.2.2 Experiment

To get a better understanding of the dehumidifier, we tested it to see how it works both in ambient air conditions and humid air conditions.

The first run involved measuring the inlet and outlet parameters for the dehumidifier in ambient air conditions, where the dehumidifier was set in a regular office set up with average ambient temperature and average relative humidity levels. Our dehumidifier had two working modes, one low and one high speed mode, so we operated in both of these modes.

The recorded inlet and outlet air properties can be seen in the Table 4.3.

Table 4.3 Measurement of air properties for first preliminary setup

	Initial	Low Speed		High Speed	
		10 min	20 min	0 min	10 min
Room Temperature (C)	23.5	27.4	29.7	24.7	26.1
Room Relative Humidity (RH)	45.7	37.5	34.2	42.9	40
Inlet Temperature	28.7			27.2	
Inlet Humidity	39.2			38.6	
Outlet Temperature	28.7	32.5	33.1	32.3	
Outlet Humidity	32.6	28.7	27.9	29.7	
Tray (kg)				1097.74	1111.17
Velocity (m/s)	1	2	3	4	5
1	0.71	0.97	1.17	1.2	0.98
2	0.98	1.03	0.97	0.89	1.1
3	0.95	1.02	1.07	0.98	1.15
4	0.98	1	0.98	0.94	1.05
5	0.94	0.92	0.83	0.85	1.15

Our second preliminary dehumidifier setup involved measuring the inlet and outlet parameters in humid air conditions. For this set up, our dehumidifier was stationed in an empty classroom where the air was humidified with a steam sprayer (Figure 4.9). We took three rounds of measurements, the first two in low speed operating conditions and the third one in high speed conditions. The recorded inlet and outlet air properties can be seen in Tables 4.4, 4.5 and 4.6 for each round.



Figure 4.9 Steam spray setup in classroom

Table 4.4 First set of measurements for the steam spray setup

	Initial	Low Speed			
		10 min	20 min		
Room Temperature (C)	20.6	21.1	22.4		
Room Relative Humidity (RH)	72.6	65.9	58.3		
Inlet Temperature	20.6	25.8	22		
Inlet Humidity	75.8	50.4	59.5		
Outlet Temperature	20.3	33.3	33.4		
Outlet Humidity	69.7	35.1	31.7		
Tray (kg)	1098.16		1212.48	114.32	
Low Speed					
Velocity (m/s)	1	2	3	4	5
1	0.58	0.56	0.55	0.52	0.59
2	0.86	0.95	0.92	0.98	1.03
3	0.92	0.96	0.9	0.97	1.11
4	0.93	1	0.97	0.93	1.06
5	0.6	0.77	1.01	0.78	1.07

Table 4.5 Second set of measurements for the steam spray setup

	Initial	Low Speed	
		10 min	20 min
Room Temperature (C)	21.6	22.7	23.4
Room Relative Humidity (RH)	69.8	64	59.7
Inlet Temperature	21.8	22.3	23
Inlet Humidity	72.1	64.8	60.1
Outlet Temperature	22.5	34.5	34.5
Outlet Humidity	77.9	33.4	31.5
Tray (kg)	1404.27	1494.62	1536.58

Table 4.6 Third set of measurements for the steam spray setup

	Initial	High Speed			
		0 min	10 min	20 min	
Room Temperature (C)	21.2		21.6	23.9	
Room Relative Humidity (RH)	72.5		65.4	54.8	
Inlet Temperature	21.2	21.2	21.4	23.3	
Inlet Humidity	70.4	70.9	66.1	55.8	
Outlet Temperature	21.2		33.1	33.1	
Outlet Humidity	69.9		33.7	32.4	
Tray (kg)	1212.48			1404.27	191.79
High Speed					
Velocity (m/s)	1	2	3	4	5
1	0.88	0.98	0.66	0.74	1.2
2	1	1.13	1.1	1.1	1.25
3	1.03	1.07	1.05	1.08	1.39
4	1.1	1.05	1	1.06	1.39
5	0.95	1.02	0.94	1.1	1.26

The results suggested that the dehumidifier was working properly and efficiently. The steam sprayer raised the relative humidity in the classroom up to 70% and the dehumidifier was able to lower this to as low as 30%. With this feat, we started to design our one-dimensional simulation model to replicate these results computationally.

4.3 Dryer Oven Setup

As mentioned in Chapter 1, this one dimensional modelling and experimental analysis of mechanical dehumidification work started as part of a larger project that examines heat pump drying of food. As part of the larger experimental analysis a closed loop drying oven (Figure 4.10) was built using our Trotec 100 K dehumidifier as the heat pump of the system. As this thesis project aims to model the said dehumidifier using Simcenter Amesim program, the output of this project will be the basis of modelling of the heat pump dryer oven in our laboratory. Hence, we used this oven as a second setup in our experimental analysis of our dehumidifier, and tested our Simcenter Amesim model against these measurements.



Figure 4.10 Dryer Oven

4.3.1 Dryer Oven Setup Details and Measurement Tools

The oven configuration placed the dehumidifier below the main cabin. The cabin has 20 cm radius connector apparatus on each side, and the dehumidifier is connected to the cabin using flexible ducts (Figure 4.11). Thermocouples have been placed throughout the established heat pump dryer, including the top and bottom of these canals for temperature monitoring (Figure 4.12).

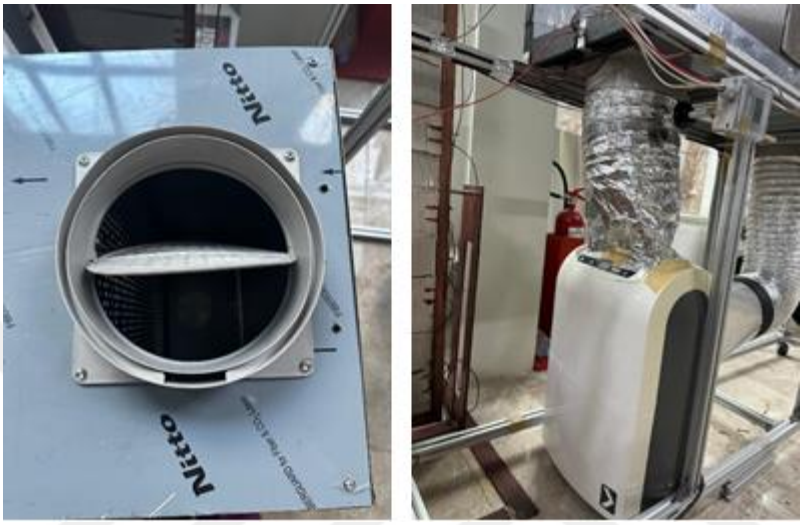


Figure 4.11 Flexible duct connection to the cabin



Figure 4.12 Thermocouples in the oven cabin

A Sense 355 Duct type Temperature and Humidity Sensor (Figure 4.13) has been placed in the left flexible duct canal connecting the exit of the dehumidifier to the main cabin. On the right side, an EMS ST-2XX Temperature and Humidity Duct Type Transmitter was used in the canal connecting the inlet of the dehumidifier to the main cabin (Figure 4.14). Technical data for the sensor are shown in Table 4.2.

All the thermocouples and humidity sensors were connected to Agilent 34972A Data Logger (Figure 4.15) to collect data.

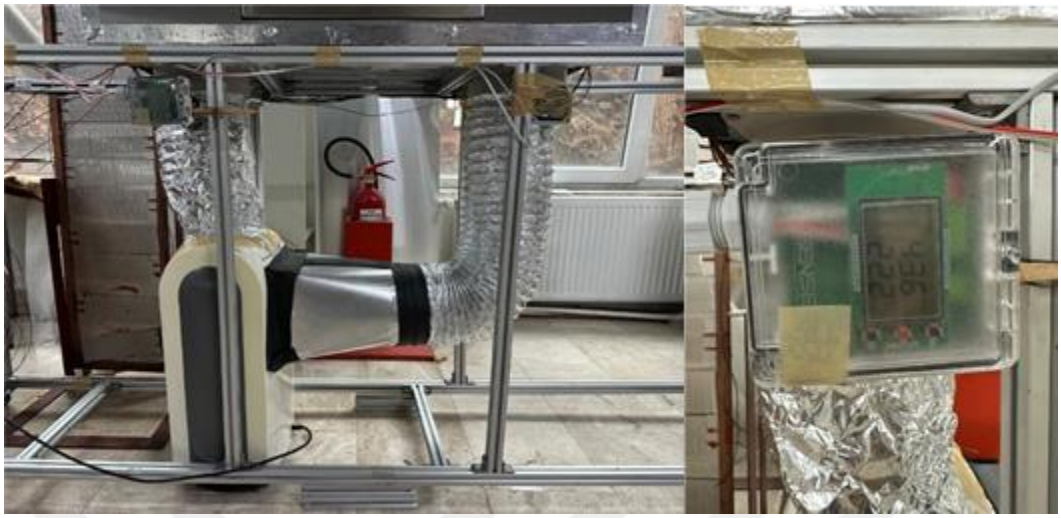


Figure 4.13 Positioning of Sense humidity sensor



Figure 4.14 Positioning of the EMS humidity sensor



Figure 4.15 Agilent data logger

The flexible inlet duct was connected to the dehumidifier by a stainless steel four-edged expanding passage hand made for this set-up by Emre Arpacı, and rubber bands were used to seal all connecting edges (Figure 4.16). A small hole was drilled on this passage where the height of duct was 19.5 cm, for accommodating the manual insertion of the Testo velocity probe (Figure 4.17) at certain time intervals to measure the inlet air speed.



Figure 4.16 Handmade stainless steel duct for inlet

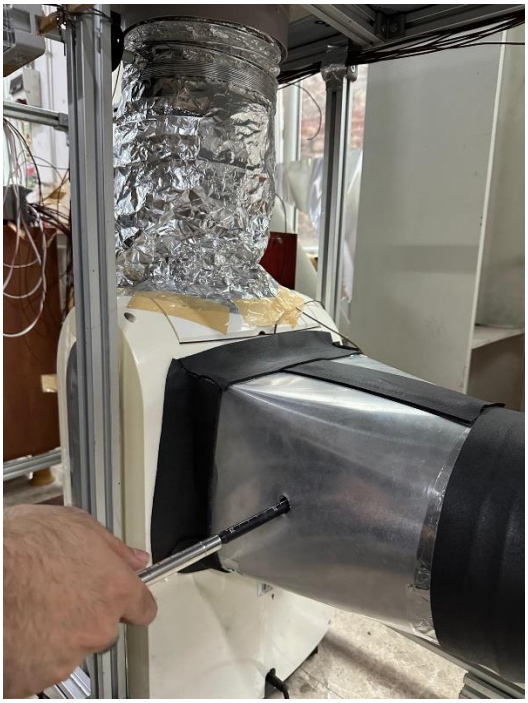


Figure 4.17 Measuring with velocity probe

4.3.2 Experiment

The first runs of the heat pump dryer oven established for Emre Arpacı's project consisted of drying tomato slices, and provided the principal data from the primary setup of this project. This experiment took over 10,5 hours, during which time the dehumidifier constantly operated on high speed mode and the air circulated in the closed-loop oven system. The analyzer monitored the system and took temperature and humidity data every 30 seconds at all points. We took measurements of the inlet air flow rate with the velocity probe every half hour manually (Figure 4. 18). Simultaneously, a designated tomato tray was weighed by Emre (Figure 4.19).

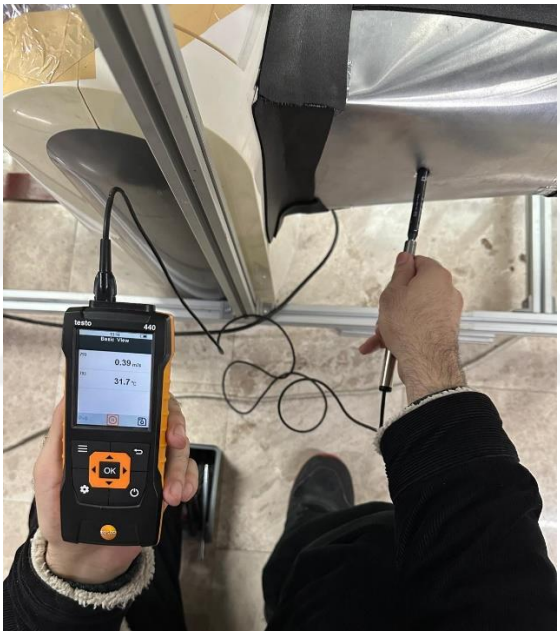


Figure 4.18 Manual measuring



Figure 4.19 Weighing tomato trays

The data output from the analyzer was in a list format as seen in Table 4.7. Manually measured data of the velocity proble was recorded in a similar format as seen on Table 4.8.

Table 4.7 Format of data logger results for dryer oven

Scan	Time	221 <Sence_Temperature> (C)	222 <Sense_Humidity>	321 <EMS_Humidity>	322 <EMS_Temperature> (C)
1	4.12.2024 10:34:40:263	22,066,584	62,313,506	67,349,156	21,687,238
2	4.12.2024 10:35:10:247	22,219,211	56,632,106	65,131,612	21,700,525
3	4.12.2024 10:35:40:247	2,265,165	43,334,781	55,098,825	2,172,045
4	4.12.2024 10:36:10:247	23,349,122	36,571,649	484,847	21,821,431
5	4.12.2024 10:36:40:247	24,022,089	33,908,816	46,738,831	22,073,875
6	4.12.2024 10:37:10:247	24,769,236	32,593,783	46,006,731	22,321,012
7	4.12.2024 10:37:40:247	25,569,525	31,824,527	45,752,956	22,569,469
8	4.12.2024 10:38:10:247	26,197,077	31,198,441	45,612,119	22,811,288
9	4.12.2024 10:38:40:247	26,854,061	30,514,287	4,547,925	23,053,106
10	4.12.2024 10:39:10:247	27,583,229	29,802,698	45,121,844	23,302,894
11	4.12.2024 10:39:40:247	28,217,707	29,210,973	44,748,487	23,682,894
12	4.12.2024 10:40:10:247	28,764,949	28,551,592	44,515,969	23,940,656
13	4.12.2024 10:40:40:247	29,284,756	27,975,048	44,263,519	24,194,431
14	4.12.2024 10:41:10:247	29,782,321	27,573,906	43,761,288	24,429,606
15	4.12.2024 10:41:40:247	30,300,931	27,193,407	43,506,181	24,801,631
16	4.12.2024 10:42:10:247	30,675,836	26,807,314	43,280,306	25,076,669
17	4.12.2024 10:42:40:247	31,091,629	26,488,611	43,034,506	25,313,169
18	4.12.2024 10:43:10:247	31,555,235	26,181,895	42,641,219	25,539,044
19	4.12.2024 10:43:40:247	31,892,849	25,863,322	423,808	2,565,995
20	4.12.2024 10:44:10:247	32,204,628	25,770,762	42,161,569	25,937,644

Table 4.8 Velocity measurements

	Evaporator Inlet (High Speed)						
Time	Measurement	1. Point	2. Point	3. Point	4. Point	5. Point	6. Point
10:35	Speed	1.69	1.38	0.65	0.32	0.25	0.26
	Temperature	23.1	23	23	23	22.8	22.8
10:36	Speed	1.51	1.14	0.65	0.36	0.34	0.23
	Temperature	22.8	22.8	22.9	22.9	22.9	22.8
11:01	Speed	0.65	0.46	0.37	0.16	0.16	0.16
	Temperature	24.8	25.1	25.4	25.8	26	26.2
11:01	Speed	0.55	0.42	0.3	0.21	0.17	0.16
	Temperature	26.8	27.3	27.7	27.9	28	28.1
11:31	Speed	0.92	0.42	0.34	0.2	0.25	0.14
	Temperature	27.9	29.2	29.6	29.6	29.5	29
11:31	Speed	0.97	0.95	0.87	0.4	0.24	0.32
	Temperature	29.2	31.6	32.2	32.3	32.2	32
12:00	Speed	0.93	0.76	0.47	0.42	0.29	0.2
	Temperature	29.4	30.3	30.6	30.6	30.3	30.1
12:01	Speed	0.82	0.97	0.75	0.39	0.25	0.21
	Temperature	30.2	32.8	33.2	33.2	33.1	32.9
12:31	Speed	0.93	0.68	0.5	0.52	0.39	0.22
	Temperature	31.3	32	32.2	32.3	32.3	32.1
12:32	Speed	0.98	0.93	0.9	0.43	0.3	0.27
	Temperature	33.3	34.4	34.8	34.9	34.9	34.7

At the end of the experiment, we gathered continuous temperature and relative humidity data for both the inlet and the outlet of the dehumidifier, as well as inlet air speed. Both data sets were formatted to be used as data input to our computational model discussed in the modelling chapter.

5
MODELLING

5.1 Simcenter Amesim

The software chosen for this one-dimensional modelling project, Simcenter Amesim, is a powerful simulation software, extensively utilized to model, simulate, and analyze multidisciplinary systems. Dehumidification process, as mentioned earlier, can be a part of various complex industries, therefore, Simcenter was chosen to model and optimize our process, so it can be further developed into a larger system.

Simcenter can model processes such as drying or humidification chambers, and engineers in food processing industries can optimize the operating conditions to achieve the desired moisture content by use of such simulations involving heat and mass transfer. This is part of the broader impact of this project.

5.1.1 Overview of Simcenter Amesim

Simcenter Amesim serves as a cutting-edge simulation platform designed to facilitate the modelling, analysis, and optimization of mechatronic systems across various domains. Its primary objective is to enable engineers to assess and enhance system performance at the earliest stages of development. This capability supports a comprehensive design approach by integrating system-level simulations into the early phases of the product lifecycle. As a commercial software solution, Simcenter Amesim excels in multi-domain simulations, seamlessly bridging diverse physical systems within a unified modelling environment.

The software is a vital component of the Siemens Digital Industries Software Simcenter portfolio, which incorporates a holistic suite of tools, including 1D and 3D simulations, physical testing, and advanced data analytics. This integration

fosters the development of intelligent, interconnected products by employing predictive engineering analytics to meet the growing demands of modern industries. [71]

5.1.2 Historical Development

The origins of Simcenter Amesim trace back to 1987, when Imagine S.A. was founded by Dr. Michel Lebrun at the University Claude Bernard in France. The software was initially developed to control complex dynamic systems, with its first major application addressing the elevation of sinking Ekofisk North Sea petroleum platforms. By the 1990s, collaboration with Professor C. W. Richards from the University of Bath culminated in the first commercial release of the software in 1995, which was dedicated to fluid control systems. [71]

Over the years, Simcenter Amesim has evolved into a pivotal tool for the automotive, aerospace, and advanced manufacturing industries. Siemens AG acquired the software through its acquisition of LMS International in 2012, integrating it into the Simcenter portfolio and expanding its capabilities to address modern engineering challenges.[71]

5.1.3 Working Principles

Simcenter Amesim features a vast array of pre-built multiphysics libraries, enabling users to quickly construct models and conduct precise analyses. These libraries are tailored to meet the needs of specific industries and applications, ensuring a high degree of flexibility and efficiency. Powered by advanced numerical methods, the software's solver dynamically selects from 17 algorithms to handle ordinary differential equations (ODEs) and differential-algebraic equations (DAEs), optimizing computation based on the system's dynamics. [72]

Simcenter Amesim is equipped with an extensive suite of tools designed to model and predict the behavior of complex mechatronic systems. These systems are characterized by nonlinear, time-dependent analytical equations that describe interactions across hydraulic, pneumatic, thermal, electric, and mechanical domains. This approach offers a distinct advantage over 3D CAD models by enabling early-stage simulations, even before detailed geometric designs are available. Such capabilities are instrumental in accelerating the design process and mitigating potential issues at later stages.

To develop simulation models, users utilize predefined component libraries encompassing various physical domains. These components are interconnected through ports, ensuring proper causality by linking inputs and outputs systematically. This modular framework promotes ease of use and adaptability, catering to a wide range of applications across industries.

The platform's physical libraries are implemented using programming languages such as C, Python, and Modelica—an open-source, object-oriented language specifically designed for modelling complex physical systems. Simcenter Amesim operates seamlessly on Linux and Windows platforms, ensuring broad accessibility for users across different environments. [71]

Simcenter Amesim supports multi-domain modelling across diverse physical domains, including hydraulics, pneumatics, mechanics, electrical systems, and thermodynamics. Rooted in bond graph theory, the software provides a structured methodology for analyzing energy exchange within and across systems. The platform's compatibility with the GNU Compiler Collection (GCC) and Intel compilers ensures flexibility and adaptability for developers.[71]

Engineers rely on Simcenter Amesim for a variety of purposes, including system-level simulations, model customization and early-stage validation. With Simcenter Amesim engineers can predicting system performance and identify optimization opportunities to enhance efficiency. They can also develop tailored components using pre-existing libraries or creating new models through custom programming. Simcenter Amesim enables simulations during the conceptual design phase before detailed CAD (computational aided design) models are developed.

The capabilities of Simcenter Amesim include the following:

- Graphical User Interface (GUI): An intuitive, interactive interface that simplifies model creation, simulation management, and results visualization.

- Advanced Analysis Tools: Features such as table editors, 3D animations, visualization dashboards, and linear analysis tools (eigenvalues, modal shapes, transfer functions) provide comprehensive analytical capabilities.

- Optimization and Robustness Testing: Tools for conducting design of experiments (DOE), Monte Carlo simulations, and parameter optimization to improve system resilience.

- Diverse Numerical Solvers: An extensive collection of solvers, including LSODA, DASSL, and fixed-step methods, ensures precise and efficient computations for various system dynamics.

- Integration and Co-simulation: Support for co-simulations with external software, functional mock-up interfaces (FMU), and real-time simulation targets enables seamless integration into existing workflows.

- Customization and Scripting: Python scripting, parameter grouping, and application design utilities allow users to adapt the platform to their specific requirements. [71]

Simcenter Amesim provides an extensive library collection, offering components tailored to various physical domains, including control systems, electrical networks, mechanical dynamics, fluid systems, thermodynamics, aerospace and defense applications and internal combustion engines. These libraries empower users to construct detailed models that span multiple physical domains, enabling the simulation of complex systems with high accuracy. The modular structure facilitates both industrial applications and academic research. [72]

This software has established itself as a valuable resource in engineering education and research. Universities utilize it as a teaching tool to introduce students to system dynamics, modelling, and simulation. Researchers leverage its advanced capabilities to support interdisciplinary projects, particularly in Europe, where it serves as a reference framework for numerous initiatives. The platform's ability to model and analyze complex systems positions it as an essential tool for advancing engineering knowledge. [71]First released in 1995 as AMESim, this project used Simcenter Amesim 2021.1 version released in April 2021.

Simcenter Amesim represents a versatile and powerful simulation platform, enabling engineers and researchers to model, analyze, and optimize intricate systems with unprecedented efficiency. Its comprehensive libraries, advanced solvers, and customization options make it a cornerstone of modern engineering practices [72].

5.2 Modelling

5.2.1 Overview of Simcenter Amesim Modelling

The dehumidifier, or the dehumidification part of our dryer oven, is regarded as a system made up of several components. Although the experimental model is a lot more complex, for the sake of this project, analytical model only consists of essential components. These components were chosen from list of submodels from several libraries. The discussion of utilized submodels is presented below.

5.2.2 Submodels

Simcenter Amesim makes use of submodels embedded in its software to model a complex system where the user can put in numerous parameters for each element and turn it into the unique element needed. For our system, four main elements are compressor, condenser, evaporator and capillary tube, so our model consists of submodels for these three elements.

5.2.2.1 Compressor

The compressor model chosen for this modelling project is "ACVDICCOMP04 - variable displacement compressor for internal control (R)" (Figure 5.1.)

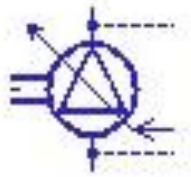


Figure 5.1 Compressor submodel icon [73]

This submodel provides a detailed representation of a variable displacement compressor, capable of employing either volumetric, isentropic, or mechanical efficiencies, or alternatively, polynomial coefficients to define its operational parameters such as mass flow rates and enthalpy losses. The methodology used for determining the mass flow rate depends on the configuration, deriving it from either volumetric efficiency or direct volumetric flow rate data. This flexibility makes the submodel adaptable to a variety of simulation scenarios. [73]

This model offers 4 input ports and 4 output ports as shown in Figure 5.2.

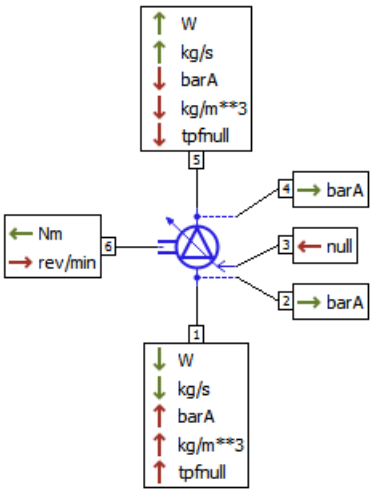


Figure 5.2 Compressor port inlet and outlets [73]

The model integrates a dimensionless analysis framework, leveraging key compressor variables such as suction and discharge pressures, operational speed, refrigerant density, and displacement. When polynomial coefficients are employed, they streamline computations by transforming variables into reduced forms, significantly simplifying equation systems.

This submodel is especially effective in simulating externally regulated compressors where pressure regulation is achieved via internal control valves. The utilization of polynomial coefficients enhances interpolation accuracy, offering precise behavioral predictions from limited data sets. It is particularly advantageous in scenarios where displacement data are unavailable or variable.

The external variables for this compressor submodel are shown on the port schematic, Figure 5.3.

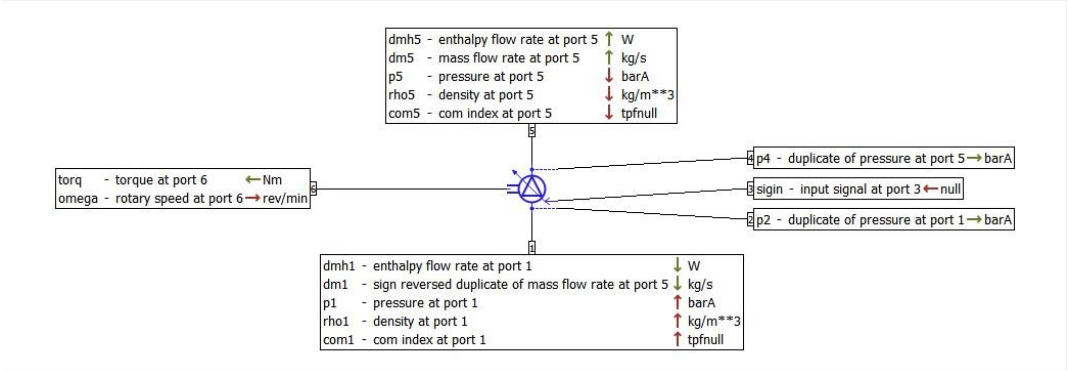


Figure 5.3 External variables for compressor submodel [73]

The parameter settings required for the simulation encompass various aspects crucial for defining and managing the system. One of the primary parameters is the index of the fluid to be used during the simulation. This determines the specific fluid properties and their behavior within the model. Another critical parameter addresses input data that falls outside the range defined by the ASCII files. In such cases, users can select between using extreme values or extrapolation to compute efficiencies or mass flow rates.[73]

The parameters defined on our model can be seen in Figure 5.4. For compressor submodel we entered mostly the parameters that were on its data sheet (Figure 5.5) and used default settings for the rest.

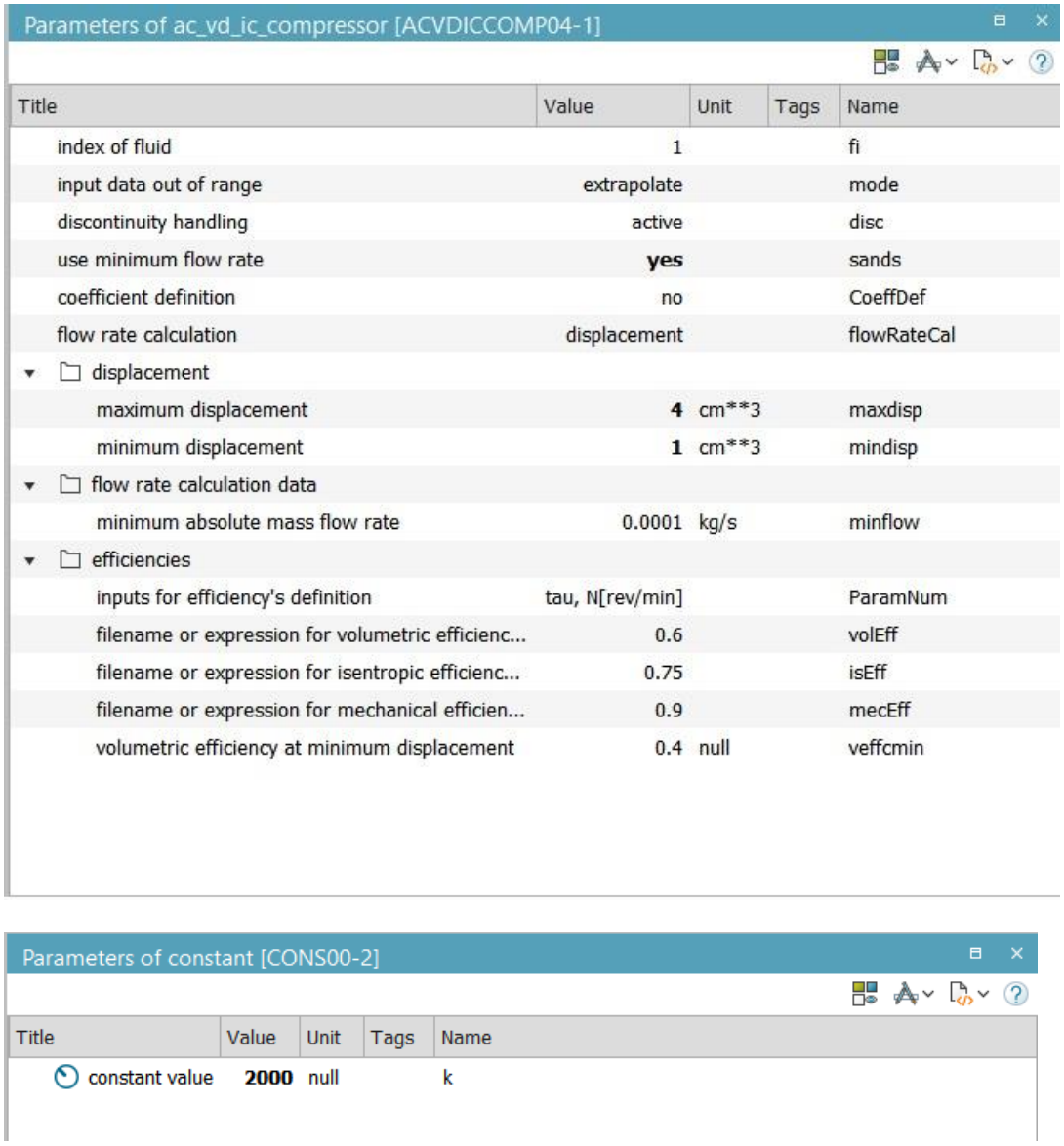


Figure 5.4 Parameters entered and signal input for compressor submodel



Figure 5.5 Compressor data sheet

5.2.2.2 Heat Exchangers

For both heat exchangers on our model, namely for our condenser and evaporator, we have chosen to use the supercomponent ACMAFT0 - TPF EMA fins and tubes heat exchanger (Figure 5.6) to create a more detailed design.

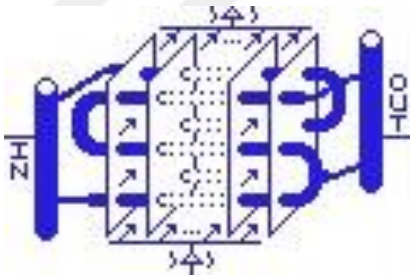


Figure 5.6 Heat exchanger submodel icon [73]

This advanced model facilitates the detailed design and simulation of fins and tubes heat exchangers. It incorporates global geometric configurations and physical parameters for tubes and moist air flows, supporting a wide range of design and operational scenarios. Key features include comprehensive heat exchange correlations applicable at both fin and tube levels, detailed pressure drop calculations for tubes and bend connections and versatile arrangement options, configurable through a dedicated designer application, "fins and tubes heat exchanger designer app." The designer app simplifies the configuration of tube banks and their interconnections, ensuring user-friendly setup processes even for

intricate geometries. Modular definitions allow for computational efficiency, enabling simulations of large-scale heat exchangers without sacrificing precision. [73]

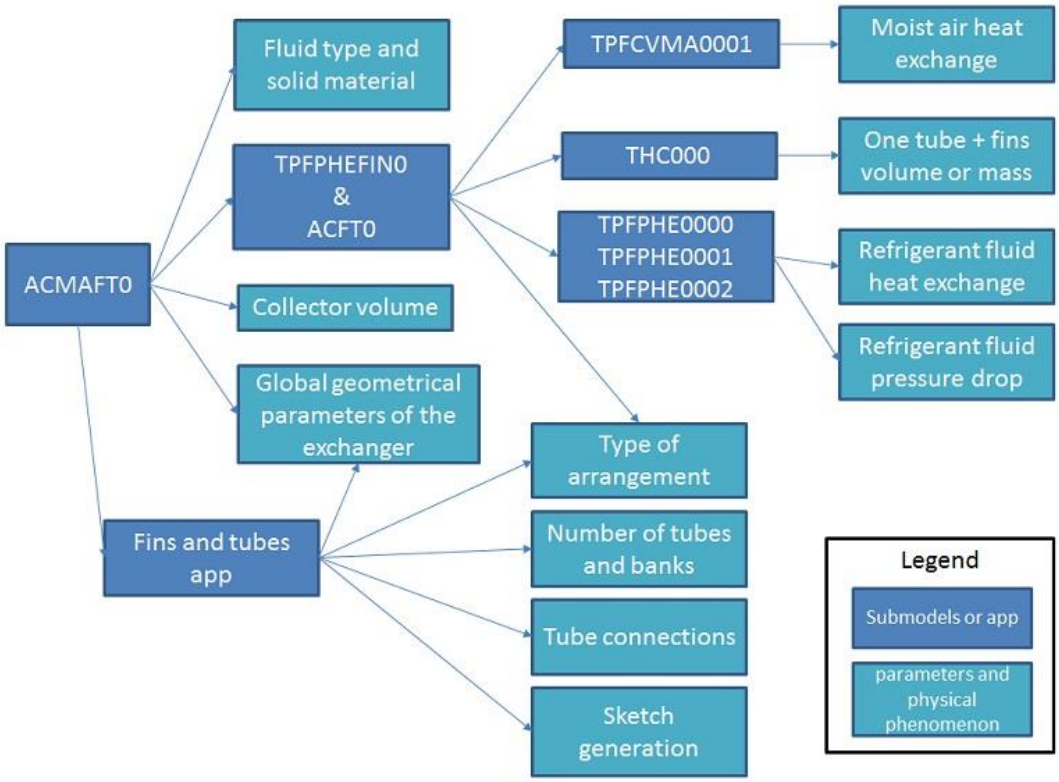


Figure 5.7 The features of designer app [73]

This supercomponent is designed for modelling a fins and tubes heat exchanger, offering a range of configurable parameters to tailor the simulation. The ACMAFT0 component allows users to set key attributes, including the heat exchange correlations at the fins level (for moist air) and the tubes level (for refrigerants). It also enables adjustments for pressure drops occurring in the tubes and bends, selection of materials for fins and tubes, specification of the arrangement type, and global geometry settings to define essential geometrical parameters (Figure 5.7). [73]

Additionally, the associated fins and tubes heat exchanger designer application must be launched to configure specific parameters unique to the design process. This app exclusively facilitates the definition of the number of tube banks and the number of tubes per bank, both parallel and perpendicular to the airflow. It also provides options for configuring the connections between tubes and enables the

automatic generation of sketches, streamlining the design process. [73]How geometry parameters are defined can be seen in Figures 5.8 and 5.9.

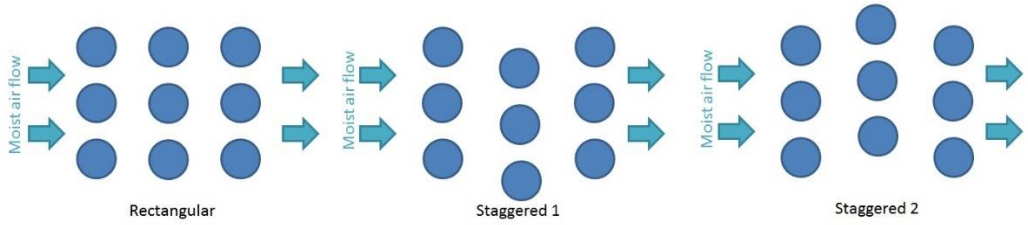


Figure 5.8 Arrangement types offered for heat exchanger tubes [73]

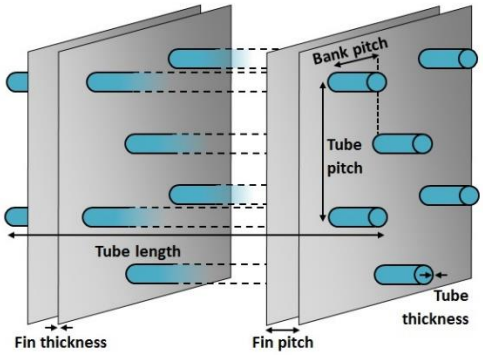


Figure 5.9 Geometry parameters defined for heat exchanger [73]

The app also allows to define a repeatable pattern, therefore simplifying the generation process and as illustrated in the example Figure 5.10.

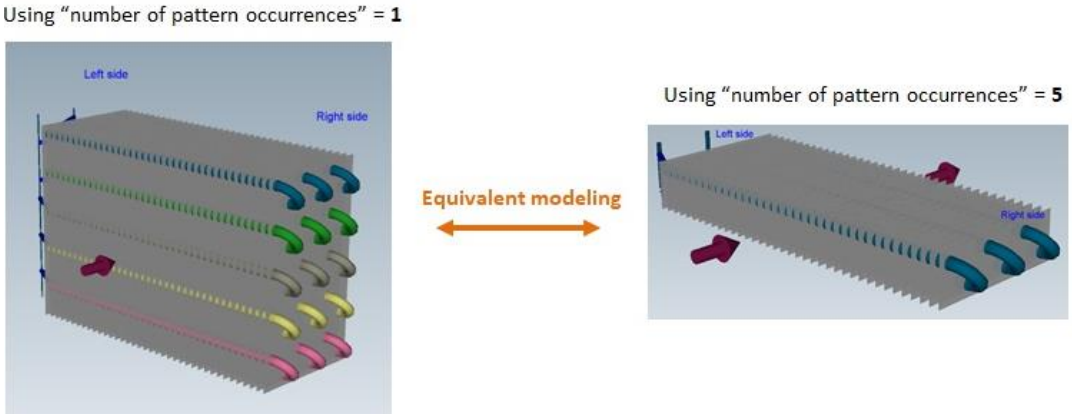


Figure 5.10 Creating a repeatable pattern for the heat exchanger [73]

The external variables for this heat exchanger supercomponent are shown on the port schematic in Figure 5.11.

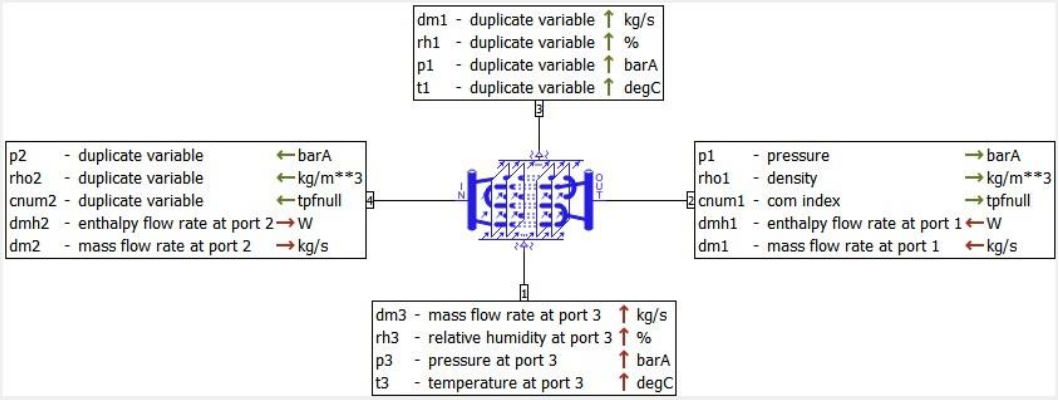


Figure 5.11 External variables for the heat exchanger submodel [73]

5.2.2.3 Condenser

By using the fins and tubes heat exchanger designer app, we have designed our condenser model with the measured geometry and parameters from the experiment (Figure 5.12). The illustrations from the app as seen in Figures 5.13 and 5.14 show the constructed model and related parameters.

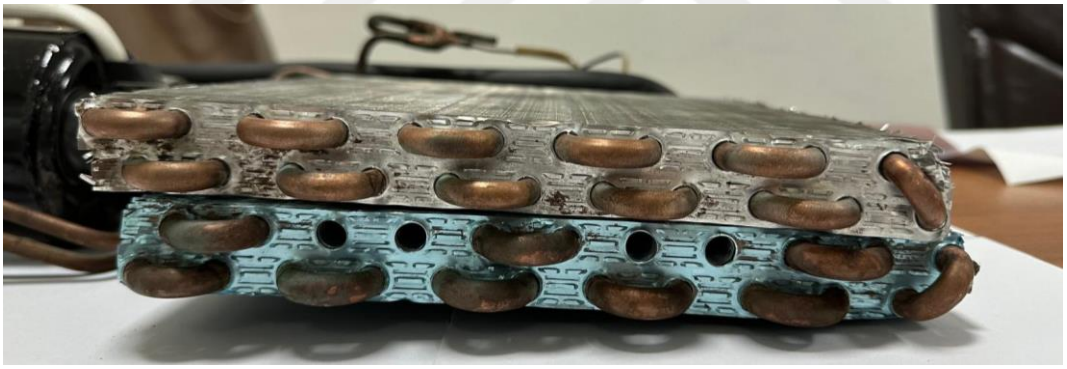


Figure 5.12 Heat exchangers of the dehumidifier

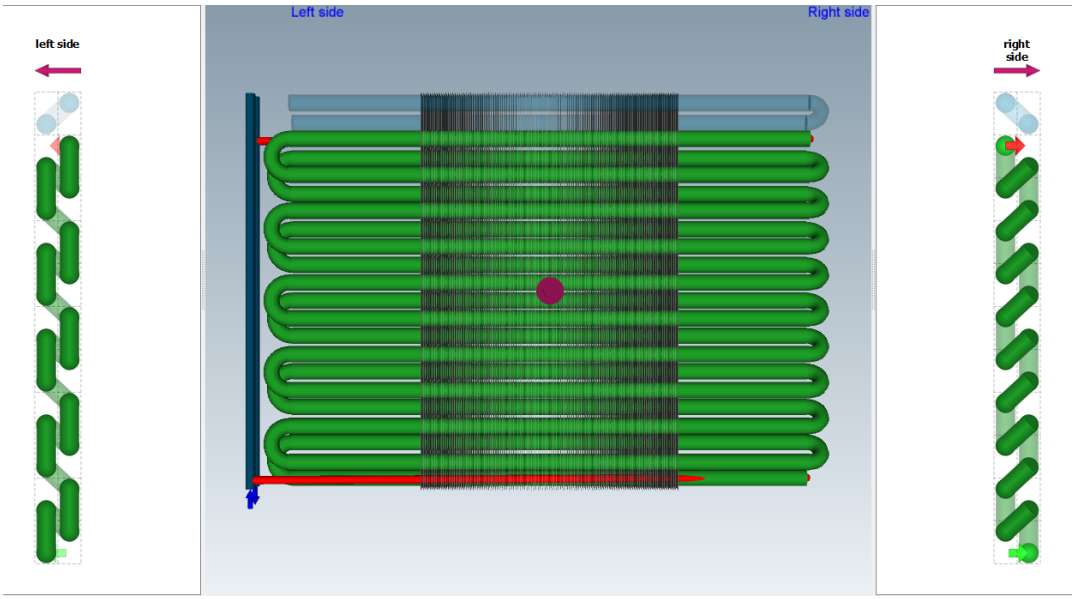


Figure 5.13 Condenser geometry illustrated by the designer app

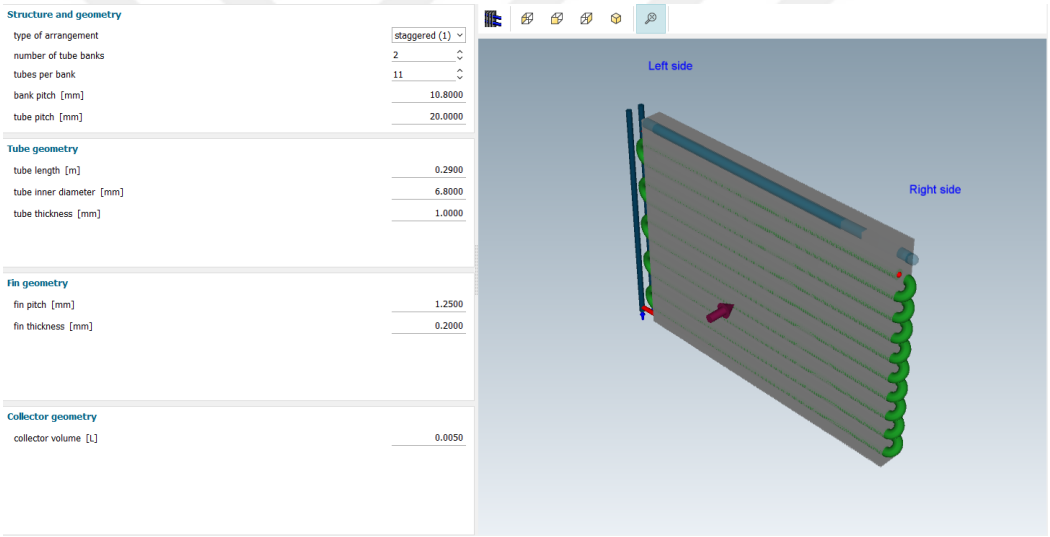


Figure 5.14 Condenser parameters entered in the designer app

5.2.2.4 Evaporator

The same procedure followed for condenser was repeated for the evaporator. By using the fins and tubes heat exchanger designer app, we have designed our evaporator model with the measured geometry and parameters from the experiment. The illustrations from the app shows the constructed model and related parameters (Figures 5.15 and 5.16).

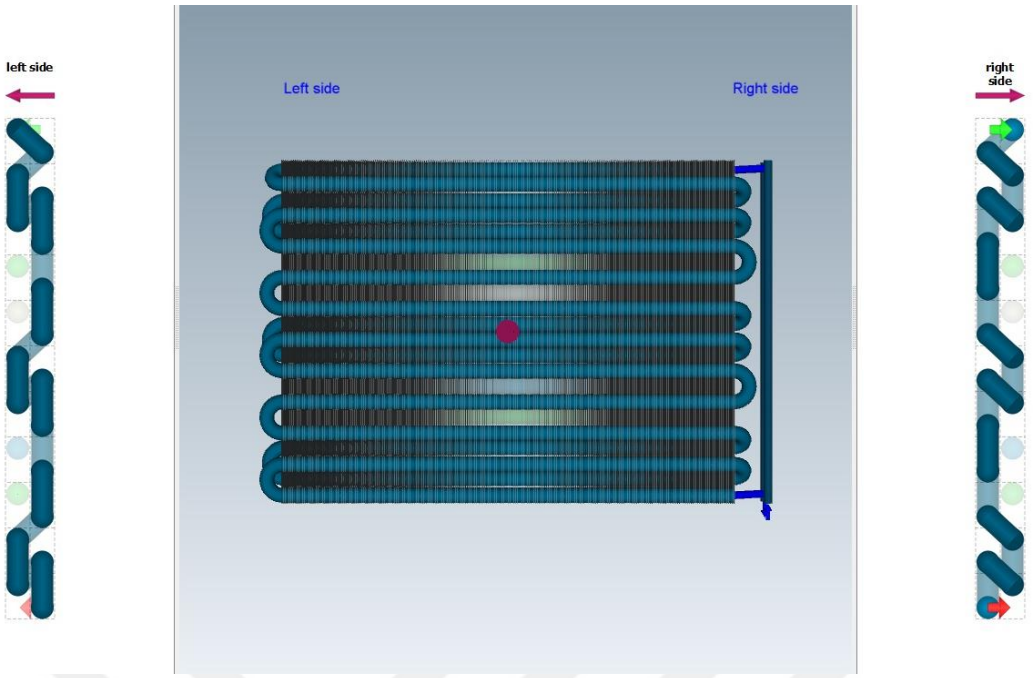


Figure 5.15 Evaporator geometry illustrated by the designer app

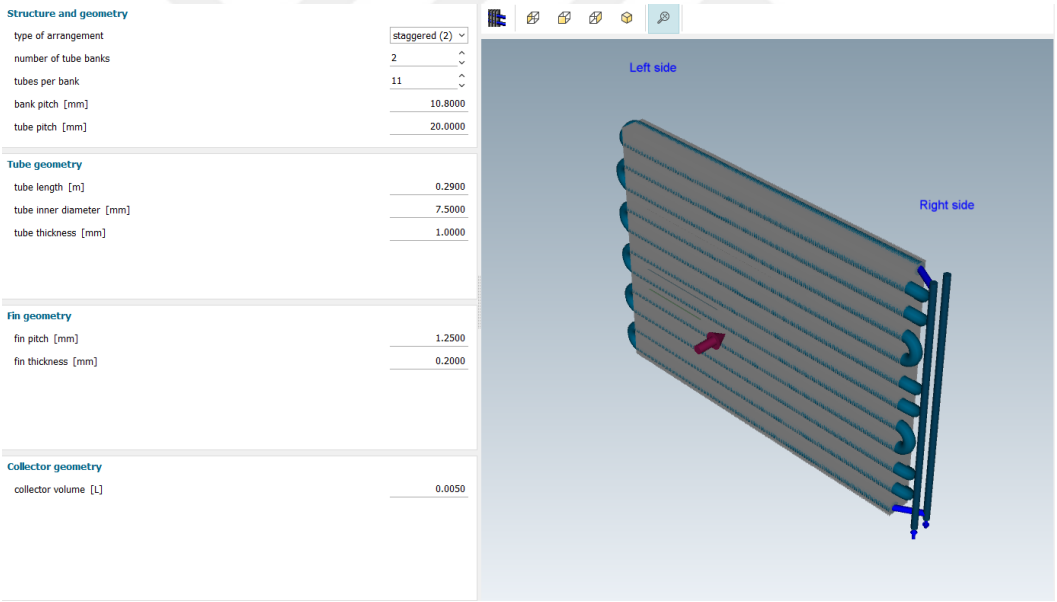


Figure 5.16 Evaporator parameters entered in the designer app

5.2.2.5 Capillary Tube

To simulate the capillary tube in our humidifier we chose to use TPFP004 - adiabatic pipe (R-C-R) (Figure 5.17).



Figure 5.17 Capillary tube submodel icon

This model addresses the interplay of compressibility and friction-induced pressure losses. It supports diverse flow regimes through established correlations, including Mac Adams, Cicchitti, Dukler, Friedel, and Muller-Steinhagen models. The user specifies essential geometric and initialization parameters such as hydraulic diameter, cross-sectional area, and fluid attributes. Outputs include precise pressure and enthalpy flow rates. [73]

The external variables for this adiabatic pipe submodel are shown on the port schematic in Figure 5.18. The parameters for our model can be seen in Figure 5.19.

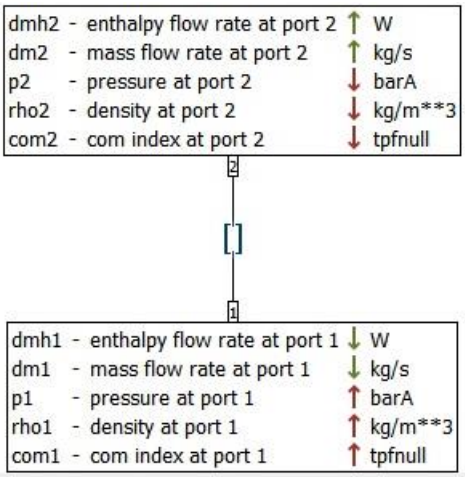


Figure 5.18 External variables for the capillary submodel

Parameters of tpf_pipe_1 [TPFP004-1]

Title	Value	Unit	Tags	Name
index of fluid	1			fi
two-phase flow frictional pressure drop correlation	Mac Adams correlation			dp2pcorr
acceleration pressure drop calculation	**yes**			acc
type of initialization	**pressure and temperature**			hcond
pressure	**1.013**	barA		pini
temperature	**25**	degC		tini
frictional pressure drop gain	1	null		kdp
length	**380**	**mm**		le
cross-sectional area	**Pi*(.85)^2**	mm**2		area
hydraulic diameter	**1.7**	mm		hdiam
absolute roughness	0	mm		rabs

Figure 5.19 Parameters entered for capillary tube

5.2.2.6 Pipes

For pipes connecting the compressor to evaporator and compressor to condenser we utilized TPFP001 - adiabatic pipe (C-R) and TPFP002 - adiabatic pipe (R-C) as submodels respectively (Figure 5.20).



Figure 5.20 Adiabatic pipe icon [73]

These two submodels differs only in that the variables at ports 1 and 2 are interchanged as seen in Figure 5.21 showing the external variables.

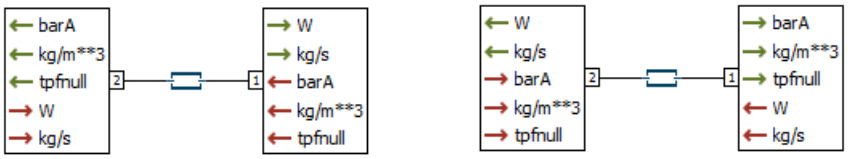


Figure 5.21 External variables for adiabatic pipe submodels [73]

The list of parameters that need to be specified and our inputs to the model can be seen in Figures 5.22 and 5.23 respectively.

Parameters of tpf_pipe_5 [TPFP001-1]

Title	Value	Unit	Tags	Name
index of fluid	1			fi
two-phase flow frictional pressure drop correlation	Mac Adams correlation			dp2pcorr
acceleration pressure drop calculation	no			acc
type of initialization	**pressure and gas mass fraction**			hcond
pressure	3	barA		pini
gas mass fraction	**0.2**	null		gmfini
frictional pressure drop gain	1	null		kdp
length	**1.175**	m		le
cross-sectional area	**pi*8.5*8.5/4**	mm**2		area
hydraulic diameter	**8.5**	mm		hdiam
absolute roughness	0	mm		rabs

Figure 5.22 Parameters for adiabatic pipe connecting compressor to evaporator

Parameters of tpf_pipe [TPFP002-1]

Title	Value	Unit	Tags	Name
index of fluid	1			fi
two-phase flow frictional pressure drop correlation	Mac Adams correlation			dp2pcorr
acceleration pressure drop calculation	no			acc
type of initialization	**pressure and temperature**			hcond
pressure	**15**	barA		pini
temperature	**30**	degC		tini
frictional pressure drop gain	1	null		kdp
length	**0.94**	m		le
cross-sectional area	**pi*7.8*7.8/4**	mm**2		area
hydraulic diameter	**7.8**	mm		hdiam
absolute roughness	0	mm		rabs

Figure 5.23 Parameters for adiabatic pipe connecting compressor to condenser

5.2.2.7 Moist Air Source

The air source we have chosen for our model is ACMAS0000 - moist air source (Figure 5.24).



Figure 5.24 Moist air source submodel icon [73]

This submodel generates a controlled source of moist air, with relative humidity as a primary input parameter. The system ensures consistent outputs across its designated ports, including signals for temperature, pressure, and humidity. Internal calculations encompass absolute humidity and specific enthalpy, enabling detailed characterizations of the air's thermodynamic state. [73]

The external variables for moist air source are shown on the port schematic in Figure 5.25.

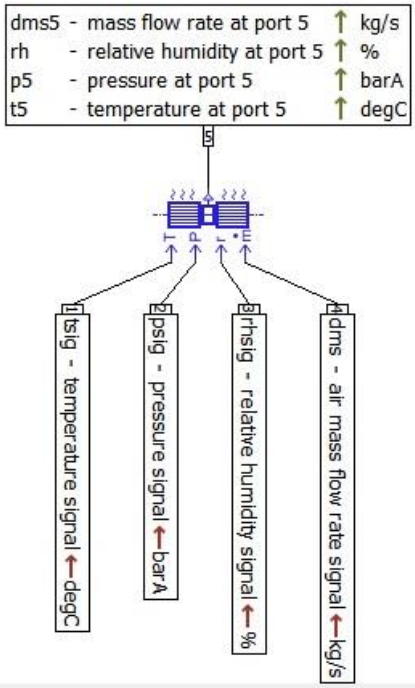


Figure 5.25 External variables for moist air source submodel [73]

There are no parameters to set for this component. The inputs are added as signals to the ports.

5.2.2.8 Input Signals

For inputs to moist air source, we have used two different signal components.

For our constant input, that is, pressure, we used CONS00 -constant signal (Figure 5.26).

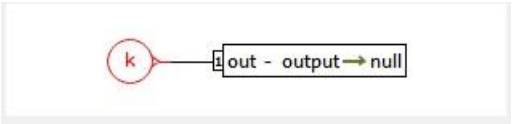


Figure 5.26 Constant input signal icon [73]

This component puts out a signal with specified value. We used this signal for air pressure input and the parameter we used for this can be seen in the Figure 5.27.

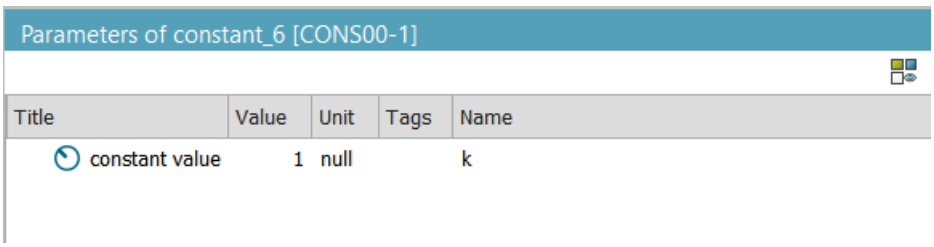


Figure 5.27 Parameter for air pressure input for moist air source

For the other three inputs of moist air, that is for temperature, relative humidity and mass flow rate, we chose to use SIGUDA01 - interpolate 1D or XY table with respect to time (Figure 5.28).

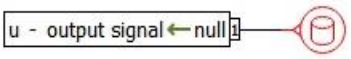


Figure 5.28 Interpolate signal input icon [73]

This utility interpolates time-dependent signals from 1D or XY data tables, offering flexibility in output generation. With support for linear, cubic, and constant interpolation methods, it accommodates diverse simulation requirements while ensuring high fidelity.

The format of data file specified by the user can either be 1D table or XY multi-column table. The output value can be set to the values of *u(t)* but also to its first and second derivatives *u'*, or *u''* . [73]

If the data file contains a 1D table, the data must be stored in the following order:

Table format: 1D

$x_1 \quad u_1$
$x_2 \quad u_2$
$x_3 \quad u_3$
...
$x_N \quad u_N$

with data separated by any number of space, tab or return.

XY table requires the user to specify which column is used for setting the *u* variable(s), by setting the *column to use for u* parameter(s) (in the range [2,N]). The first column ($u_{*,1}$) is always used for x. Data must be stored in the following order:

Table format: XY

$u_{1,1} \quad u_{1,2} \quad u_{1,3} \quad \ldots \; u_{1,N}$
$u_{2,1} \quad u_{2,2} \quad u_{2,3} \quad \ldots \; u_{2,N}$
$u_{3,1} \quad u_{3,2} \quad u_{3,3} \quad \ldots \; u_{3,N}$
...
$u_{M,1} \quad u_{M,2} \quad u_{M,3} \quad \ldots \; u_{M,N}$

with M as the number of rows and N as the number of columns.

The output value can be set either to u, du/dx_i or d^2u/dx^2. However, note that the second derivative d^2u/dx^2 is always zero in case of linear interpolation. [73]

The data interpolation is done in one of three options, linear, cubic, and stairs (constant interpolation). Figure 5. 29 shows the 3 curves produced using the same data points (blue squares) but different interpolation types.[73]

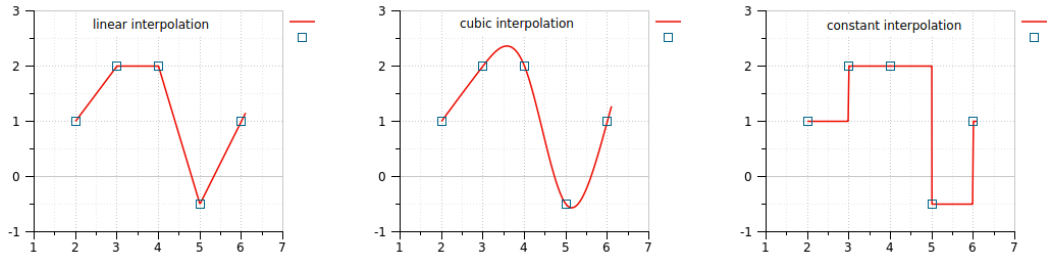


Figure 5.29 Interpolation types for interpolate signal input submodel [73]

The model allows users to configure various parameters, including boundary conditions, data extrapolation modes, and output derivatives. Designed to handle monotonic input data, it supports advanced initialization techniques, enabling smooth curve fitting and precise signal representation. The utility is particularly valuable in scenarios requiring dynamic signal generation aligned with time-varying input data. [73]

For our model input data, we organized our experiment data in 1D table for each of temperature, relative humidity and mass flow rate measurements against time. The parameter windows and our data files can be seen below in Figure 5.30 and 5.31 respectively.



Figure 5.30 Parameters entered for moist air source submodel

4.12 olcum sicaklik.txt - Notepad

File Edit Format View Help

0	21.71
60	21.95
1560	32.08
3360	37.84
5100	40.23
5160	40.28
6960	41.46
7020	41.47
8700	41.97
10500	42.23
12300	42.38
14100	42.49
15900	42.62
15960	42.75
17700	42.51
17760	42.51
19500	42.76
21300	42.66
21360	42.73
23100	42.86
23160	42.91
24900	43.15
24960	43.15
26700	43.30
26760	43.28
28500	43.41
28560	43.40
30300	43.63
30360	43.67
32100	43.80
32160	43.93
33900	44.30
33960	44.31
35700	44.66
35760	44.68
37500	45.50

4.12 olcum debi.txt - Notepad

File Edit Format View Help

0	0.038728
60	0.035664
1560	0.015608
3360	0.017446
5100	0.023258
5160	0.025657
6960	0.024356
7020	0.028641
8700	0.022838
10500	0.021844
12300	0.02531
14100	0.02098
15900	0.018778
15960	0.020044
17700	0.020064
17760	0.02342
19500	0.017494
21300	0.01727
21360	0.022682
23100	0.018128
23160	0.02682
24900	0.019056
24960	0.023134
26700	0.019112
26760	0.026371
28500	0.022053
28560	0.026123
30300	0.017209
30360	0.023191
32100	0.015332
32160	0.024668
33900	0.018868
33960	0.01997
35700	0.016599
35760	0.01987
37500	0.018407

4.12 olcum nem.txt - Notepad

File Edit Format View Help

0	60.12
60	47.61
1560	37.38
3360	33.22
5100	31.74
5160	31.73
6960	31.24
7020	31.30
8700	30.88
10500	30.63
12300	30.51
14100	30.32
15900	30.02
15960	30.02
17700	29.90
17760	29.91
19500	29.53
21300	29.29
21360	29.30
23100	28.93
23160	28.93
24900	28.73
24960	28.67
26700	28.56
26760	28.50
28500	28.31
28560	28.17
30300	27.95
30360	27.95
32100	27.57
32160	27.51
33900	26.83
33960	26.77
35700	25.83
35760	25.71
37500	24.17

Figure 5.31 Screenshot of data files entered for moist air source inputs

5.2.2.9 Refrigerant

For the refrigerant in the system, Simcenter Amesim presents a generic submodel, TPF_FP01 - refrigerant thermodynamic properties (Figure 5.32).



Figure 5.32 Refrigerant submodel icon [73]

This generic submodel allows to define properties of a fluid accessible from one of four databases: common fluids, refrigerants, organic compounds and noble gases. The list of refrigerants available list can be seen as an example in Table 5.1.

Table 5.1 List of refrigerants available [73]

Usual name	Available	Validity domain (Tmin [K], Tmax [K],	Default
R22	Helmholtz	115.73 / 550.0 / 600.0 / 1721.60	IIR
R32	Helmholtz	136.34 / 435.0 / 700.0 / 1429.28	IIR
R123	MBWR	166.0 / 600.0 / 400.0 / 1774.00	IIR
R125	Helmholtz (H1	172.52 / 500.0 / 600.0 / 1691.11	IIR
R134a	MBWR	169.85 / 600.0 / 700.0 / 1591.70	IIR
R13b1	Peng-Robinson	105.15 / 600.0 / 500.0 / 2978.20	NBP
R143a	Helmholtz	161.34 / 650.0 / 1000.0 / 1332.05	IIR
R152a	MBWR	154.56 / 500.0 / 600.0 / 1193.54	IIR
R227ea	Helmholtz	146.35 / 475.0 / 600.0 / 1878.82	IIR
R236ea	Helmholtz (H1	242.0 / 500.0 / 600.0 / 1591.09	IIR
R236fa	MBWR	179.52 / 500.0 / 400.0 / 1718.04	IIR
R245fa	Helmholtz	171.05 / 440.0 / 2000.0 / 1648.79	IIR
R1233zd(E)	Helmholtz	195.15 / 550. / 1000. / 1488.96	IIR
R1234yf	Helmholtz (H1	240.0 / 400.0 / 400.0 / 1327.45	IIR
R1234ze(E)	Helmholtz	168.62 / 420.0 / 200.0 / 1512.19	IIR
R1336mzz(Z)	Helmholtz	182.65 / 500.0 / 460.0 / 1637.27	IIR
Novec 649	Helmholtz	165.0 / 500.0 / 500.0 / 1972.12	IIR
Novec7000	Helmholtz	150.65 / 500.0 / 200.0 / 1777.69	IIR

Our dehumidifier uses R410a as the refrigerant. Fluid index chosen can be seen among rest of the properties that have to be specified in the parameter window in Figure 5.33.

Parameters of two_phase_props [TPF_FP01-1]

Title	Value	Unit	Tags	Name
index of fluid	1			skfi
fluid index in database	**R410a**			dbfi
equation of state	Pseudo pure fluid			eosi12
reference state	default			refq
use charge and temperature	**yes**			loadinit
charge and temperature				
type of global initialization	priority to bottle filling			typeinit
initial temperature	**30**	degC		temp
charge of fluid	**0.425**	kg		load
oil content				
additional oil mass content	0	percent		yOil
absolute viscosity of oil	100	cP		muOil

Figure 5.33 Parameters entered for refrigerant submodel

5.2.2.10 Air Sink

THMASINK00 – moist air sink is the submodel (Figure 5.34) chosen to close a moist air port. The inputs for the port can be seen in the illustration and no parameters are set for this submodel (Figure 5.35).



Figure 5.34 Moist air sink submodel icon [73]

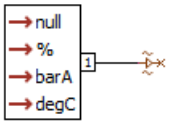


Figure 5.35 External variables for moist air sink submodel [73]

5.2.2.11 Solid

In order to define thermal properties of evaporator and condenser solids, we utilized the generic submodel, THSD00 – thermal solid properties (Figure 5.36).



Figure 5.36 Solid submodel icon [73]

The properties for the solids can be specified either by setting as constant or as a function of temperature, or by picking predefined materials within the software. We have chosen pure aluminum for our model (Figure 5.37).

Parameters of th_solid_data [THSD00-1]

Title	Value	Unit	Tags	Name
solid type index	1			soli
material definition	pure aluminum (Al)			materialType

Figure 5.37 Parameters entered for solid submodel

5.2.3 Final Model

The final model for the system can be seen in Figure 5.38. The moist air source, linked with four input signals, is connected to port 1 of the evaporator. Moist air line continues out from port 3 of the evaporator connecting directly to port 1 of condenser and leaving the condenser at port 3 to the air sink. The compressor is connected to the adiabatic pipe and this pipe is connected to the condenser at port 4. This refrigerant line continues out from the condenser at port 2, getting to the capillary tube and capillary tube is connected to the evaporator at port 2. The evaporator is connected to the compressor through the second adiabatic pipe, completing the refrigerant circulation.

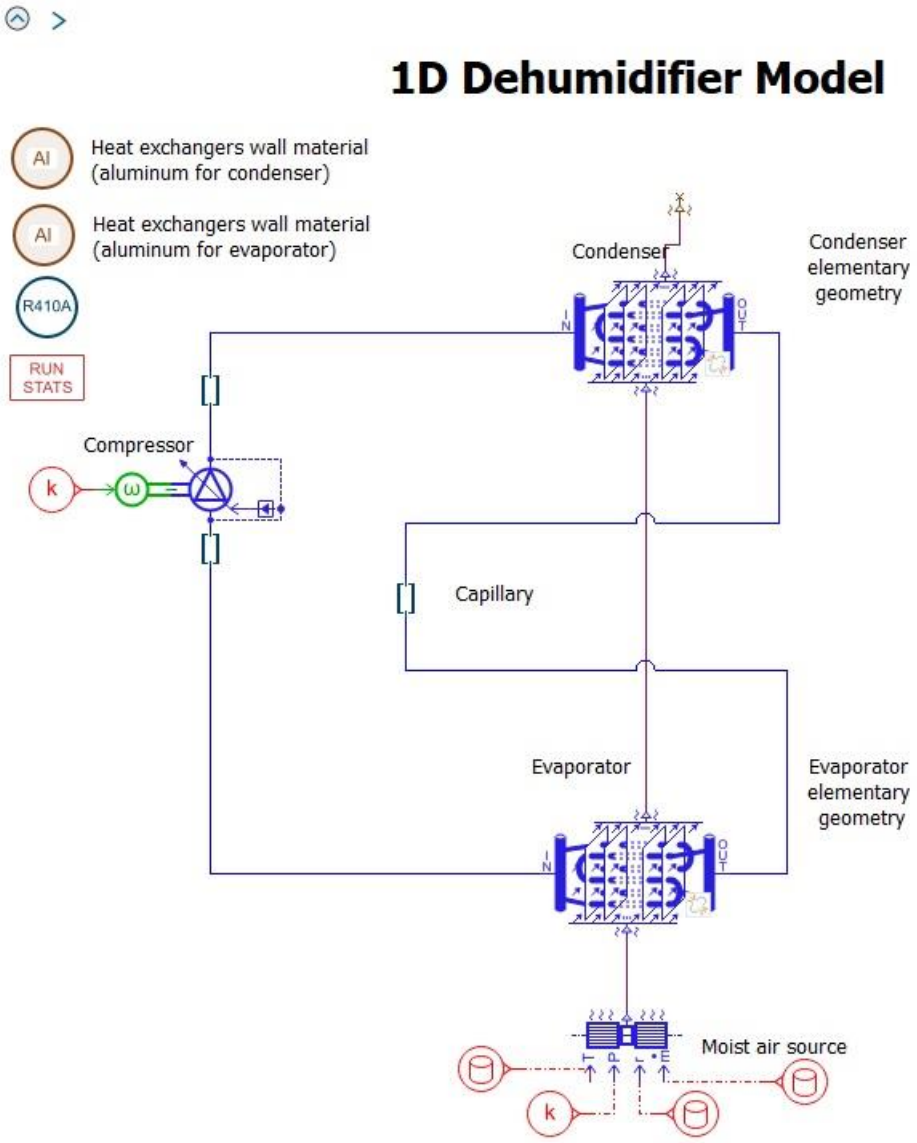


Figure 5.38 One dimensional dehumidifier model

Once the model was confirmed to run smoothly, the results have been evaluated. The run parameters (Figure 5.39) and performance analyzer results (Figure 5.40) are given. For the data sets discussed above, the time interval has been set at 60 seconds, final time being 37560 seconds.

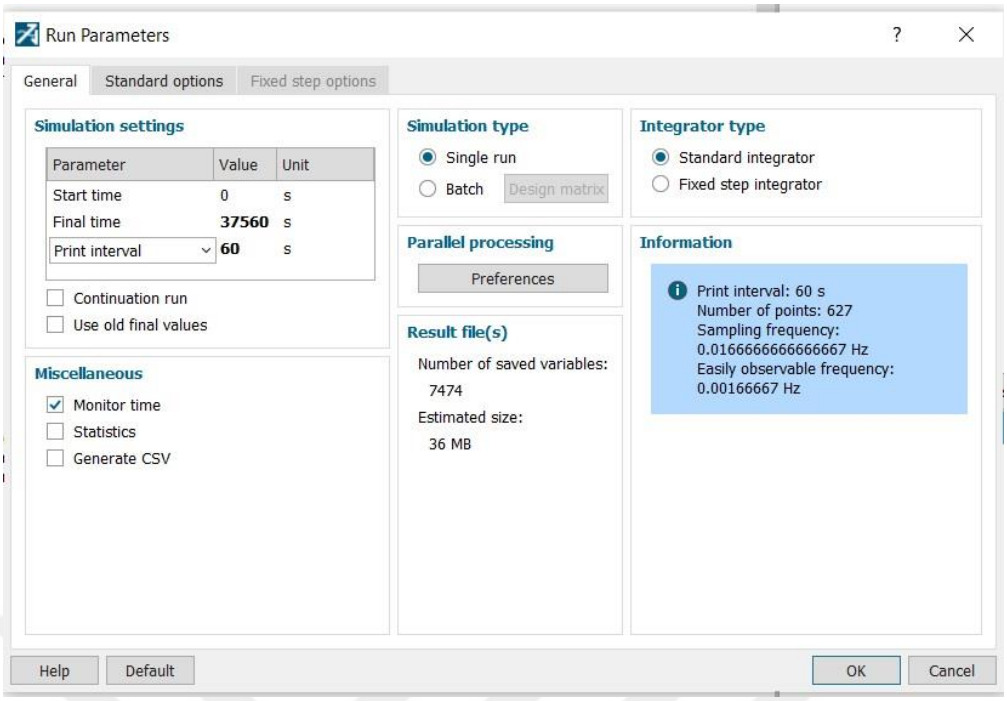


Figure 5.39 Run parameters used for the model

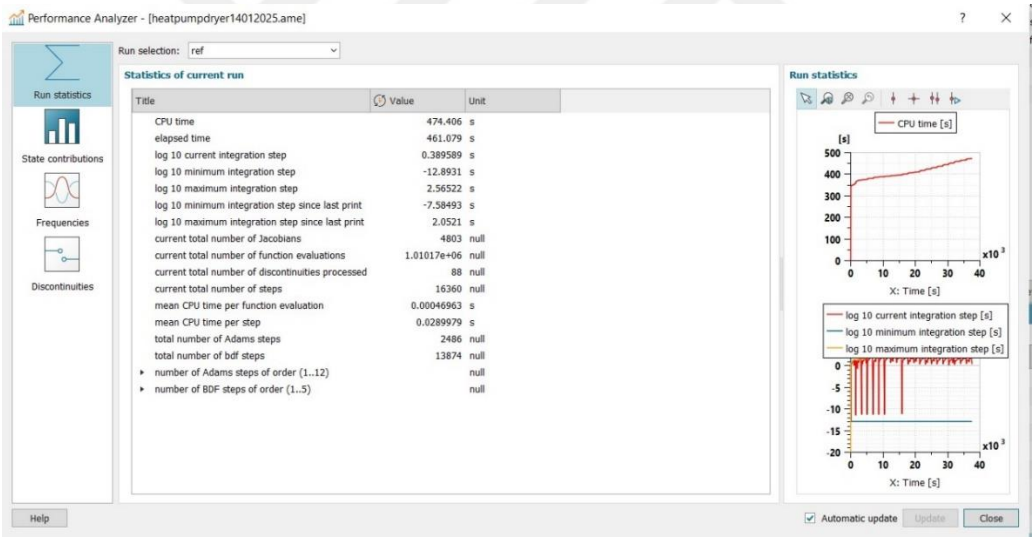


Figure 5.40 Performance analyzer results

We ran first our preliminary setup values to validate our model. Once this was confirmed, the second setup, that is heat pump dryer oven setup data is fed to the systems. Results from the physical experiment and computational model were compared and the discussion on this is done in the conclusion and results chapter. Lastly, we experimented with changing some parameters on the model, namely the fluid used in the system, to see the effects on the outcome.

6
CONCLUSION

In this chapter we compare the results of our experiments to the output of our Simcenter Amesim simulation model. Table 6.1 shows the experiments we carried out, where the preliminary setup experiments are our validation set and our dryer oven setup experiments are our test set.

Table 6.1 List of Experiments

Experiments		
Preliminary Setup		**Dryer Oven Setup**
Ambient Air Conditions	Humid Air Conditions	Closed loop
1 set of data	3 sets of data	1 set of data

6.1 Validation

For validation of our model, we used our preliminary setup which was operating and monitoring results of our dehumidifier in a middle-sized room first with ambient air conditions and second with humid air conditions.

The results of our model for the ambient conditions can be seen in Figures 6.1 and 6.2. The model outputs for temperature and relative humidity values at condenser exit (port 3) are graphed respectively. The results show correlation with our experimental measurements; the condenser outlet air temperature increases and the humidity ratio decreases as we have seen during the dehumidifier experiment runs.

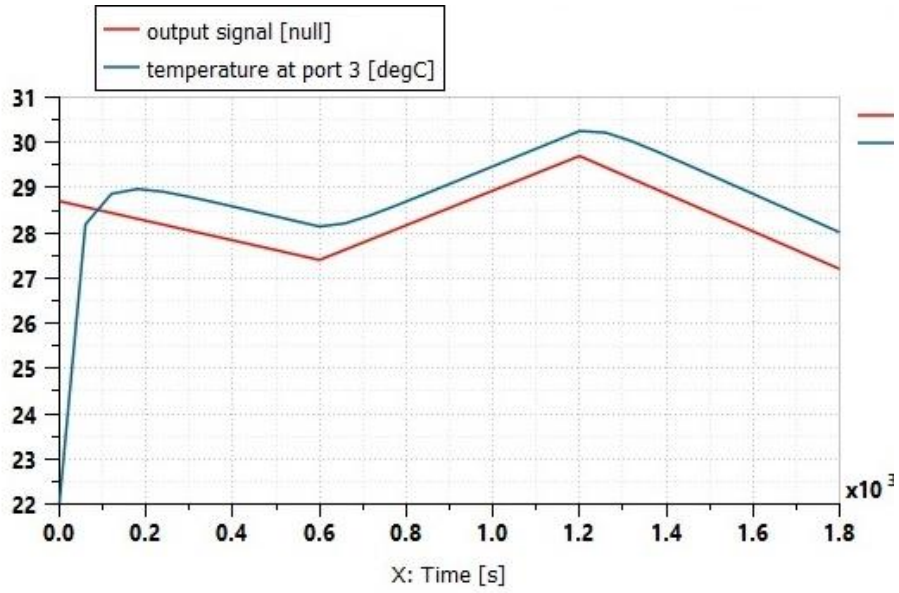


Figure 6.1 Results from the preliminary setup at ambient temperature: exit temperature shown as blue and inlet temperature shown as red (degrees C on y-axis)

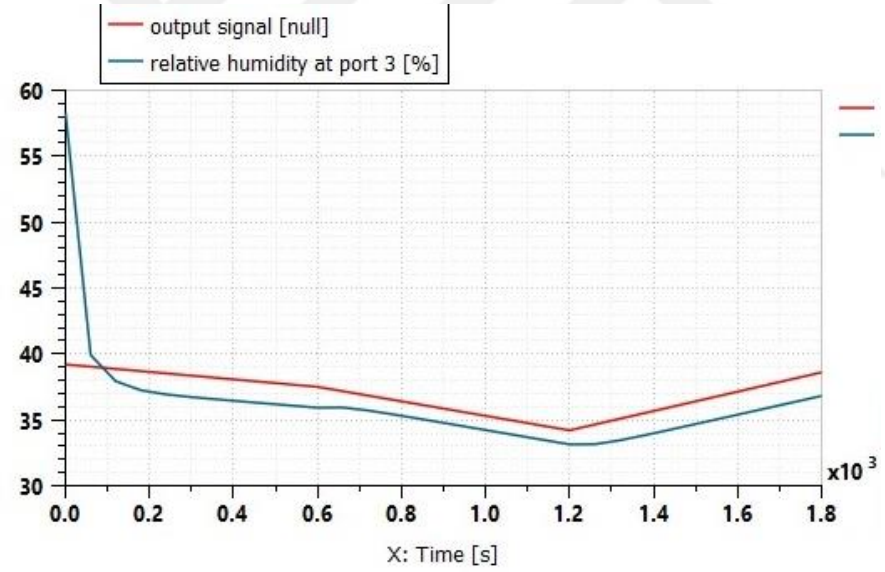


Figure 6.2 Results from the preliminary setup at ambient temperature: exit relative humidity shown in blue and inlet relative humidity shown in red (% value on the y-axis)

The second set of experiments with our preliminary setup involved raising the humidity level of the room with a steam sprayer and running our dehumidifier in humid air conditions. We ran three sets of measurements for these conditions. In Figures 6.3, 6.4 and 6.5, condenser exit air temperature results of our model are

graphed. In Figures 6.6, 6.7 and 6.8 the humidity levels at port 3 of condenser can be evaluated.

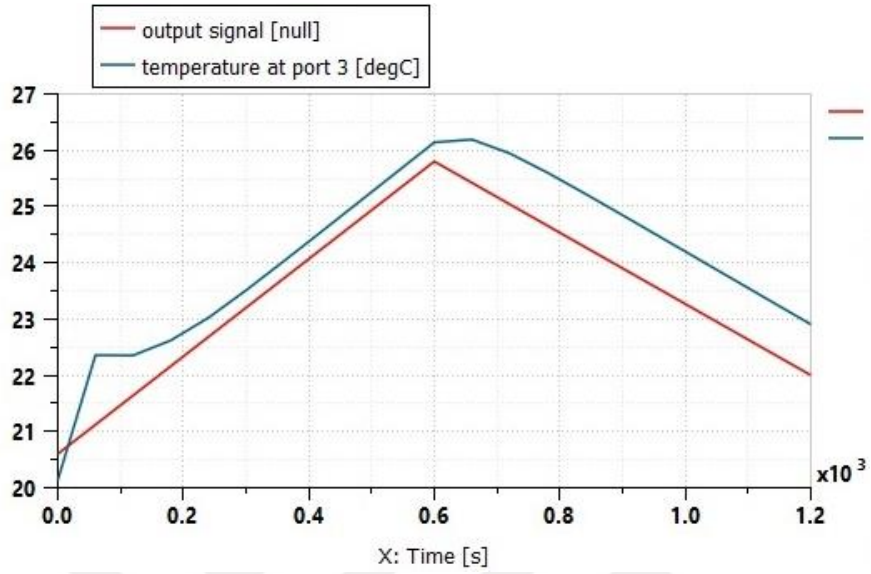


Figure 6.3 Results from the preliminary setup at humid conditions: exit temperature shown as blue and inlet temperature shown as red (degrees C on y-axis) – Experiment 1

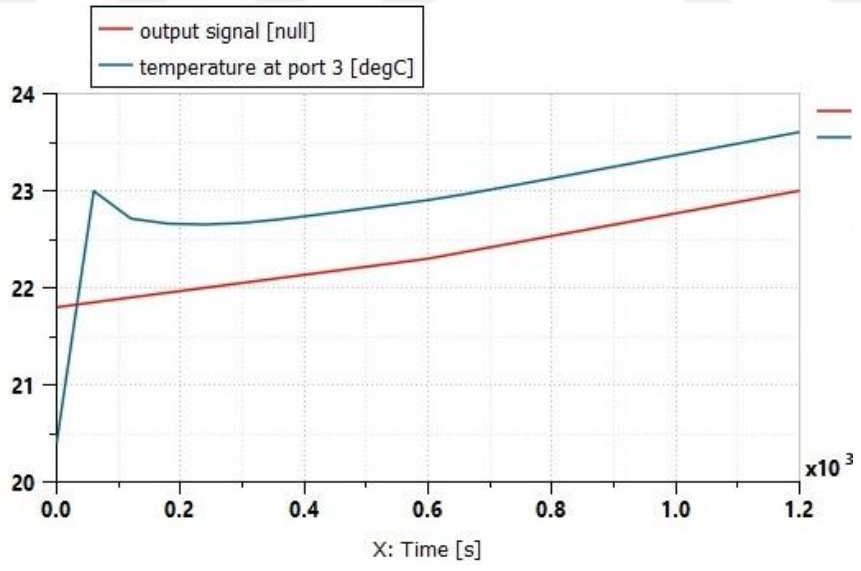


Figure 6.4 Results from the preliminary setup at humid conditions: exit temperature shown as blue and inlet temperature shown as red (degrees C on y-axis) – Experiment 2

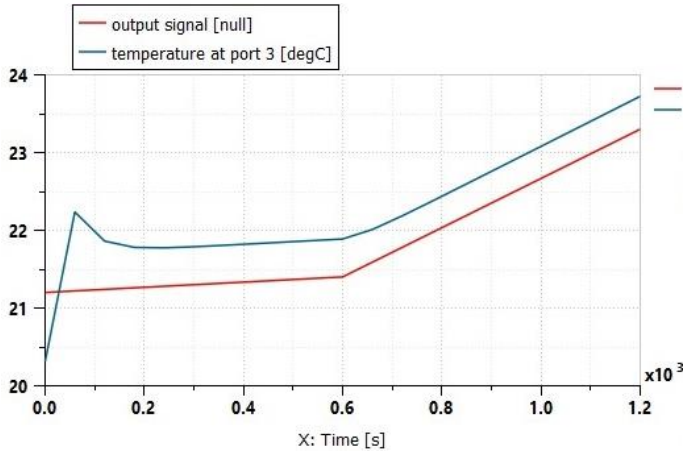


Figure 6.5 Results from the preliminary setup at humid conditions: exit temperature shown as blue and inlet temperature shown as red (degrees C on y-axis) – Experiment 3

In all three runs of this setup, the model shows correlation to our temperature measurement. There is an increase in outlet temperature.

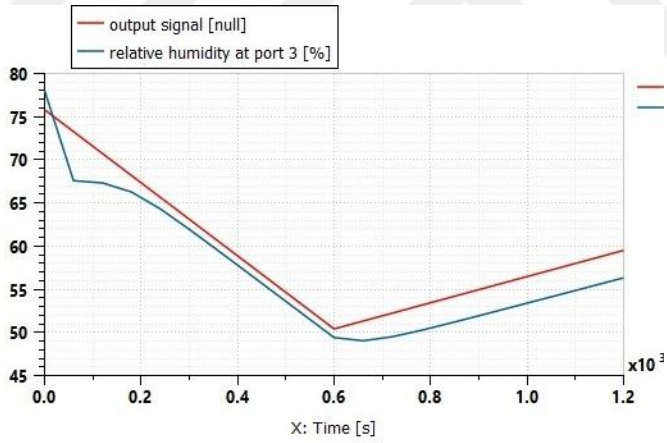


Figure 6.6 Results from the preliminary setup at humid conditions: exit relative humidity shown in blue and inlet relative humidity shown in red (% value on the y-axis) – Experiment 1

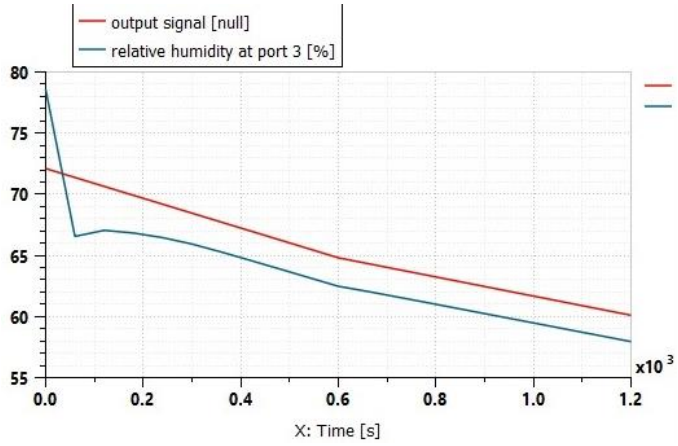


Figure 6.7 Results from the preliminary setup at humid conditions: exit relative humidity shown in blue and inlet relative humidity shown in red (% value on the y-axis) – Experiment 2

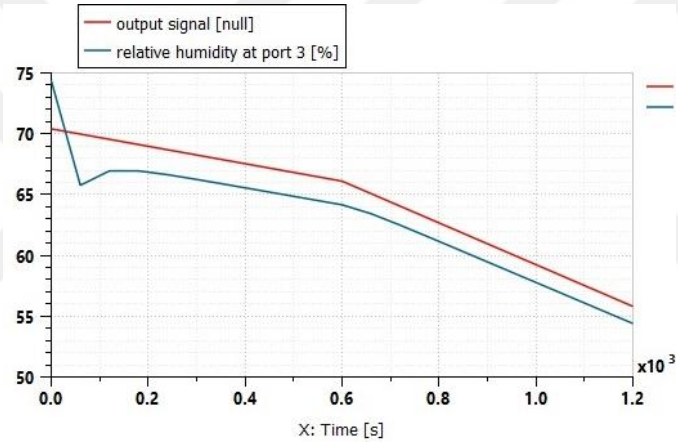


Figure 6.8 Results from the preliminary setup at humid conditions: exit relative humidity shown in blue and inlet relative humidity shown in red (% value on the y-axis) – Experiment 3

In all three runs of this setup, the model shows correlation with our relative humidity measurement. There is a decrease in outlet humidity.

We observe that the one-dimensional model results show correlation with experimental measurements for both temperature and relative humidity properties, so the model is validated with experimental results.

6.2 Test Results

For the heat pump dryer oven setup, the inlet data given to the model was prepared from the physical experiment measurements as an XY table for the specific time stamps as explained in Chapter 5. The results taken from the model for this set of data is again compared with the actual experiment measurements.

For psychrometric analysis, the starting evaporator inlet and ending condenser outlet air properties for both the experiment and model data can be seen in Figures 6.9 and 6.10 respectively.

1254	4.12.2024 21:01:10:247	53,0779	0	15,42988	0
1255	4.12.2024 21:01:40:247	53,11245	0	15,42948	0
1256	4.12.2024 21:02:10:247	53,115106	0	15,3545	0
1257	4.12.2024 21:02:40:247	53,116431	0	15,33093	0

Scan	Cont	Start Action:				
Scan		Time	321 <EMS_Nem>	Alarm 321	322 <EMS_Sicaklik> (C)	Alarm 322
1		4.12.2024 10:34:40:263	67,349156	0	21,687238	0
2		4.12.2024 10:35:10:247	65,131612	0	21,700525	0
3		4.12.2024 10:35:40:247	55,098825	0	21,72045	0

Figure 6.9 Experiment starting evaporator inlet and ending condenser outlet air properties

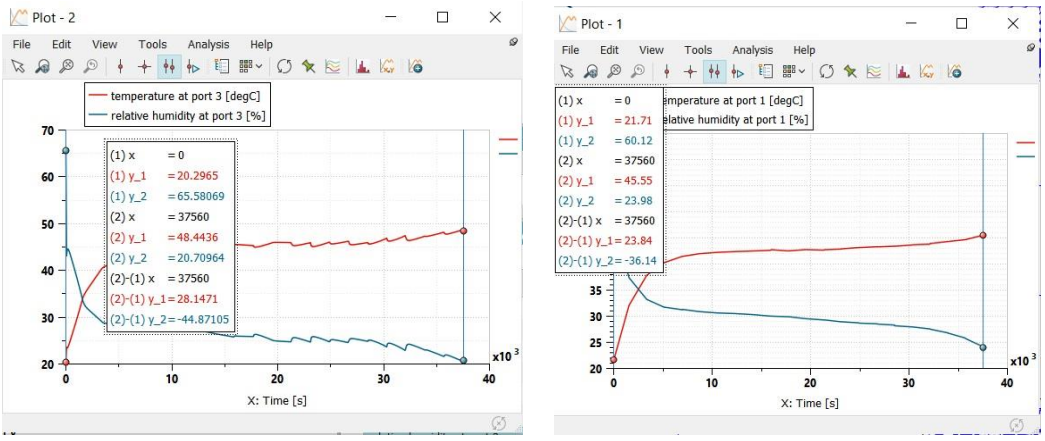


Figure 6.10 Model starting evaporator inlet and ending condenser outlet air properties

T (°C) dry bulb	rH (%) rel.humidity	TDP (°C) dew point	W (kg/kg) abs. humidity	h (kJ/kg) enthalpy	Tw (°C) wet bulb	sp. vol (m³/kg)		
21.7	67.4	15.4	0.01091	49.5	17.3	0.85	Calculate	Remove
53.1	15.4	19.2	0.01393	89.6	27.5	0.95	Calculate	Remove
21.7	60.1	13.7	0.00974	46.6	16.3	0.85	Calculate	Remove
48.4	20.7	20.2	0.01487	87.1	27	0.93	Calculate	Remove

Add line

Figure 6.11 Psychrometric air properties at starting evaporator inlet and ending condenser outlet points

The psychrometric properties for these points were calculated using an online psychrometric calculator [74] (Figure 6.11) and the dehumidification process between these points were graphed. The psychrometric graph for the experimental results (Figure 6.12) and model results (Figure 6.13) both reflect drying, with downward movement on the chart, and heating, with right way movement on the chart.

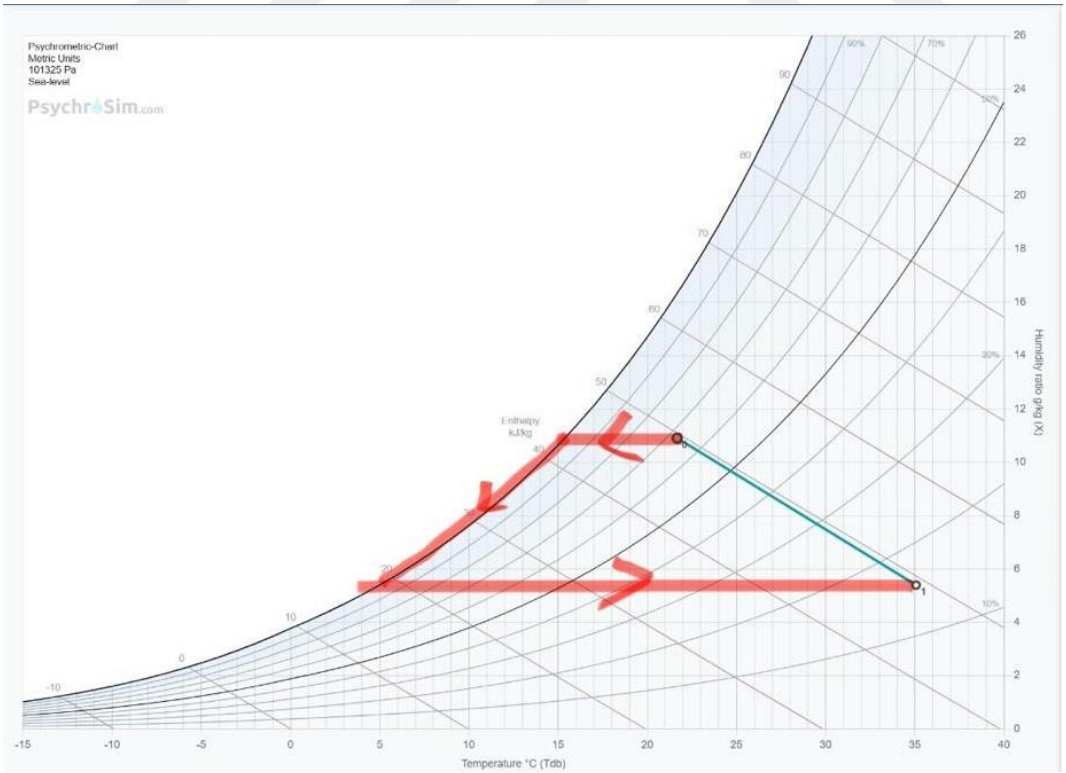


Figure 6.12 Psychrometric dehumidification process of the dryer oven experiment

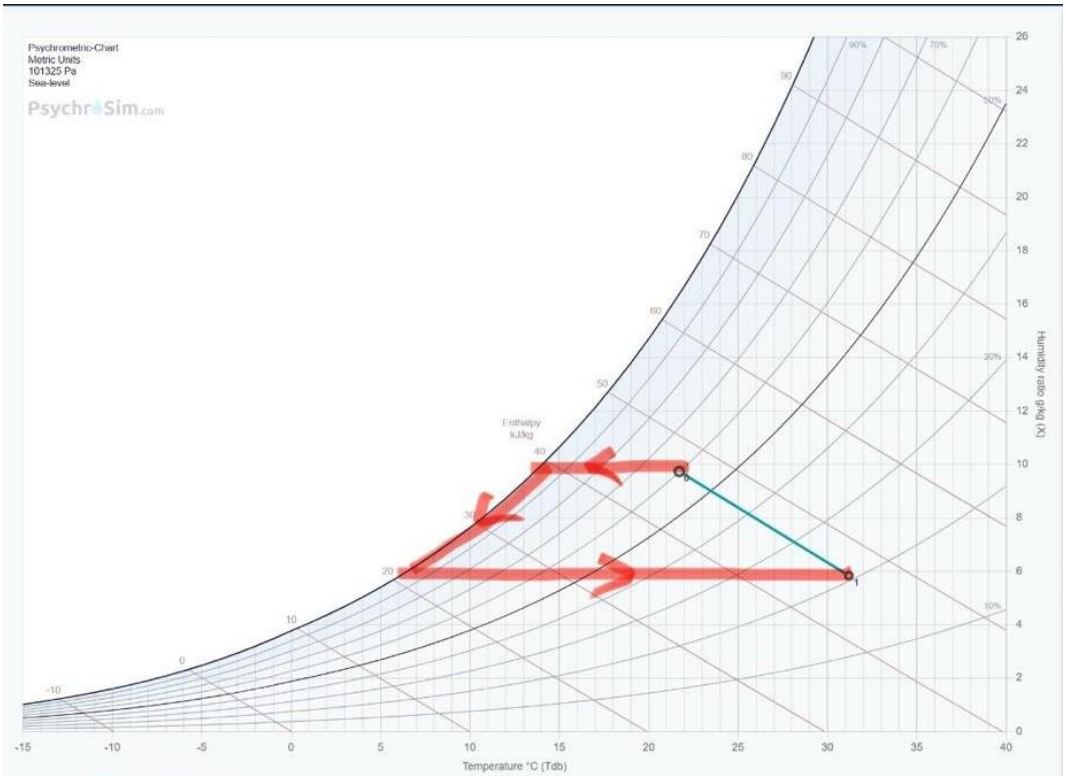


Figure 6.13 Psychrometric dehumidification process of the simulation model

Comparison between results from the model and actual experiment measurements are done for temperature and relative humidity data. The input data to the model are the temperature, relative humidity and mass flow rate measurements of the dryer oven evaporator inlet at certain time stamps. The air properties simulated by the model for the condenser exit are compared with the dryer oven measurements taken at the exit of the condenser duct with thermocouples and humidity sensor. The graphs for the model exit air properties are shown in Figures 6.14 and 6.15 below.

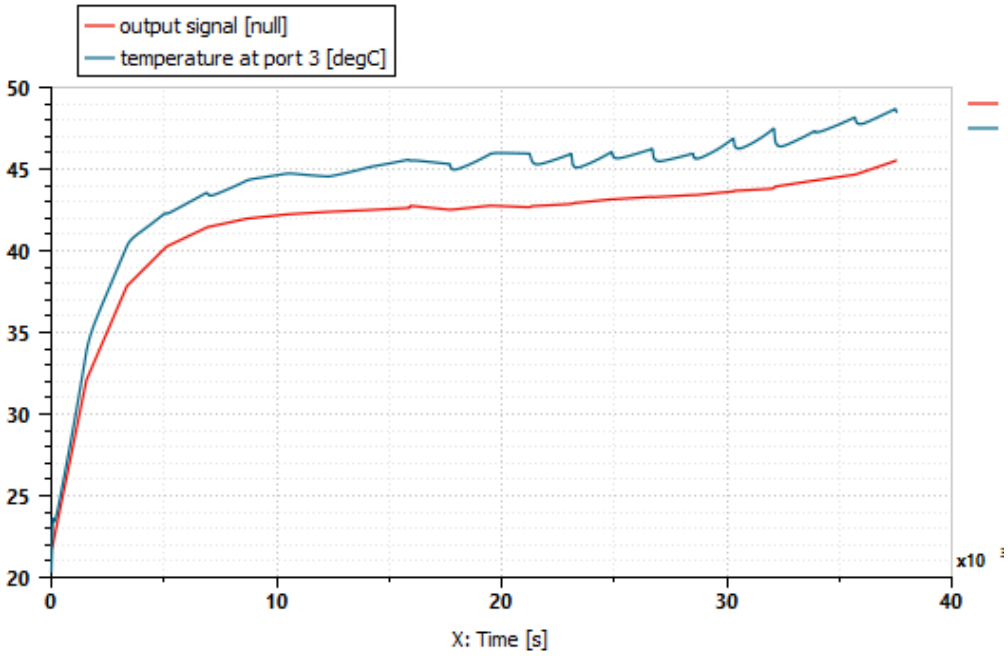


Figure 6.14 Model exit temperature results for dryer oven setup shown in blue, inlet temperature shown in red (degrees C on the y-axis)

The heat pump dryer oven model designed on Simcenter Amesim shows steep increase in exit temperature for up to 2,5 hours (around 10000 seconds) in time data. After this point, the acceleration of increase is lower, but temperature continues to gradually increase through the simulation runtime.

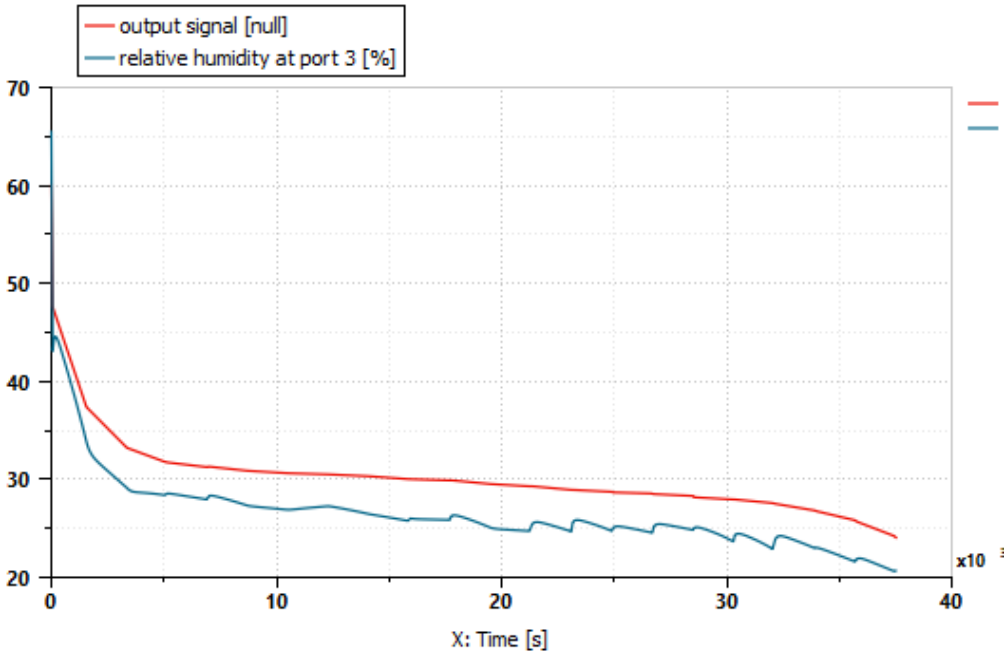


Figure 6.15 Model exit relative humidity results for dryer oven setup shown in blue, inlet relative humidity shown in red (% values on the y-axis)

The heat pump dryer oven model designed on Simcenter Amesim shows steep decrease in exit relative humidity levels for up to 1,5 hours (around 5000 seconds) in time data. After this point, the acceleration of decrease is lower, but humidity level continues to gradually decrease through the simulation runtime.

The experimentally measured data for condenser exit of heat pump dryer oven logged by the analyzer was organized for the same time stamps as our model input data in order to compare the results of the model and the experiment. The comparison graphs are shown in Figures 6.16 and 6.17.

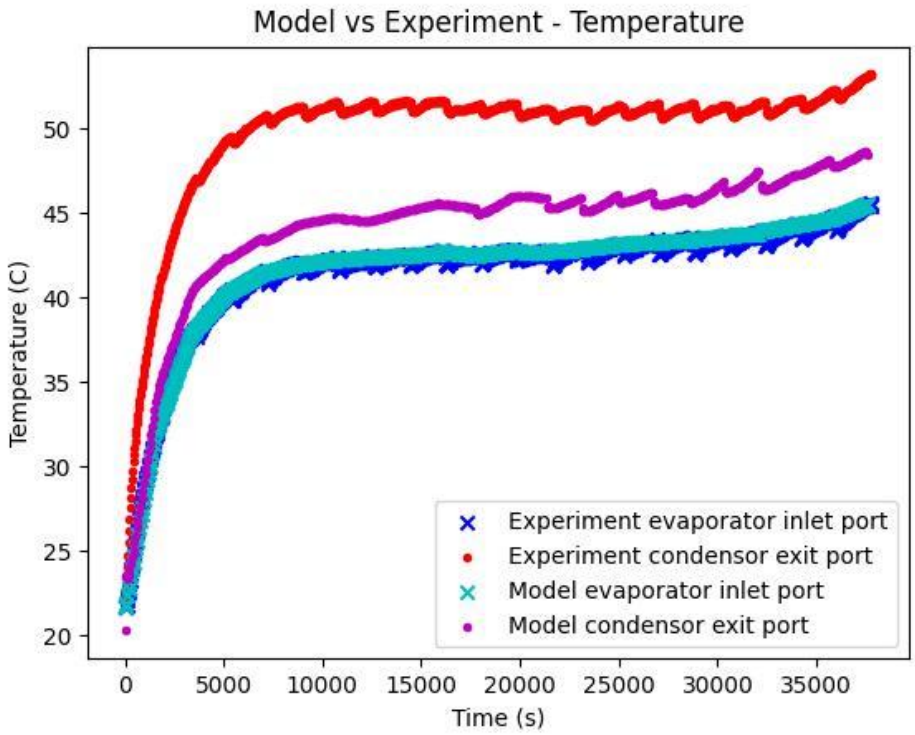


Figure 6.16 Comparison graph for dryer oven and model output temperature data

The temperature results for condenser exit in real life experiment show the same trend of steep increase in the first quarter of runtime. After this point the temperature nearly plateaus, very gradually increasing towards the end.

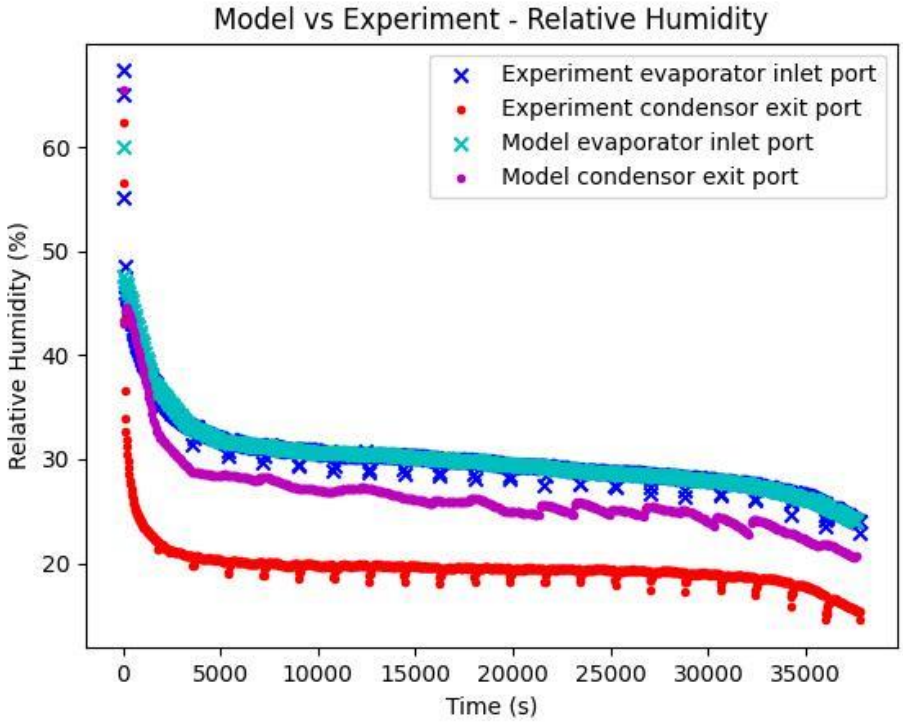


Figure 6.17 Comparison graph for dryer oven and model output relative humidity data

The relative humidity results for condenser exit in real life experiment show the same trend of steep decrease in the first hour of runtime. After this point the humidity continues to very gradually decrease towards the end.

It can be seen from the comparison graphs that the model results and experiment measurements show some correlation. The temperature plots show similar trend in increase over the time period, initial steep increase gradually slowing down. The relative humidity plots also show the same trend and shape of decrease, sharp initial decrease slowing with time.

For both data sets however, the actual temperature degrees and relative humidity ratios do not show an exact match. Temperatures measured at our dryer oven condenser exit are higher at all points than our model outputs. Similarly, the relative humidity ratios measured at our heat pump dryer oven condenser exit are lower at all points than our model outputs.

We have used some evaluation metrics to show these observations in numbers. We have compared our experiment data with our model data at evaporator inlet and condenser outlet for temperature and relative humidity time series. Firstly, we have

calculated the error between the model and experiment series. Then we took the absolute value of errors and averaged them to get Mean Absolute Error (MAE), as our first metric. MAE focuses on measuring the accuracy or error of predictions or model outputs. Secondly, we took the squares of the errors between data and took their average, to get Mean Squared Error (MSE). Finally we used MAPE (Mean Absolute Percentage Error) as our last metric. MAPE is calculated with formula

$$\text{MAPE} = \frac{1}{n}\sum_{i}^{n}\left|\frac{y_i - \hat{y}_i}{y_i}\right| \times 100\% \qquad (6.1)$$

where y_i is the actual value, $\hat{y}_i$ is the forecast value and n is the number of fitted points. MAPE indicates how accurate a forecast system is and expresses errors as a percentage, making it scale-independent and interpretable. To better understand the correlation between our time series, we also calculated Pearson correlation coefficient. It measures the strength of the linear relationship between two variables. It has a value between -1 to 1, with a value of -1 meaning a total negative linear correlation, 0 being no correlation, and + 1 meaning a total positive correlation. The results of our calculations on the error and error percentages are shown in Table 6.2.

Table 6.2 Evaluation metric results on time series comparisons

Experiment vs Model	MAD (Mean Absolute Error)	MSE (Mean Squared Error)	MAPE (Mean Absolute Percentage Error)	Pearson Correlation Coefficient
Evaporator Inlet Temperature	0,22	0,09	0,54	1,00
Condenser Exit Temperature	5,64	32,75	11,38	0,97
Evaporator Inlet Relative Humidity	3,58	13,46	12,14	0,98
Condenser Exit Relative Humidity	10,47	113,15	53,33	0,86

Among these metrics, the one that makes most sense about our data comparison is MAPE. This value represents the percentage deviation between actual and forecast values where our experiment data is considered actual and model data is considered forecast results. For example, temperature values at condenser exit deviates 11.38%; our dryer oven provides higher temperatures. The relative humidity at the

same point on the other hand has a larger deviation; the experiment providing 53% lower humidity levels.

The Pearson coefficients alternatively suggest very high linear correlation between all data sets compared. Inlet temperature data confirms entering the same data points into the model as Pearson coefficient is calculated as 1, whereas exit temperature values have 0.97 correlations, suggesting different values but similar trends. Lowest Pearson coefficient for our data is for condenser exit relative humidity. As discussed earlier, the trend of the two time series at condenser exit have sharp decrease during the first half hour of runtime (where the difference in values are higher) but then stabilize, giving a close correlation like 0.86.

The graphs in Figures 6.18 thru 6.21 show experiment and model data plotted against each other in blue, and a trend line running through the data points, showing the correlation between data sets. Temperature data seems very much correlated all throughout the experiment, where relative humidity data is better correlated when humidity levels are lower, which corresponds to latter half of our experiment run.

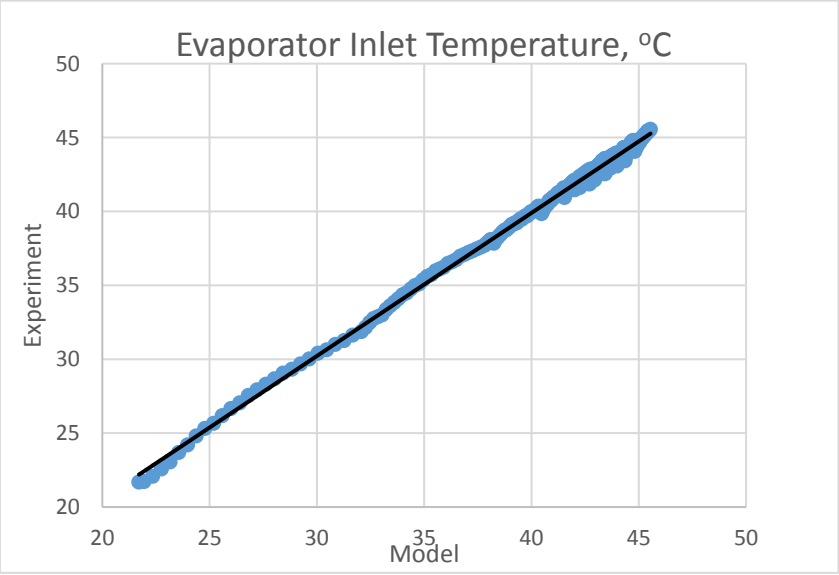


Figure 6.18 Correlation between experiment and model data temperature at evaporator inlet

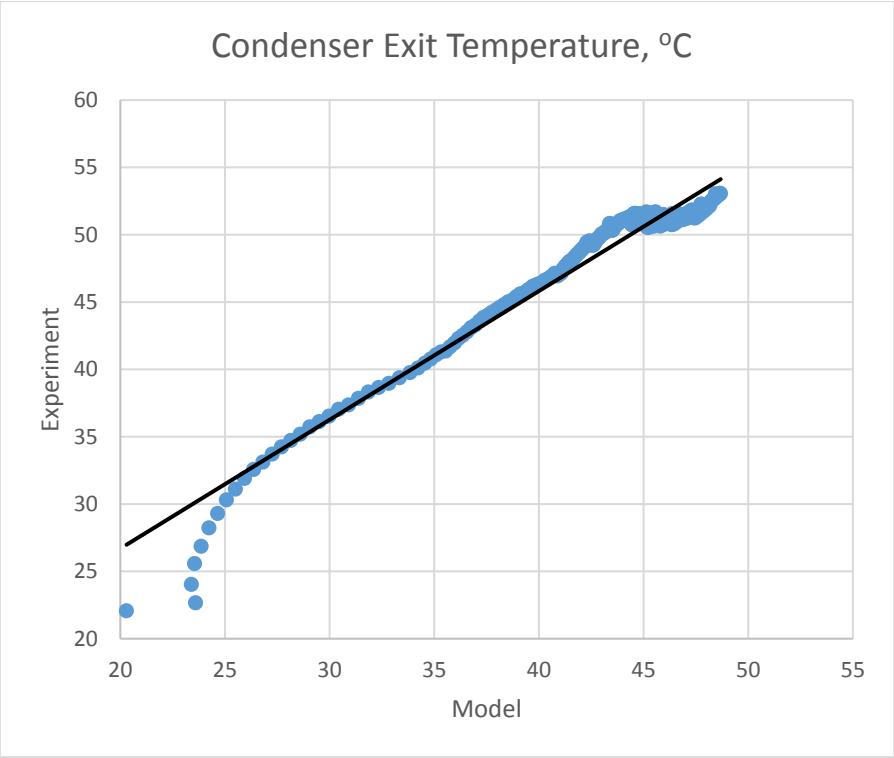


Figure 6.19 Correlation between experiment and model data temperature at condenser exit

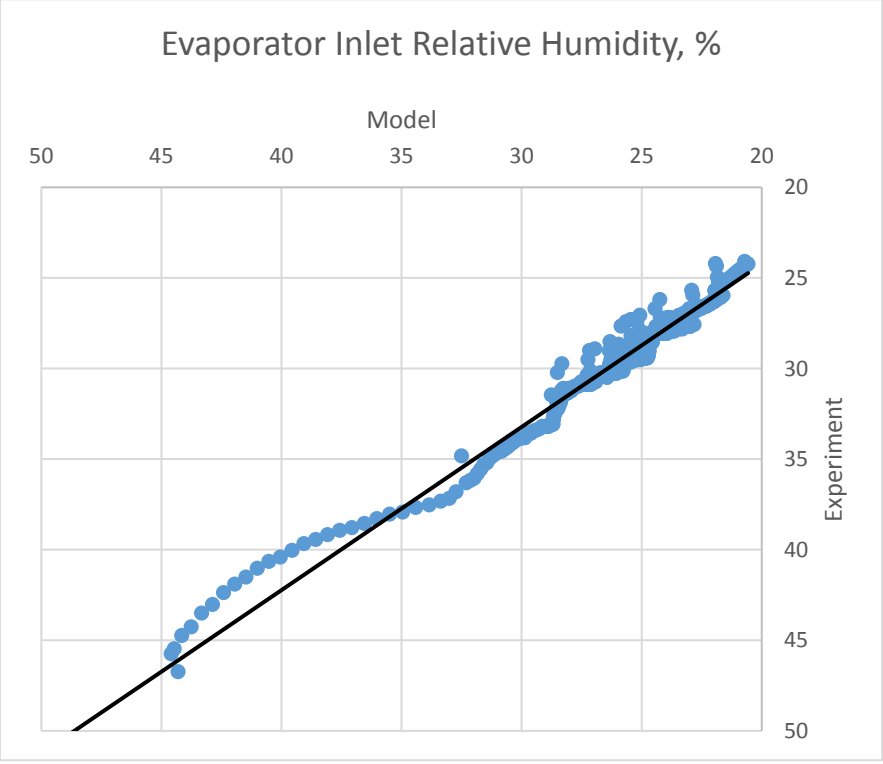


Figure 6.20 Correlation between experiment and model data relative humidity at evaporator inlet

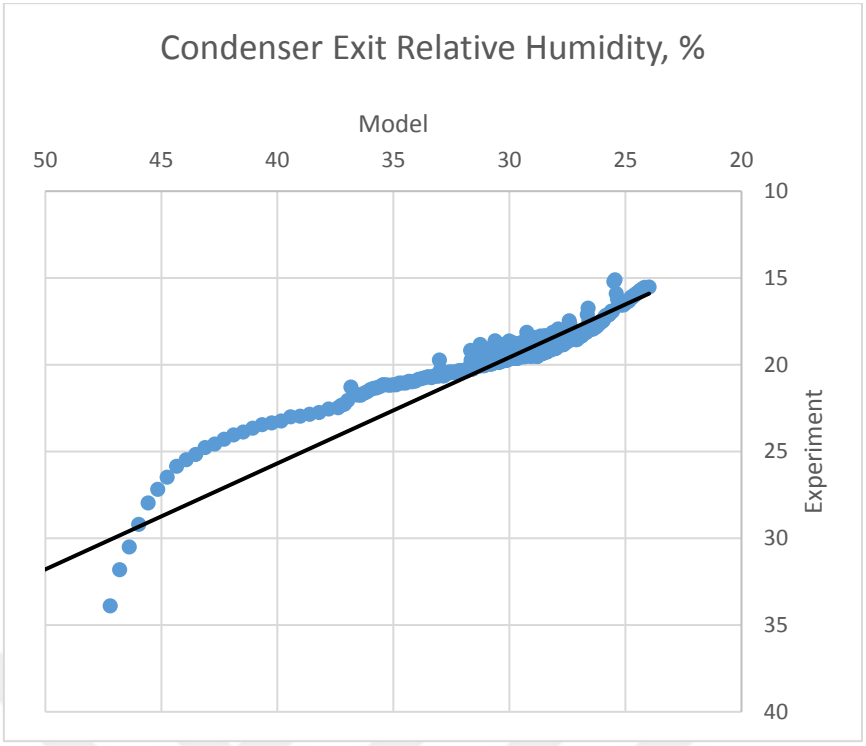


Figure 6.21 Correlation between experiment and model data relative humidity at temperature at condenser exit

With these evaluation metrics and correlation graphs, we once again see that there is a relating trend between our experiment data and model data, but also there are deviations and variances in values. There might be a couple of reasons for these differences. The first probable reason for this difference might be the fact that the condenser exit measurement on the oven setup is about 30 cm above the dehumidifier exit, at the upper end of the duct connecting to the main cabin. The model data is read at the exit port of the condenser. This difference in measurement points might be the reason in the difference in the results. There are also probable energy loses in the setup framework, such as leakage or convection loses, resulting in the variance seen between model and experiment results. Another reason can be inaccurate inlet data given to the model. The measurement of the inlet air properties using the velocity probe is a meticulous operation where the flow of air might have been affected while measuring, due to human error factor. The measurement reading also took time to stabilize. Both might have caused readings to be different than the actual real time parameters. There are also inherent shortcomings of our model that might have caused this difference in results. We have simplified the

dehumidifier system for our model, combining only essential components. Leaving out parts like the fan may be causing the discrepancies. Moreover, we were not able to measure and input all the real time parameters for components. There may also be errors for the parameters we have physically measured since measuring required great precision and were prone to human error. All these shortcomings might be contributing to divergencies in results.

This difference in the results can be examined and might be corrected with calibration. This might be confirmed with new runs of the experiment and sets of data.

6.3 Variations on the Model

Although not exact, seeing the accurate correlation on the model with the experiment leads us to further investigate the oven setup on the one-dimensional Simcenter Amesim model to give insights for future adjustments and improvements in our heat pump dryer oven. Among the many modification options, the one in the scope of this project is to change the fluid in the system to see the variations in results. This is an element that can be adapted on the physical model as well, hence chosen.

The fluid in our dehumidifier is refrigerant R410a. This is a commonly used fluid for our purposes, however there are many more options that are being evaluated in research. Therefore, it was reasonable for us to experiment with an organic compound trending in recent applications, as well as a secondary refrigerant fluid. We have chosen organic compound R290 and refrigerant R32 to test and compare in our model using the same inlet air data used for R410a.

Figures 6.22 and 6.23 show the temperature and humidity result comparison plots for using R410a refrigerant and R290 organic compound, respectively. The correlations in results for both properties are very high. The graphs follow the same trends. However, the outlet temperature for R290 is observed to be higher and the relative humidity is observed to be lower than R410a results for the same inlet data points. This outcome leads us to think that R290 can be a more efficient fluid for the dehumidification system.

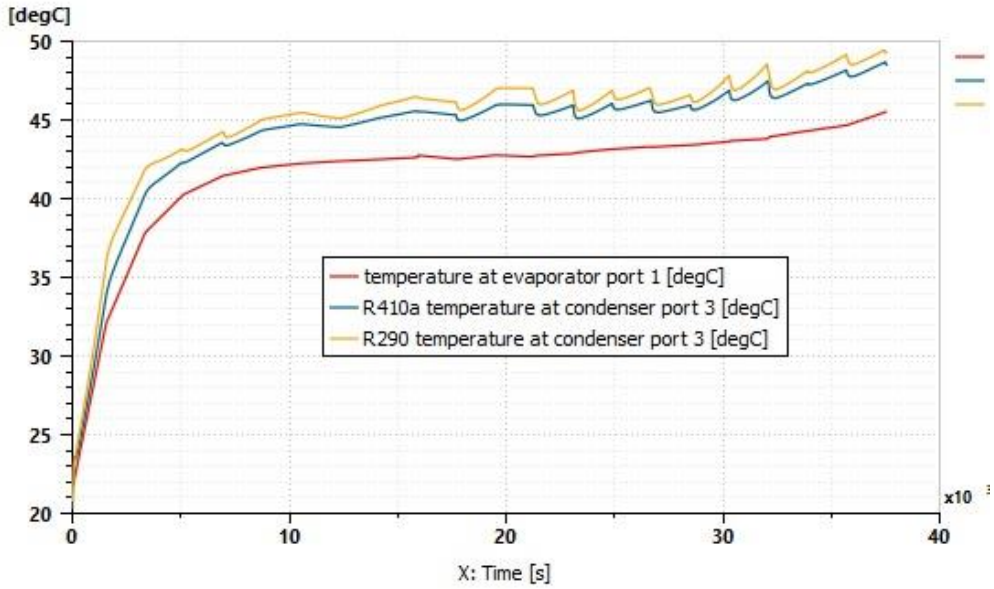


Figure 6.22 Comparison graph for model output temperature using R290 and R410a

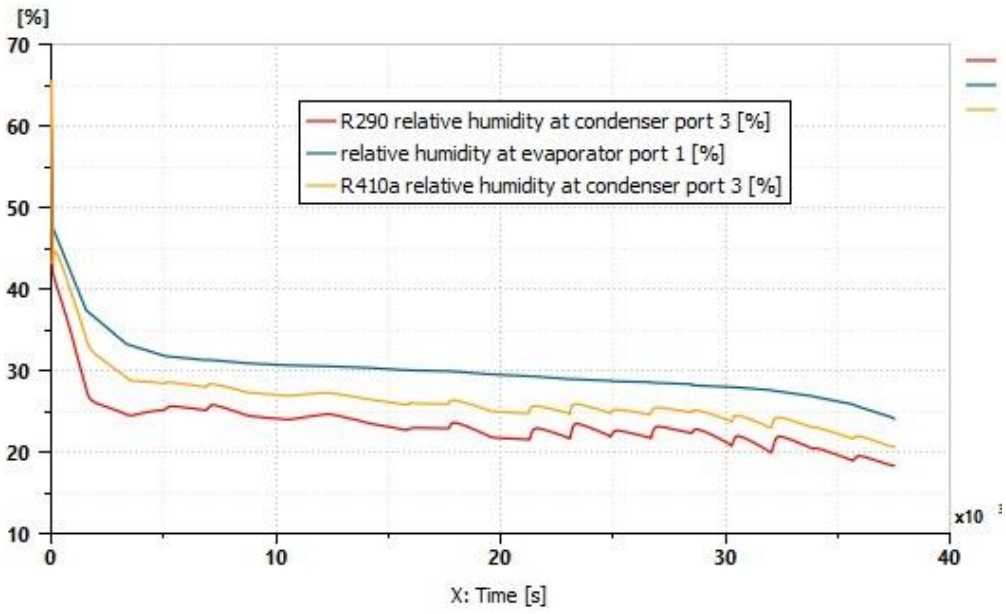


Figure 6.23 Comparison graph for model output relative humidity using R290 and R410a

To enhance the comparison and see the relativeness of efficiency increase observed from the use of R290, we have added the plot of results of model using another refrigerant, namely R32, another common refrigerant for such applications. Figure

6.24 shows the exit temperature comparison of the three fluids and Figure 6.25 shows the relative humidity comparison of the three fluids.

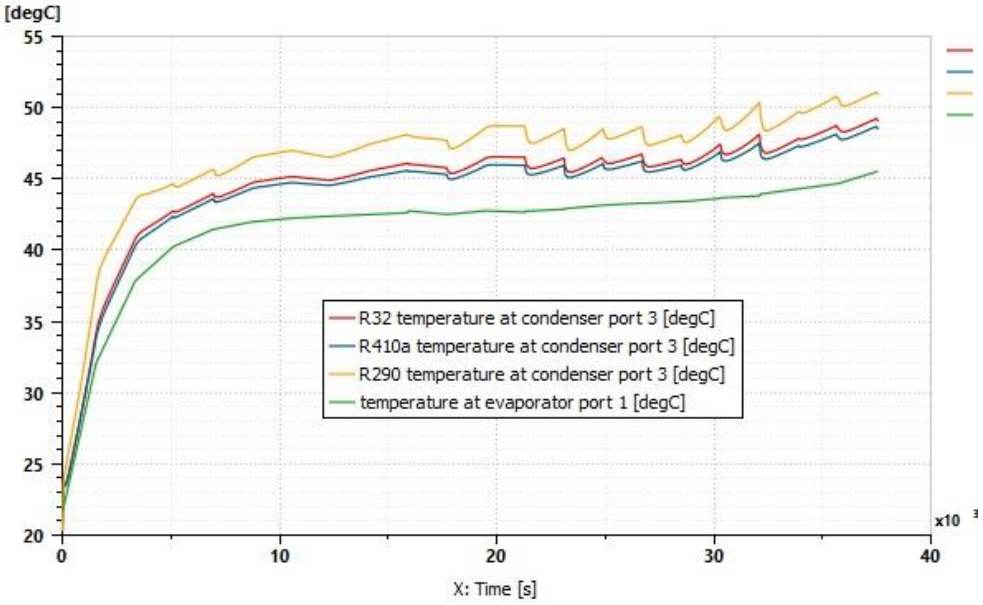


Figure 6.24 Comparison graph for model output temperature using R290, R32 and R410a

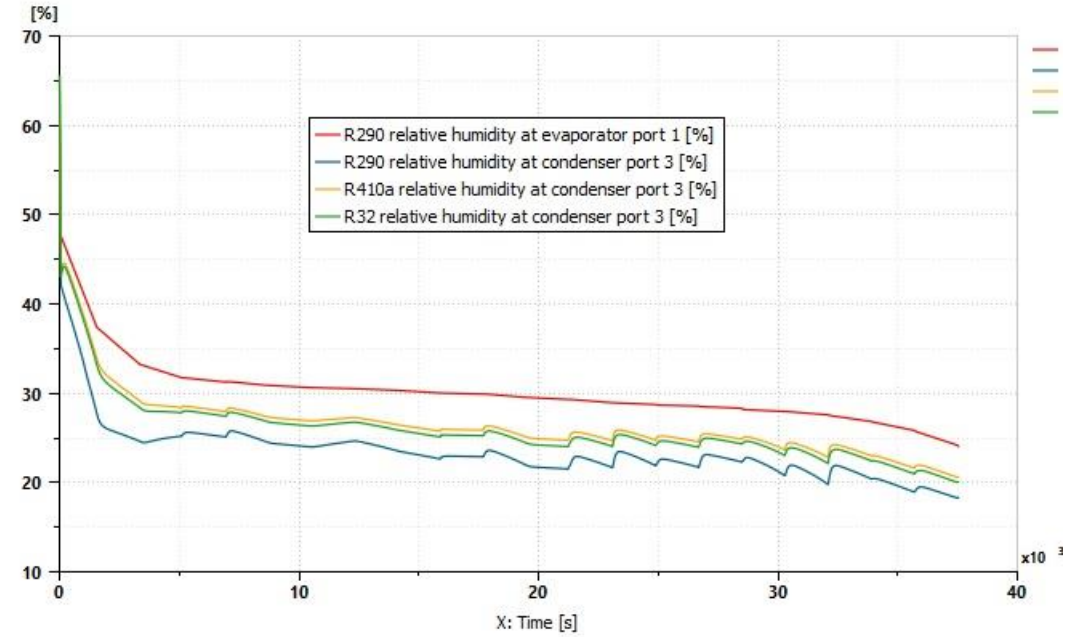


Figure 6.25 Comparison graph for model output relative humidity using R290, R32 and R410a

It is observed in these comparisons that all three fluids show correlated trends in both parameters. However, it can be detected that the results for R32 and R410a

show greater similarity in value, R32 having slightly higher temperature and slightly lower humidity levels, whereas R290 show relatively higher exit temperature and relatively lower exit humidity values. It can be concluded that R290 give better results for the same inlet values.

These comparisons exemplify the practicality of making variations on the model and demonstrate the advantages of a one-dimensional model to make decision for real-life applications.

6.4 Conclusion

The project's one-dimensional model was validated by comparing its outputs with experimental data. Experimental runs in a medium-sized room demonstrated that the model effectively replicated the dehumidification process, showing consistent trends in evaporator outlet air temperature and corroborating results with manual psychrometric analyses.

Graphs illustrating model results revealed a strong correlation between experimental and simulated data. For example, trends in relative humidity showed a consistent decline over time, while temperature increased predictably. Discrepancies in absolute values were attributed to factors such as differences in measurement points, potential energy losses (e.g., leakage or convection), and human error during data collection. Calibration and additional experimental runs were suggested to refine the model further.

The oven setup provided a more complex testing environment, integrating inlet air data measured during physical experiments into the model. The comparison of model and experimental data for temperature, relative humidity, and mass flow rates revealed close alignment in overall trends. However, slight deviations in absolute values persisted due to differences in measurement locations and potential inaccuracies in inlet data. Energy losses within the experimental framework also contributed to these discrepancies.

Despite these challenges, the validated model proved to be a robust tool for exploring system variations. For instance, changing the working fluid in the model demonstrated potential improvements in efficiency. These findings underscore the model's adaptability and its role in optimizing dehumidification systems.

6.5 Future Work

This one-dimensional model for the drying oven is a basic one, open to development and alterations. As this model will be used as a starting point for modelling a heat pump dryer oven system in our laboratory as part of a doctoral student's project, there are many improvements that can be done in relation to the physical setup as well.

The dryer oven setup in our lab is designed as a closed-loop system. The air in the cabin goes back to the inlet of the dehumidifier and this is the only air stream entering the dehumidifier. We have measured the inlet data on the physical model at certain timestamps and given this data as the inlet air source data on our model. The closed loop factor has not been totally factored into our model. This is the next step in developing our model.

Exploration of the Simcenter Amesim program for better more suitable submodels is another direction of improvement. The correlation between the physical components of the dehumidifier and the model can also be enhanced.

There are also many variations and changes that can be tested on the model for the development of the dryer oven according to our need. Using the model for enhancement of the setup and related research has been a major goal of the ongoing project from the beginning. Trying on different compressor speeds, different evaporator or condenser geometries are a few examples of what can be evaluated with this model.

6.6 Future of Dehumidification

There are many directions mechanical dehumidification technology goes to improve efficiency and effectiveness in terms of sustainability. This can range from developing more efficient compressor designs to writing better control algorithms for optimization for energy efficiency improvements. Ways of utilizing waste heat generated during the process is another area of interest. Integrating smart controls and automation systems, utilizing modular and scalable designs, using renewable energy sources can be listed as other trending directions for improving mechanical humidification design.

The one-dimensional model prepared for this project will be utilized as part of modelling a larger system. This system will consist of a heat pump dryer oven designed for food drying processes. This project is under construction at our heat lab at Yildiz Technical University. Beyond the immediate model, this project offers broader implications for mechanical dehumidification. Future enhancements in system efficiency, integration with renewable energy sources and smart automation systems aligns with sustainability goals, making dehumidification systems more environmentally friendly and cost-effective.

Since Simcenter Amesim provides a platform for various industries, our design can be adapted for dehumidification processes and applicaitons in other industries. With this simple model simulating the complex interactions between thermodynamic, fluid flow, and heat transfer phenomena, it is comtemplated that engineers can gain further valuable observations towards understanding and improving mechanical dehumidification systems.

REFERENCES

[1] "Online Interactive Pyschrometric Chart." Accessed: Jan. 19, 2025. [Online]. Available: https://www.flycarpet.net/en/psyonline

[2] Dehumidifier Corporation, "Psychrometric Processes and Dehumidification." Accessed: Jan. 21, 2025. [Online]. Available: https://dehumidifiercorp.com/blog/psychrometric-processes-and-dehumidification/

[3] G. Gürlek, Ö. Akdemir, and A. Güngör, "Usage of Heat Pump Dryer in Food Drying Process and Apple Drying Application," *Pamukkale University Journal of Engineering Sciences*, vol. 21, no. 9, pp. 398–403, 2015, doi: 10.5505/pajes.2015.35761.

[4] L. J. Goh, M. Y. Othman, S. Mat, H. Ruslan, and K. Sopian, "Review of heat pump systems for drying application," Dec. 2011. doi: 10.1016/j.rser.2011.07.072.

[5] K. J. Chua, S. K. Chou, J. C. Ho, and M. N. A. Hawlader, "Heat pump drying: Recent developments and future trends," *Drying Technology*, vol. 20, no. 8, pp. 1579–1610, 2002, doi: 10.1081/DRT-120014053.

[6] G. Chassériaux and O. Gaschet, "A MULTIFUNCTION DEHUMIDIFYING HEAT PUMP FOR GREENHOUSES," *Acta Hortic*, no. 893, pp. 469–476, Apr. 2011, doi: 10.17660/ActaHortic.2011.893.46.

[7] G. Li, Y. Liao, Y. Dou, J. Sun, J. Nan, and J. Chen, "Comparative analysis of radiant air-conditioning systems combined with two different types of solar-powered dehumidification methods," *J Phys Conf Ser*, vol. 2838, no. 1, p. 012038, Sep. 2024, doi: 10.1088/1742-6596/2838/1/012038.

[8] M. F. El Tantawy, T. mohamed Mansour, T. Nabil, and M. K. Dawood, "Enhanced Performance of Humidification-Dehumidification Desalination Systems through PCM Integration: An Experimental and Numerical Review," *Suez Canal Engineering, Energy and Environmental Science*, vol. 2, no. 1, pp. 79–95, Jul. 2024, doi: 10.21608/sceee.2024.273386.1018.

[9] A. K. M, K. G, S. M, R. S, and S. S. R, "Performance Comparison of Tray, Bed and Integrated Drying Chamber in Closed Loop Heat Pump Dryer for Bermuda Grass," *E3S Web of Conferences*, vol. 399, p. 06005, Jul. 2023, doi: 10.1051/e3sconf/202339906005.

[10] J. A. Assadeg, A. H. Al-Waeli, and K. Bin Sopian, "Solar Assisted Heat Pump System for High Quality Drying Applications: A Critical Review," 2020. [Online]. Available: https://www.researchgate.net/publication/340163128

[11] X.-M. Huang, L.-S. Xiong, Y.-W. Zheng, H.-Q. Liu, Y.-Z. Xu, and Y.-C. Li, "Comparative investigation of performance of gas dryer and two other types of domestic clothes dryers," *International Journal of Low-Carbon*

Technologies, vol. 16, no. 2, pp. 294–304, May 2021, doi: 10.1093/ijlct/ctaa064.

[12] A. B. T. Loemba, B. Kichonge, and T. Kivevele, "Comprehensive assessment of heat pump dryers for drying agricultural products," Aug. 01, 2023, *John Wiley and Sons Ltd*. doi: 10.1002/ese3.1326.

[13] J. Yu, L. Su, K. Li, and Y. Fang, "An investigation on dehumidification and heat transfer characteristics of a minichannel heat exchanger for heat pump system of electric vehicles," *Int J Energy Res*, vol. 46, no. 13, pp. 18294–18311, Oct. 2022, doi: 10.1002/er.8445.

[14] M. A. Elazab, A. E. Kabeel, M. Salem, hamouda Abueldahab, and M. S. Elhadidy, "A Review of Hybrid Humidification and Dehumidification Desalination Systems," *Journal of Engineering Research*, vol. 7, no. 5, pp. 77–88, Nov. 2023, doi: 10.21608/erjeng.2023.235477.1237.

[15] N. Ghaddar, K. Ghali, and A. Najm, "Use of desiccant dehumidification to improve energy utilization in air-conditioning systems in Beirut," *Int J Energy Res*, vol. 27, no. 15, pp. 1317–1338, Dec. 2003, doi: 10.1002/er.945.

[16] R. Zylla, S. P. Abbas, K. W. Tai, S. Devotta, F. A. Watson, and F. A. Holland, "The potential for heat pumps in drying and dehumidification systems I: Theoretical considerations," *Int J Energy Res*, vol. 6, no. 4, pp. 305–322, 1982, doi: 10.1002/er.4440060402.

[17] A. R. Nurieva and N. P. Nikitina, "Functional, technological, constructive and compositional solutions of ski complexes," *Russian Journal of Construction Science and Technology*, vol. 9, no. 2, p. 0902005, 2023, doi: 10.15826/rjcst.2023.2.003.

[18] B. R. Toal, R. Morgan, and J. T. McMullan, "Experimental studies of low-temperature drying by dehumidification. Part 1—Apparatus and theory," *Int J Energy Res*, vol. 12, no. 2, pp. 299–314, Mar. 1988, doi: 10.1002/er.4440120211.

[19] K. Hamid, U. Sajjad, K. S. Yang, S. K. Wu, and C. C. Wang, "Assessment of an energy efficient closed loop heat pump dryer for high moisture contents materials: An experimental investigation and AI based modelling," *Energy*, vol. 238, Jan. 2022, doi: 10.1016/j.energy.2021.121819.

[20] C. Arpagaus, F. Bless, M. Uhlmann, J. Schiffmann, and S. S. Bertsch, "High temperature heat pumps: Market overview, state of the art, research status, refrigerants, and application potentials," *Energy*, vol. 152, pp. 985–1010, Jun. 2018, doi: 10.1016/j.energy.2018.03.166.

[21] B. Wang, J. Shen, L. Jiang, and W. Wei, "Research on Two-stage Humidification-dehumidification Heat Pump Desalination System," *J Phys Conf Ser*, vol. 2473, no. 1, p. 012003, Apr. 2023, doi: 10.1088/1742-6596/2473/1/012003.

[22] W. Li, J. Wei, Y. Yuan, L. Yang, C. Zhang, and B. Li, "Experimental Investigation on Performance of Multi-Stage Dehumidification Heat Pump Tower Corn Drying System in High Cold Regions," *Heat Transfer Engineering*, vol. 44, no. 16–18, pp. 1671–1685, Oct. 2023, doi: 10.1080/01457632.2022.2140632.

[23] M. K. Bezrodny and T. O. Misiura, “ENERGY ANALYSIS OF A HEAT PUMP AIR HANDLING UNIT FOR THE DEHUMIDIFICATION AND AIR CONDITIONING OF A PRODUCTION PREMISE,” *Thermophysics and Thermal Power Engineering*, vol. 44, no. 1, pp. 55–64, May 2022, doi: 10.31472/ttpe.1.2022.7.

[24] I. A. Ikem, M. I. Ibeh, D. Osim-Asu, O. E. Nyong, and A. E. Edem, “A review on possibilities for the development of heat pump cocoa drying in Ikom (Cross River State), Nigeria,” *International Journal of Engineering Trends and Technology*, vol. 38, no. 3, pp. 158–157, Aug. 2016, doi: 10.14445/22315381/IJETT-V38P229.

[25] T. Kivevele and Z. Huan, “A review on opportunities for the development of heat pump drying systems in South Africa,” 2014, *Academy of Science of South Africa*. doi: 10.1590/sajs.2014/20130236.

[26] E. Öztürk and A. Güngör, “THERMODYNAMICS AND PSYCHROMETRIC ANALYSIS OF INDOOR SWIMMINGPOOL DEHUMIDIFICATION UNITS,” *Mugla Journal of Science and Technology*, vol. 2, no. 1, pp. 77–82, 2016.

[27] A. Santrallerinin, T. Ve, and A. Gungor, “THERMODYNAMICS AND PSYCHROMETRIC ANALYSIS OF INDOOR SWIMMINGPOOL DEHUMIDIFICATION UNITS KAPALI YÜZME HAVUZU NEM,” 2016. [Online]. Available: https://www.researchgate.net/publication/311100884

[28] L. B. Taclan, E. Y. Taclan, R. M. Ephraim Umpad, D. Garduque, J. S. Balila, and M. P. Narbarte, “Dehumidification Efficiency (DHE) of the Automated Multi Commodity Heat Pump Dryer (AMCHPD).”

[29] A. D. Tuncer, R. Mavuş, C. Gökçe, M. Koşan, and M. Aktaş, “Efficient Energy Systems Models for Sustainable Food Processing,” *Turkish Journal of Agriculture - Food Science and Technology*, vol. 7, no. 8, pp. 1138–1145, Aug. 2019, doi: 10.24925/turjaf.v7i8.1138-1145.2439.

[30] T. Suyono *et al.*, “Performance of desiccant wheel for low humidity drying system.” [Online]. Available: https://www.researchgate.net/publication/287567175

[31] Ü. İşkan, A. Yüksel, and C. Tunçkal, “An experimental research on the effect of infrared and carbon fiber film heater integration in heat pump food drying system on drying performance,” *International Journal of Energy Studies*, vol. 9, no. 4, pp. 601–618, Dec. 2024, doi: 10.58559/ijes.1540479.

[32] Z. Zhuman, N. Khanzharov, and B. Abdizhapparova, “DESIGNING AND TESTING A HEAT PUMP UNIT FOR DRYING, LOW-TEMPERATURE PROCESSING, AND STORING OF FOOD PRODUCTS,” *Eastern-European Journal of Enterprise Technologies*, vol. 5, no. 8(131), pp. 33–41, 2024, doi: 10.15587/1729-4061.2024.313339.

[33] N. Mishra, S. K. Jain, and N. K. Jain, “Recent Developments of Heat Pump Dried Agriculture Produce: An Overview of Technical and Theoretical Application,” *Environment and Ecology*, vol. 41, no. 3C, pp. 1910–1916, Sep. 2023, doi: 10.60151/envec/NPRU7616.

[34] F. Salehi, “Recent Applications of Heat Pump Dryer for Drying of Fruit Crops: A Review,” 2021, *Bellwether Publishing, Ltd.* doi: 10.1080/15538362.2021.1911746.

[35] M. Yazici and R. Kose, “Evaluation beyond a Review: Developments in Heat Pump Dryers from the Recent Past to the Present,” *Journal of Energy Research and Reviews*, pp. 52–71, Apr. 2022, doi: 10.9734/jenrr/2022/v10i430264.

[36] K. J. Chua, S. K. Chou, and W. M. Yang, “Advances in heat pump systems: A review,” 2010, *Elsevier Ltd*. doi: 10.1016/j.apenergy.2010.06.014.

[37] J. Wang *et al.*, “Brief introduction of dehumidification technology and research progress,” in *IOP Conference Series: Earth and Environmental Science*, IOP Publishing Ltd, Sep. 2020. doi: 10.1088/1755-1315/568/1/012020.

[38] H. Rostamzadeh, “Indirect mechanical heat pump assisted humidification-dehumidification desalination systems,” *Int J Energy Res*, vol. 45, no. 11, pp. 15892–15920, Sep. 2021, doi: 10.1002/er.6822.

[39] M. Hamid Rajab, M. Anwar Abdullah, M. Noori Mohammed, and T. Khalil Ibrahim, “Investigation of the Performance of Heat Pump Waste Heat Regeneration Runner Dehumidification of Air Conditioning Systems,” 2021.

[40] C. Guo *et al.*, “Study on performance optimization of a liquid desiccant air conditioning system driven by photovoltaic thermal–air source heat pump,” *Physics of Fluids*, vol. 36, no. 9, Sep. 2024, doi: 10.1063/5.0220870.

[41] J. Yu and L. Sheng, “Experimental investigation on dehumidification and heating performance of a heat pump system concerning dew or fog removal for electric vehicles,” *Proceedings of the Institution of Mechanical Engineers, Part D: Journal of Automobile Engineering*, vol. 238, no. 1, pp. 89–99, Jan. 2024, doi: 10.1177/09544070221125344.

[42] W. Yaïci, E. Entchev, P. Talebizadeh Sardari, and M. Longo, “Recent Developments of Combined Heat Pump and Organic Rankine Cycle Energy Systems for Buildings,” in *Product Design*, IntechOpen, 2020. doi: 10.5772/intechopen.93130.

[43] K. Salhein, C. J. Kobus, M. Zohdy, A. M. Annekaa, E. Y. Alhawsawi, and S. A. Salheen, “Heat Transfer Performance Factors in a Vertical Ground Heat Exchanger for a Geothermal Heat Pump System,” *Energies (Basel)*, vol. 17, no. 19, p. 5003, Oct. 2024, doi: 10.3390/en17195003.

[44] Bhatu R. Borane, V. H. Patil, Tushar Koli, and Kishor Mahajan, “An Experimental and Psychrometric Analysis of Desiccant Wheel with Comparative Study of Dehumidification using Desiccant Material used in hybrid Air Conditioning,” *International Journal of Research in Engineering, Science and Management*, Jun. 2019.

[45] C. Ghiaus, “Computational psychrometric analysis as a control problem: case of cooling and dehumidification systems,” *J Build Perform Simul*, vol. 15, no. 1, pp. 21–38, 2022, doi: 10.1080/19401493.2021.1995498.

[46] V. H. Tailor, D. Ragesh, G. Kapadia, and M. E. Student, “A Literature review on an energy and exergy analysis of psychrometric processes,” *© 2014 IJEDR*, vol. 2, no. 1, 2014, [Online]. Available: www.ijedr.org

[47] F. Kuru and D. Kumlutaş, “A novel method for measuring and improving the dehumidification process inside a direct contact condensation unit,” *European Mechanical Science*, vol. 7, no. 2, pp. 109–121, Jun. 2023, doi: 10.26701/ems.1275329.

[48] K. Maslak and S. Nimmermark, “Thermal energy use for dehumidification of a tomato greenhouse by natural ventilation and a system with an air-to-air heat exchanger.”

[49] S. Gendelis, A. Timuhins, A. Laizans, and L. Bandeniece, “Mathematical Modeling of Dual Layer Shell Type Recuperation System for Biogas Dehumidification,” *Latvian Journal of Physics and Technical Sciences*, vol. 52, no. 6, pp. 49–60, Dec. 2015, doi: 10.1515/lpts-2015-0035.

[50] J. Chu, W. Choi, C. A. Cruickshank, and S. J. Harrison, “Modeling of an Indirect Solar Assisted Heat Pump System for a High Performance Residential House,” *J Sol Energy Eng*, vol. 136, no. 4, May 2014, doi: 10.1115/1.4027486.

[51] V. Singh, D. Harursampath, S. Dhawan, M. Sahni, S. Saxena, and R. Mallick, “Physics-Informed Neural Network for Solving a One-Dimensional Solid Mechanics Problem,” 2024, doi: 10.3390/modelling.

[52] F. Clavica, J. Alastruey, S. J. Sherwin, and A. W. Khir, “One-dimensional modelling of pulse wave propagation in human airway bifurcations in space–time variables,” in *2009 Annual International Conference of the IEEE Engineering in Medicine and Biology Society*, IEEE, Sep. 2009, pp. 5482–5485. doi: 10.1109/IEMBS.2009.5334564.

[53] F. Russo, O. Pereira Taranto, H. Silva Santana, and K. Andreola, “Mathematical modeling of the air dehumidification using Peltier modules,” Oct. 2017. doi: 10.19146/pibic-2017-78875.

[54] T. Zarei and M. R. Miroliaei, “Performance evaluation of an HDH desalination system using direct contact packed towers: experimental and mathematical modeling study,” *Journal of Water Reuse and Desalination*, vol. 12, no. 1, pp. 92–110, Mar. 2022, doi: 10.2166/wrd.2022.095.

[55] H. M. Abd-Ur-Rehman and F. A. Al-Sulaiman, *Mathematical Modeling of Bubbler Humidifier for Humidification-Dehumidification (HDH) Water Desalination System*.

[56] R. Enayatollahi, T. Anderson, and R. Nates, “Mathematical modeling of a solar powered humidification dehumidification desalination prototype.”

[57] A. Laknizil *et al.*, “Modeling and Thermal Analysis of Small Scale Desalination System using Humidification-Dehumidification Process Driven by Solar Energy,” in *2018 6th International Renewable and Sustainable Energy Conference (IRSEC)*, IEEE, Dec. 2018, pp. 1–6. doi: 10.1109/IRSEC.2018.8702981.

[58] D. Barochia, H. Nikkhah, and B. Beykal, “Design and Optimization of a Multipurpose Zero Liquid Discharge Desalination Plant,” Jul. 2024, pp. 705–710. doi: 10.69997/sct.142929.

[59] F. A. Marion, S. V. Masson, F. J. Betz, and D. H. Archer, “Cogeneration System Performance Modeling,” in *ASME 2008 2nd International Conference on Energy Sustainability, Volume 1*, ASMEDC, Jan. 2008, pp. 801–808. doi: 10.1115/ES2008-54256.

[60] T. Jafarinejad, H. Yousefi, and K. Choubineh, “Techno-Economic Assessment of Heat Recovery in Series Condensers Arrangement: Hot and Humid Regions,” *Environmental Energy and Economic Research*, vol. 2, no. 3, pp. 219–228, 2018, doi: 10.22097/eeer.2019.163929.1063.

[61] J. Wang, S. Sivashankar, E. Arvanitis, and D. Reed, “Modeling and Simulation of Two Patient Single Ventilator Systemwith Simcenter Amesim,” in *2024 Design of Medical Devices Conference*, American Society of Mechanical Engineers, Apr. 2024. doi: 10.1115/DMD2024-1042.

[62] C. Husar *et al.*, “Simcenter Amesim virtual validation of a BEV using EMR methodology,” in *2021 IEEE Vehicle Power and Propulsion Conference (VPPC)*, IEEE, Oct. 2021, pp. 1–6. doi: 10.1109/VPPC53923.2021.9699204.

[63] H. Nguyen, S. I. Ngo, H. Bui, T. Vu, B. Tran, and H. Pham, “Simulation of Battery Air Cooling Performance of Electric Vehicle by SIMCENTER AMESim,” in *2023 Asia Meeting on Environment and Electrical Engineering (EEE-AM)*, IEEE, Nov. 2023, pp. 1–4. doi: 10.1109/EEE-AM58328.2023.10395204.

[64] A. Reveillere, M. Longeon, and I. Rossi, “Dynamic simulation of a combined cycle for power plant flexibility enhancement,” *E3S Web of Conferences*, vol. 113, p. 01005, Aug. 2019, doi: 10.1051/e3sconf/201911301005.

[65] L. Romagnuolo, E. Frosina, C. R. de Hieronymis, G. Bordini, and A. Senatore, “Innovative and self-adaptive energy recovery system in hydraulic cylinders for cyclic operations,” *J Phys Conf Ser*, vol. 2893, no. 1, p. 012059, Nov. 2024, doi: 10.1088/1742-6596/2893/1/012059.

[66] W. Fiebig and W. Prastiyo, “Reduction of Dynamic Loads in Piston Compressors Through the Use of Mechanical Resonance,” in *2024 International Maha Fluid Power Conference*, Denmark: River Publishers, 2024, pp. 105–122. doi: 10.13052/rp-9788770047456.008.

[67] S. Szabłowski, “Projektowanie mechatroniczne w środowisku Simcenter Amesim 1D,” *Dydaktyka Informatyki*, vol. 15, pp. 133–140, 2020, doi: 10.15584/di.2020.15.9.

[68] Z. Ren *et al.*, “Analysis and research on the constant-rate penetration mechanism of the seabed cone penetration test system,” *Front Mech Eng*, vol. 9, Jun. 2023, doi: 10.3389/fmech.2023.1110951.

[69] Trotec GmbH, “TTK 100 E Nem Alma Cihazı TALIMATLAR.”

[70] Inc. Degree Controls, “Efficient Ventilation for Safe Workplace Air.” Accessed: Jan. 22, 2025. [Online]. Available: https://www.degreec.com/efficient-ventilation-for-safe-workplace-air/

[71] “Simcenter Amesim,” Wikipedia. Accessed: Jan. 20, 2025. [Online]. Available: https://en.wikipedia.org/wiki/Simcenter_Amesim#:~:text=Simcenter%20Amesim%20is%20a%20part,Digital%20Industries%20Software%20Simcenter%20portfolio.

[72] Siemens Digital Industries Software, “Mechanical system simulation software.” Accessed: Jan. 20, 2025. [Online]. Available: https://plm.sw.siemens.com/en-US/simcenter/simulation-test/mechanical-system-simulation/

[73] Siemens Industry Software NV, “Simcenter Amesim ,” 2021.1.

[74] Tornado, “Free online Psychrometric Calculator”, Accessed: Jan. 21, 2025. [Online]. Available: http://www.hvac-calculator.net/index.php?v=2

PUBLICATIONS FROM THE THESIS

Conference Papers

1. Ş. Satoğlu and H. Demir, "One Dimensional Modelling and Experimental Investigation of Mechanical Dehumidification," in *12. ULUSLARARASI İSTANBUL BİLİMSEL ÇALIŞMALAR KONGRESİ*, Istanbul, 2024, pp. 401–401.